EUROPEAN COMMISSION

nuclear science and technology

Development of NDA procedures for the QA/QC characterisation of large-volume radioactive waste packages

(Large Waste Assay)

L.P.M. van Velzen[1], J. Botte [2], A. Lyoussi[3], R. Thierry[3], A. Dodaro[4], N. Cherubini[4], R. Strange[5], S. Daish[5], K. Svoboda[6], J. Kluson[7], A. Tiitta[8], T. Kekki[8], B. Janssen[1]

[1] NRG, NL; [2] Belgoprocess, BE; [3] CEA Cadarache, FR; [4] ENEA, IT; [5] NNC, UK; [6] NRI Rez, CZ; [7] Czech Technical University of Prague, CZ; [8] VTT, FI

Contract N° FIKW-CT-2000-00027

Final report

Work performed as part of the European Atomic Energy Community's research and training programme in the field of nuclear energy 1998-2002 (Fifth Framework Programme)
Key action: Nuclear fission
Area: Safety of the fuel cycle

Directorate-General for Research
2007 Euratom EUR 23098

Project coordinator

L.P.M. van Velzen	(vanvelzen@nrg-nl.com)	NRG

Project partners

J. Botte	(john.botte@belgoprocess.be)	Belgoprocess
A. Lyoussi	(lyoussi@desdsud.cea.fr)	CEA Cadarache
A. Dodaro	(alessandro.dodaro@casaccia.enea.it)	ENEA
N. Cherubini	(nadia.cherubini@casaccia.enea.it)	ENEA
R. Strange	(robin.strange@amecnnc.co.uk)	NNC
S. Daish	(steve.daish@amecnnc.co.uk)	NNC
K. Svoboda	(ska@ujv.cz)	NRI Rez
J. Kluson	(kluson@fjfi.cvut.cz)	University of Prague
A. Tiitta	(antero.tiitta@vtt.fi)	VTT
T. Kekki	(tommi.kekki@vtt.fi)	VTT

Contents

Executive summary

In most participating countries in this project the problem of how to perform a QA/QC characterization of large-volume waste packages is recognised as one of the new arising radioactive waste problems.

The objectives of this project are the development of non-destructive QA/QC procedures and methodologies for an independent QA/QC characterization of the fissile and non-fissile content of large-volume waste packages (minimum respectively maximum volume 600 l and a 6-metre standard ISO container).

This aim can be reached by defining the following sub-objectives:

- Development of special NDA equipment and procedures for the non-destructive QA/QC characterisation of fissile and non-fissile content. Special attention will be given to source localisation of fissile and non-fissile sources.
- The validation of developed equipment and procedures for non-fissile radioactive large-volume waste. Will be tested by comparison of measured specific radioactivity before and after conditioning of the waste into a large-volume waste package.
- Validation of developed equipment and procedures for fissile radioactive waste. Will be performed mainly by artificial waste.

Therefore the project work-plan consisted of six work packages:

1. Definition phase. Investigation of available and applicable NDA techniques, procedures and large-volume waste packages. Created overviews formed the starting point of new research and developments.
2. Development of NDA techniques and procedures for the NDA characterisation of fissile material in large-volume waste, focused on the applicability of a Linac to quantify fissile material (actinides).
3. Development of NDA techniques and procedures for the NDA characterisation of non-fissile material in large-volume waste, focused on accurate collimated fixed measurements as well as on fast automatic scanning of large-volume waste packages.
4. Development of a multi-energy transmission correction technique for large-volume waste packages in order to determine the matrix properties of the waste package. Special attention has been given to the assessment of the mass fraction of hydrogen.
5. In situ validation experiments. Three experiments have been performed, at the Olkiluoto NPP (Finland), in the Waste Quality Checking Laboratory (United Kingdom), and at the Saphir facility of CEA Saclay (France).
6. Evaluation of achievements.

Therefore the performed R&D had to deal with all facets of NDA QA/QC characterization for fissile material as well as for non-fissile material present in the waste. In Table 1 an overview is given of the work carried out in this project.

The R&D on the development of suitable nuclear non-destructive techniques and procedures to control and characterize fissile material (actinides) had been focused on neutron detection following neutron and photon interrogation by using a mobile electron linear accelerator and a high-energy “fixed” electron linear accelerator which are called respectively Mini Linatron and Saphir.

These R&D investigations have lead to nuclear non-destructive methods that in one hand permit to specify radiological and emission rays provided by electron linear accelerators and in the other hand to localise and to quantify fissile masses inside concrete large waste packages by measuring the neutron emission rate produced in the contaminant content following photons and neutrons irradiation provided by electron linear accelerator.

Two series of experiment campaigns have been carried out to test, assay and validate this scientific and technical approach, which is based on simultaneous neutrons and photons interrogation techniques. The first experiment used a transportable electron linear accelerator called Mini Linatron on a concrete cubic crate of 1.4 m. The added value of such a machine is firstly the ability to be transported and to carry out in situ radioactive waste measurement and secondly its ability to produce high-energy electrons (6 MeV, 9 MeV and 11 MeV) and hence high-energy photons and high photo neutron intensities. The lower detection limit corresponds to an exenterate position at a depth of 0.38 m and is equal to 12 g of ^{238}U for a 10-minute measurement. The second experiment has been performed on a cylindrical large waste concrete package by using different ^{238}U sources in different positions inside the crate.

These experiments have been performed with a fixed Linac (Saphir) and an adjusted maximum energy of 15 MeV, resulting in a minimum detectable activity for ^{238}U of about 1.58 g at a depth of 0.48 m in concrete. Other experiments confirmed the expectation that when ^{238}U is near a more concentrated cluster of hydrogen there is a non-negligible difference in the response of about 20 % without a cluster.

Table 1 Overview of work carried out and reported.

Topic	**Developments**		**Calculations**		**Experiments**	
	Theory	**Measuring devices**	**MCNP**	**Others**	**Tests**	**Validation**
Fissile material						
Passive background	●	●		●	●	
Active background	●	●		●	●	
Active photon interrogation	●	●	●	●	●	●
Active neutron interrogation	●	●	●	●	●	●
Non-fissile material						
Photons		●	●	●	●	●
Tomography	●			●		
Contamination		●			●	
Transmission						
Linear accelerator	●	●	●	●	●	●

To assay the non-fissile content of large-volume waste packages two measuring devices have been designed. The results achieved by the point-to-point-system and the 3-dimension automatic scanning (3DAS) system by the NDA characterization of a heat exchanger were in good agreement. The reported specific activity for ^{60}Co was respectively for the PTP and the 3DAS systems 6.2 ± 3 MBq,

4.2 ± 2.1 MBq (slow scan) and 5.6 ± 2.8 MBq (fast scan). The uncertainties for both systems are assessed at 50 %.

The activity of the ISO container is assessed at 66 ± 33 MBq for ^{60}Co and at 7.2 ± 3.6 MBq for ^{137}Cs. These calculated values are in a good agreement with the total nuclide specific activities of the ISO container, filled with a consignment consisting of seventy 220-l drums including the applied calibration drum, reported by WQCL (Waste Quality Checking Laboratory, UK). The reported activities are respectively of 41 MBq for ^{60}Co and 6.3 MBq for ^{137}Cs.

The above experience combined with the experience gained by NDA characterization of an ISO container has lead to the set-up of a general guideline. Both developed systems, e.g. the PTP system and the 3DAS system, can in principle be applied. However, the developed 3DAS-system is preferable for its data-acquisition efficiency.

A multi-energy transmission model has been developed, tested and improved by artificial data provided by MCNP calculations. The results showed that with the improved model the differences between hydrogen mass fractions could be calculated within 10 %, however not the true values of the hydrogen mass fractions. Experiments were performed with a fixed Linac at different maximum energies to investigate in more detail. In conclusion, more research needs to be performed on this topic before a working method for the matrix characterization of large-volume waste packages can be established.

Finally, it can be concluded that a guideline for NDA QA/QC characterization for non-fissile material in large-volume waste packages has been established. Such a guideline for fissile material (actinides) to be applied in routines is more difficult to be established.

Concerning matrix characterization and assaying the mass fractions of hydrogen, more research is needed.

1 Objectives and strategic aspects

1.1 Introduction

Independent characterisation of radioactive waste packages by specialised laboratories is a tool which is used in most European countries to improve and to control a number of aspects of a radioactive waste package on a routine basis. At this moment routine QA/QC non-destructive techniques are available for volumes up to 220 l. However, the specialised laboratories in most countries have at this moment no routine procedures and equipment available for an independent non-destructive characterisation to be applied at large-volume waste packages. The minimum volume of a large-volume waste package is considered to be at least 600 l.

In most EU Member States, nuclear facilities (e.g. nuclear power plants and nuclear research reactors) have at regular times long maintenance periods or major revisions in which the possibility exists that large components have to be released and treated as radioactive waste. This problem looks almost the same as the treatment of large radioactive components coming from dismantling or decommissioning activities of a nuclear facility into a large-volume waste package.

Due to the age of most nuclear facilities and political decisions, it can be expected that in the near future there will be an increase of offers of these large-volume waste packages to dispose in interim or final waste storage facilities or to treatments with the aim to recycle material. At this moment large-volume waste packages form a minor quantity (about 10 %) of the total produced volume of radioactive waste packages.

In the participating countries in this project the problem of how to perform a QA/QC characterisation of large-volume waste packages is recognised as one of the new arising radioactive waste problems. The problem that has to be solved has two facets:

- How can *large waste packages* (LWP) that are not amenable to current on-site and off-site checking facilities be quality checked?
- Given that large components and decommissioning rubble are inherently dense, how can the regulator be assured that large sources of activity are not mistakenly (or deliberately) concealed in the large waste packages?

These problems have to be sufficiently solved before large numbers of these large-volume packages will be offered to waste storage facilities.

1.2 Objectives

The objective of this project is the development of "non-destructive QA/QC procedures and methodologies for an independent QA/QC characterisation of the fissile and non-fissile content of large-volume waste packages". The minimum respectively the maximum volume will be restricted in this to 0.75 m^3 and 37.5 m^3 (corresponding with an ISO sea-transport container of 2.5 * 2.5 * 6 m).

1.3 General approach

The above-stated objectives can be reached by the following sub-objectives:

- Development of special NDA equipment and procedures for the non-destructive QA/QC characterisation of fissile and non-fissile content of large-volume waste packages.

Attention is given to source localisation of fissile and non-fissile sources. The newly developed NDA equipment, procedures and methodologies are based on NDA methodologies used for the QA/QC characterisation of 220-l waste packages and NDA methodologies used in high-radiation fields. In the development of the QA/QC NDA methodologies it is taken into account that large-volume waste packages cannot be transported (in general) to QA/QC laboratories. This means that NDA equipment for these large packages has to be mobile and able to function under severe physical and radiological conditions.

- Validation of developed equipment and procedures for non-fissile radioactive large-volume waste by full-scale experiments on large-volume waste packages, i.e. a heat exchanger (8.7 m^3), a concrete box filled with radioactive scrap material (5.8 m^3), a soft waste bale (0.75 m^3) and an ISO transport container (37.5 m^3).
- Validation of developed equipment and procedures for fissile radioactive waste will be performed mainly by both semi-real radioactive waste and artificial waste (concrete cubic crate of 1.4 m edge) and by using respectively Mini Linatron and Saphir electron linear accelerators. Semi-real radioactive large waste packages consist of cylindrical concrete crate containing the same but inactive wastes matrix and putting radioactive sources inside.

The following existing and innovative non-destructive techniques are taken into account during the development of NDA methods for large-volume waste packages:

Existing:
- Gamma spectroscopy.
- Passive neutron measurements.

Innovative:
- Three-dimensional scanning of large-volume waste objects.
- Transmission with the aid of a fixed linear accelerator (adjustable to 35 MeV).
- Active neutron and photon interrogation by using a transportable electron linear accelerator (Mini Linatron).
- Active neutron and photon interrogation by using a fixed linear accelerator (Saphir).
- Two-dimensional radiation (e.g. photons or neutrons) source imaging/cartography.

1.4 Strategic aspects

Most European QA/QC radioactive waste checking laboratories have performed, nationally, the first R&D for the most common waste package in Europe – a 220 l drum – and for their typical national waste forms. Now, afterwards, they are trying to balance/harmonise their developed methods as much as possible with methods developed in similar institutes in other EU Member States.

This project offers the EU the opportunity to develop QA/QC non-destructive characterisation methodologies beforehand for large-volume waste packages, to be monitored by QA/QC radioactive waste checking laboratories in the EU Member States, so that efforts to balance/harmonise methods can be minimised (in this project seven Member States are participating).

Development of methodologies for an independent QA/QC non-destructive characterisation of large-volume waste packages will also contribute to waste management strategies for the safe disposal of radioactive waste and spent fuel and thus to the safety of the fuel cycle.

Summarised, the project:

- contributes to a consensus on the key issue of monitoring waste that bypasses current facilities
- is in accord with the programme objective of improving methods and technologies for the quality checking of wastes
- provides a more secure method(s) of monitoring large-volume waste streams
- contributes to/improves public confidence and trust in the management of radioactive waste
- assists in the development of a sound basis for the management and control of decommissioning and dismantling wastes.

1.5 Description of the consortium

All partners have been and are still involved in international R&D projects of non-destructive and destructive characterisation of radioactive waste. It is important to point out that most of the laboratories which participate in this project are responsible in their countries for the quality checking of the radioactive waste packages or are considered as experts in this field. Furthermore, all partners are members of the European Network of Testing Facilities for Quality Checking of Radioactive Waste Packages.

Partners are:

- Nuclear Research and Consultancy Group, Arnhem, NL, Coordinator (L.P.M. van Velzen).
- Belgoprocess NV, Dessel, BE (J. Botte)
- Commissariat à l'énergie atomique, Cadarache, FR (A. Lyoussi)
- Ente per le Nuove tecnologie, l'Energia e l'Ambiente, Rome, IT (A. Dodaro)
- National Nuclear Corporation Limited, Dorchester, UK (R. May)
- Nuclear Research Institute Rez plc, Prague, CZ (K. Sovoda)
- Technical Research Centre of Finland, Espoo, FI (A. Tiitta).

2 Scientific results

2.1 Introduction

This project is anticipating that the number of large-volume waste packages which will be offered to interim and final storage facilities will increase. Therefore the work plan has to deal with R&D, the validation of newly developed methods and equipment, and *in situ* validation tests to show the limitations of the developed QA/QC non-destructive techniques and procedures.

This could be realized by setting up a project work-plan that consists out 6 main work-packages those are defined as:

1. Definition phase.
2. Development of NDA techniques and procedures for the NDA characterisation of fissile material in large-volume waste
3. Development of NDA techniques and procedures for the NDA characterisation of non-fissile material in large-volume waste
4. Development of a multi-energy transmission correction technique for large-volume waste packages.
5. *In situ* validation experiments.
6. Evaluation.

From the definitions of the work packages it can be seen that the development of NDA procedures for fissile and non-fissile materials run through the work packages like a continuous thread. Therefore, the scientific and technical work for the three main topics, i.e.

- NDA characterisation of fissile material,
- NDA characterisation of non-fissile material, and
- multi-energy transmission technique for large-volume waste packages,

are separated but coherently and consistently reported.

2.2 NDA characterisation of fissile material in large-volume waste packages

2.2.1 Introduction

In the frame of this project scientific and technical work have been performed with the aim to develop or adapt specific and suitable nuclear non-destructive techniques and procedures to control and characterize fissile material (actinides) present inside large-volume radioactive waste packages.

The R&D has been focused on neutron detection following neutron and photon interrogation by using a mobile electron linear accelerator, e.g. the Mini Linatron. The study started by Brems-strahlung photon production studies and Monte-Carlo simulations and calculations to determine the Bremsstrahlung spectrum produced by Mini Linatron for 6, 9 and 11 MeV electron energies. Next to the Monte-Carlo simulations also MCNP calculations were conducted to evaluate photon flux, neutron flux, photon dose rate, photon dose rate stemming from the Mini Linatron, and to support the R&D on multi-energy transmission techniques.

In view to investigate the properties of such mobile linear accelerator photonuclear calculations to determine its applicability for active interrogation, the level of neutron intensities produced by the Mini Linatron have been studied.

In order to validate these photo-neutron calculation results, series of experiments have been carried out to perform and measure the photo-neutron component produced with a Mini Linatron and an appropriate neutron converter target.

Further, series of specific active nuclear non-destructive measurements on a large concrete crate were conducted by using the Mini Linatron to test and examine different spatial positions of transuranic material inside the concrete mock-up.

The aim of these measurements is to study also performances and limitations of using such a machine for non-destructive measurements (neutron measurements) of large radioactive waste packages and their ability to localize heavy nuclides (uranium, plutonium …) inside such items.

This section is a summary of the topical report "Upgrading NDA active and passive neutron detection calibration and neutron source detection" [1].

2.2.2 Photons and neutrons production by using a Mini Linatron electron accelerator

2.2.2.1 Photons and neutrons production

Neutron yields produced through the use of electron beams are based on photonuclear reactions (γ,n) which occur on nuclei with appropriate photo-neutron production threshold. For photonuclear reaction applications for NDA characterization of fissile material in waste, relevant photon energies lie between 2 and 15 MeV. Further, there are several other characteristics of photons in this energy range that must be born in mind when applications of photonuclear reactions are considered.

- First, there are no commercial primary sources of photon beams available that emits in this high-energy range. Instead, photons are always produced as secondary beam, in general from electron beams.
- Secondly, photons experience both atomic and nuclear interactions. A consequence of the relatively weak atomic interaction is the high penetrating power of these energetic photons in materials.
- Thirdly, it is clear that it is not possible to focus photon beams magnetically.
- Fourthly, photons cannot be detected directly; photons must be converted first to charged particles.

The simplest manifestation of the interaction of photons with atoms is the attenuation of a photon beam as it penetrates bulk material. Neglecting the effects of scattered photons and secondary electrons and positrons, a photon beam undergoes exponential absorption within bulk material according to $I(r) = I_0 \exp(-\mu r)$, where r is the distance within the material and μ is the linear attenuation coefficient.

The attenuation coefficient is often expressed as the mass attenuation coefficient μ/ρ, where ρ is the density of the bulk material.

Interactions of photons with nuclei are reflected in photonuclear cross sections. Some of these reactions are given in Table 2.2.1.

2.2.2.2 Photon-neutron source calculations

Photon-neutron source calculations cannot be handled by just one programme. Therefore specific analytical programmes developed by CEA to perform (γ,n) and (γ,fission) reactions have been used.

These analytical programmes are coupled with MCNP4B to get a complete simulating tool that is applicable for Bremsstrahlung photon production and transport, photonuclear reactions, neutron transport and finally count rate level inside neutron detectors.

Table 2.2.1 Overview of main photonuclear reactions, examples and applications

Reaction	**Channel**	**Example**	**Application**
(γ , γ)	Photon elastic scattering	Resonance, fluorescence	Bulk material analysis
(γ , γ′)	Photon inelastic scattering	Photon excitation of isomers	Dosimetry
(γ , p)	Photoprotons	----------	Transmutation, doping of semiconductors
(γ , n)	*Photoneutrons*	*Antimony-beryllium source*	*Start-up source in NPP's Linac neutron sources, radioactive wastes control*
(γ , f)	Photofission	----------	Actinides in radioactive wastes

The calculations are performed with the specific CEA code called ELEPHANT consisting of the following stages:

- MCNP version 4B: calculation of the Bremsstrahlung photon production and transport.
- RAVISOURCE: for the photonuclear reactions and neutron productions with as additional input photonuclear cross-section data files. With the now obtained neutron source(s), this source can be the source term for MCNP4B.
- MCNP version 4A: Photon-neutron transport and count rate calculations.

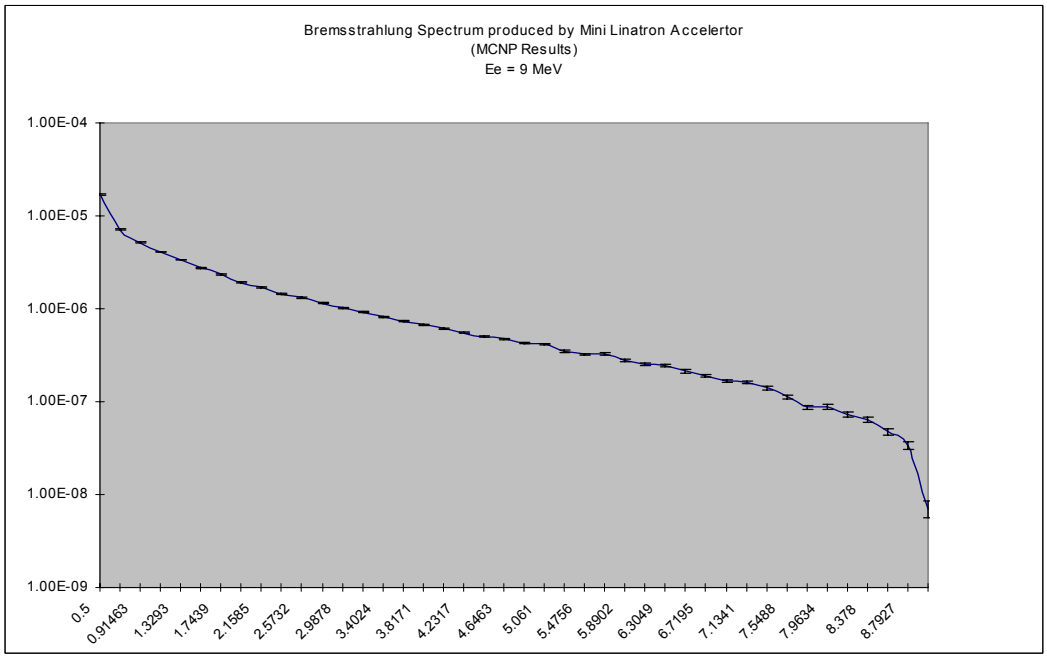

Figure 2.2.1: Mini Linatron Bremsstrahlung spectrum obtained by MCNP calculations E_e = 9 MeV

As an example of these calculations is presented in Figure 2.2.1 the calculated Bremsstrahlung by MCNP for the Mini Linatron for 9 MeV electrons and in Figure 2.2.2 results of dose rate calculations for photons and neutrons produced by a Mini Linatron. The main objectives of these calculations are to determine the optimal experimental set-up for passive neutron measurements and interrogation.

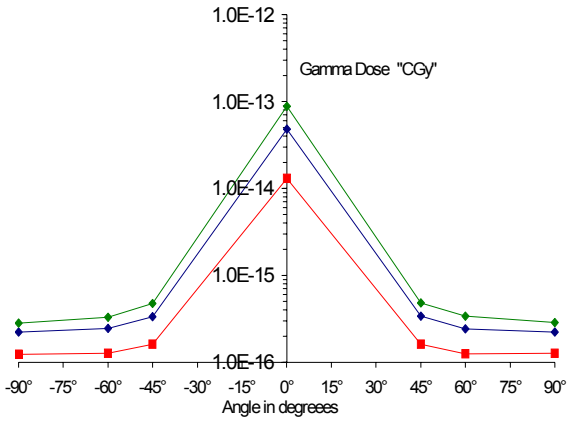

Figure 2.2.2 A

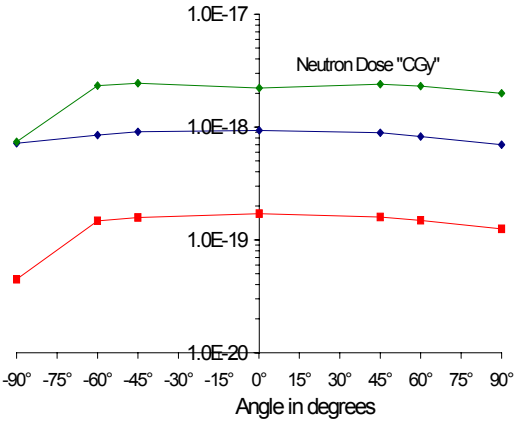

Figure 2.2.2 B

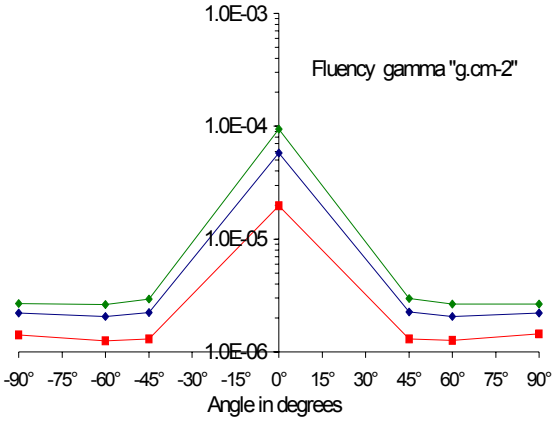

Figure 2.2.2 C

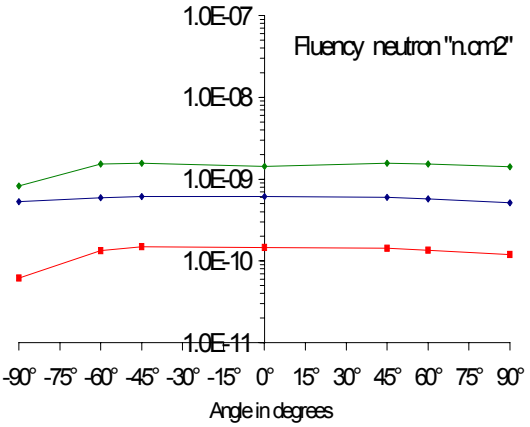

Figure 2.2.2 D

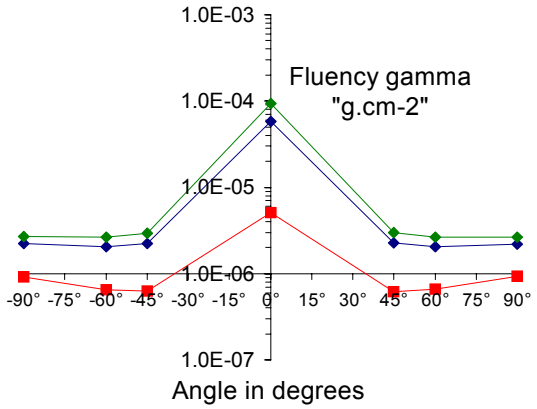

Figure 2.2.2 E

Figure 2.2.2 The results of the MCNP calculations for respectively 6 MeV (red), 9 MeV (blue) and 11 MeV (green) are given. On top: A) Gamma dose rate at 1 m; B) Neutron dose rate at 1 m; C) Photon fluency rate at 1 m; D) Neutron fluency rate at 1 m. At bottom: E) Photon fluency rate at 2 m

2.2.2.3 Experimental verification of photon-neutron source calculations

In order to validate these photo-neutron calculation results, series of experiments have been carried out to measure the photo-neutron component produced with the Mini Linatron and with an appropriate neutron converter target. The experimental set up used in these experiments was; beryllium converter target, photo-neutron measurement results and finally Mini Linatron Bremsstrahlung spatial distribution measurements results.

A series of measurements by neutron detection without and with a photon to neutron converter target were carried out (see Figure 2.2.4 for principal set up) [13]. In this case no converter target is used; the neutron component is mainly produced by photonuclear interaction in the tungsten target itself. In order to enhance Mini Linatron neutron production an appropriate beryllium converter target was placed on the electron beam axis in front of the Mini Linatron and close to the tungsten-braking target. The beryllium target is a cylinder (12 cm high and 10 cm in diameter).

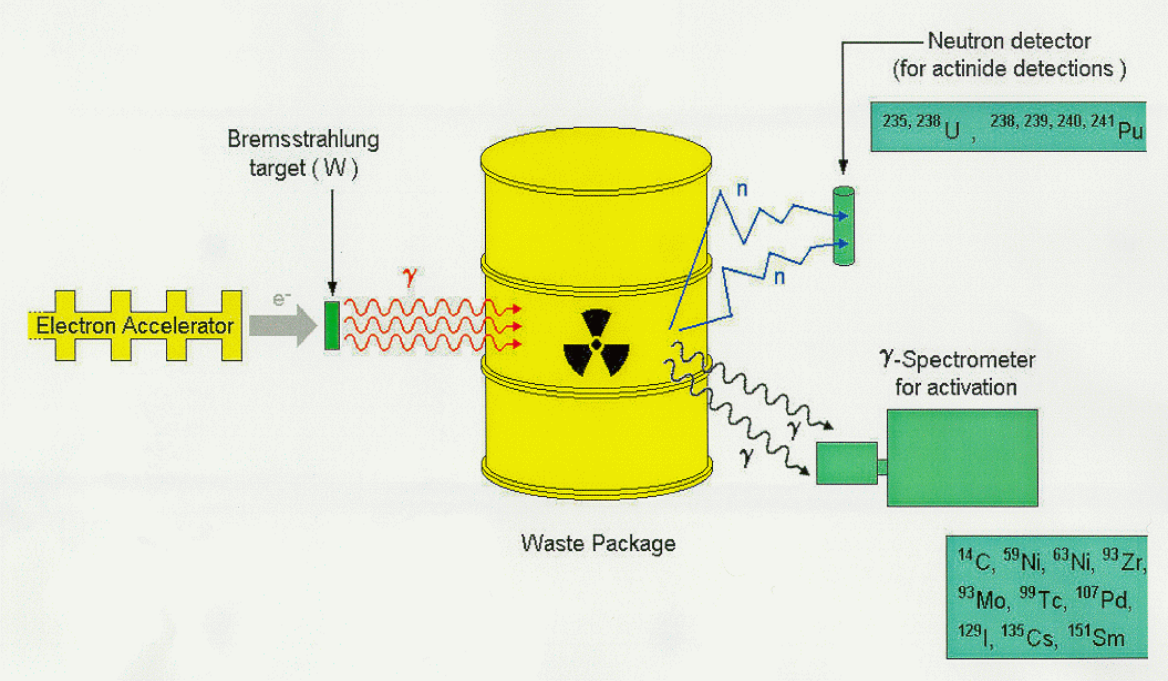

Figure 2.2.4: Principal of the experimental set up with the aid of Mini Linatron

Results of the measurements for electron energies of 6, 9 and 11 MeV are given in Table 2.2.2 for three spatial positions all at a distance of 2 m and with different angles at 90^0 (A), 45^0 (B) and 0^0 (C) degrees.

The experimental results show that the maximum neutron production corresponds to Pos C (2 m 0°) with Be target and with an electron energy of 11 MeV.

Finally, it is important to notice that photo-neutron production is significantly non-isotropic.

Table 2.2.2: Photo-neutron productions versus electron energy without and with beryllium converter target

Position	6MeV	9MeV	11MeV
Without Be target			
Pos A (2 m 90°)	2,01E+07 ($n.s^{-1}$)	7,90E+07 ($n.s^{-1}$)	1,16E+08 ($n.s^{-1}$)
Pos B (2 m 45°)	2,82E+07 ($n.s^{-1}$)	1,15E+08 ($n.s^{-1}$)	1,63E+08 ($n.s^{-1}$)
Pos C (2 m 0°)	6,33E+07 ($n.s^{-1}$)	1,79E+08 ($n.s^{-1}$)	2,59E+08 ($n.s^{-1}$)
With Be target (12 x 10 cm)			
Pos A (2 m 90°)	1,15E+10 ($n.s^{-1}$)	1,39E+10 ($n.s^{-1}$)	7,13E+09 ($n.s^{-1}$)
Pos B (2 m 45°)	1,15E+10 ($n.s^{-1}$)	1,36E+10 ($n.s^{-1}$)	6,97E+09 ($n.s^{-1}$)
Pos C (2 m 0°)	1,05E+10 ($n.s^{-1}$)	1,27E+10 ($n.s^{-1}$)	6,65E+09 ($n.s^{-1}$)

2.2.3 Concrete large waste assay by simultaneous photons and neutrons interrogation using a Mini Linatron

2.2.3.1 Objectives and set-up

According to the objectives of this R&D series of specific nuclear active non-destructive measurements on a large concrete mock-up (semi-real waste) containing fissile material in different positions have been done.

The aim of these measurements is to study also performances and limitations of using such machine for non-destructive measurement (neutron measurements) of large radioactive waste package and their ability to localize heavy nuclides (uranium, plutonium …) inside such item by means of simultaneous neutron and photon interrogation method. Therefore different spatial positions of transuranic material inside such inactive drum had been tested and examined.

2.2.3.2 Experimental and calculation procedures

The experiments have carried out by using a Mini Linatron linear accelerator. The large-volume radioactive waste package has been simulated by an inactive concrete package with three radial positions for artificial radioactive sources see Figures 2.2.5 and 2.2.6 for a schematic overview and the actual experimental set-up.

The applied ^{3}He proportional neutron detectors are coated inside with polyethylene and cadmium. In total nine counter blocks with seven ^{3}He inside each one are used (see Figures 2.2.5 and 2.2.7 for details of the CEA counter block).

Photons and neutrons produced by Mini Linatron are used as interrogating particles to induce nuclear reactions within transuranic elements inside the drum. The main photonuclear reaction applied is *photo-fission* and detecting the delayed neutron signal emitted following such reactions. As transuranic target ^{238}U was positioned in the different radial positions.

After a calibration campaign, background and forwarded signal measurements specific calculations were carried out to assay the detection limit.

The calculation of the detection limit in count per second is given by the mathematical expression:

$$LD = 4\left(\frac{1}{t_0} + \sqrt{B_a\left(\frac{1}{t_a} + \frac{1}{t_0}\right) + B_p\left(\frac{1}{t_p} + \frac{1}{t_0}\right)}\right)$$

Where:

- Ba : Neutron active background ($c.s^{-1}$),
- Bp : Neutron passive background ($c.s^{-1}$),
- t_0 : signal counting time (s),
- t_a : active background counting time (s),
- t_p : passive background counting time (s).

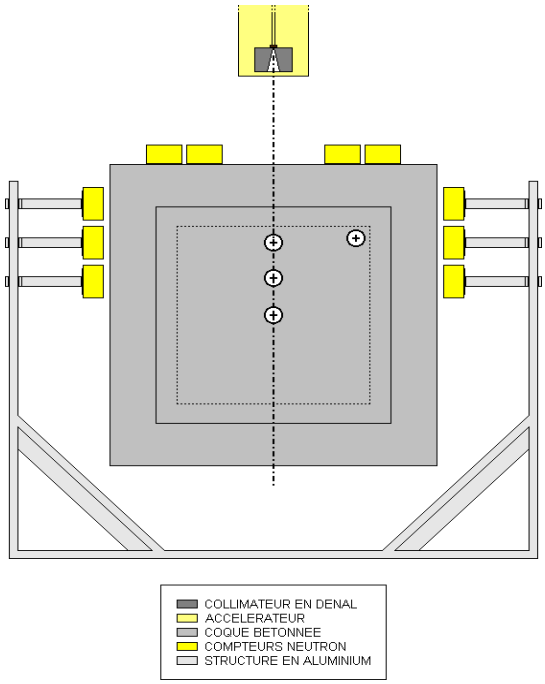

Figure 2.2.5 Schematic overview of the concrete mock-up (cubic with sides of 1.4 m^3 and 3 radial positions for radioactive sources), accelerator, ^3H proportional counters and aluminium supporting structures.

Figure 2.2.6 Picture of the actual set-up with the Mini Linatron electron accelerator in front of large concrete mock-up and the ^3H proportional counters fixed at the aluminium supporting structures.

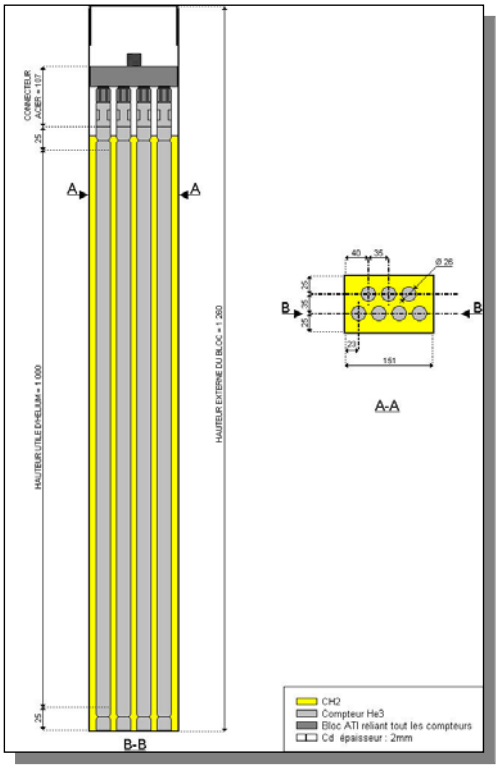

Figure 2.2.7 Description of CEA neutron detector bloc; seven ^3He proportional counters inside polyethylene and coated with cadmium.

2.2.3.3 Results

The results obtained for ^{238}U are presented in Table 2.2.3 below:

Table 2.2.3. Detection limits in gram for neutron and photon interrogation of ^{238}U at different radial positions within concrete mock-up.

	Calibration coefficients (c. s^{-1}/g)			Detection limits (g)		
Detection limits c. s^{-1}	**Centred position**	**Intermediate position**	**Exenterate position**	**Centred position**	**Intermediate position**	**Exenterate position**
0.542	$2.404\ 10^{-3}$	$6.600\ 10^{-3}$	$4.531\ 10^{-2}$	225(g)	82(g)	12(g)

For each spatial position inside the concrete mock-up hold:

Detection limit (g) = [detection limit ($c.s^{-1}$)] x [calibration coefficient ($c.s^{-1}/g$)]$^{-1}$

Duration of each measurement is 10 min for each position.

2.2.3.4 Conclusion

The performed R&D on the development of suitable nuclear non-destructive techniques and procedures to control and characterize fissile material (actinides) present inside large-volume radioactive waste packages with the aid of a Mini Linatron electron accelerator has lead to quantified characteristics of neutrons and photons production by using such a Mini Linatron.

Bremsstrahlung calculations and specifications of the Mini Linatron are essential for the prediction of the photon transmission assay.

Neutron and photon dose rates calculations by MCNP permits to establish the most advantageous location of neutron and photon experimental setups to avoid (to minimize) radiation background effect on ^{3}H neutron counters that has to will deal with.

Finally, high neutron intensity produced by Mini Linatron has been measured and well quantified, as is about 10^{10} n. $^{s-1}$. This high neutron intensity produced by such a machine is expected to be sufficient for neutron interrogation of large-volume waste packages.

The results of a specific nuclear non-destructive measurements campaign on large concrete inactive package by using photons and neutrons produced by Mini Linatron as interrogating particles at ^{238}U established detection limits of 225, 82 and 12 g for respectively the centre (depth of 70 cm), the intermediate position (depth of 54 cm) and at the exenterate position (depth of 38 cm) of the concrete mock-up.

2.2.4 Fissile material *in situ* validation experiment by using Saphir

2.2.4.1 Objectives and set-up

The objectives of the validation experiments carried out at CEA Saclay with Saphir were to determine the minimum detectable activity (MDA) of ^{238}U using active neutron interrogation and

to estimate the influence of the position of the ^{238}U source and the influence of the hydrogen content of the matrix at the results by replacing concrete by polyethylene.

2.2.4.2 Experimental and specific activity calculation procedures

In Figure 2.2.8 a schematic overview of the experimental set-up is given. The concrete mock-up has a diameter of 1.08m, height 0.4 m and has a weight of about 800 kg and has 26 voxels of 0.12 m *0.12 m. The diameter of the bangs in the voxel is 0.06 m by a length of 0.4 m.

In order to obtain the information needed for the above described objectives the following experiments have been carried out in active as well in the passive mode (e.g. with and without beam from the accelerator):

- Passive measurements. Calibration of the system. This series of measurements was performed with a ^{252}Cf source e.g. with three source configurations (positions C8, C6 and C4) and two matrix configurations (all cylinders are of concrete except the one with the source and with concrete cylinder replace by polyethylene cylinders, see Figure 2.2.8)
- Active background measurements. In order to subtract the active background.
- Active interrogation measurements. The passive measurements carried out with the Spontaneous fission source (Cf^{252}) were repeated with the beam on substituting with ^{238}U the ^{252}Cf.
- MDA determination. To determine the MDA, the source was placed in position C4 and was measured with two different sources of uranium characterized by masses of respectively of 115.0 g and 8.5 g. The accelerator has been set at 15 MeV of maximum energy.

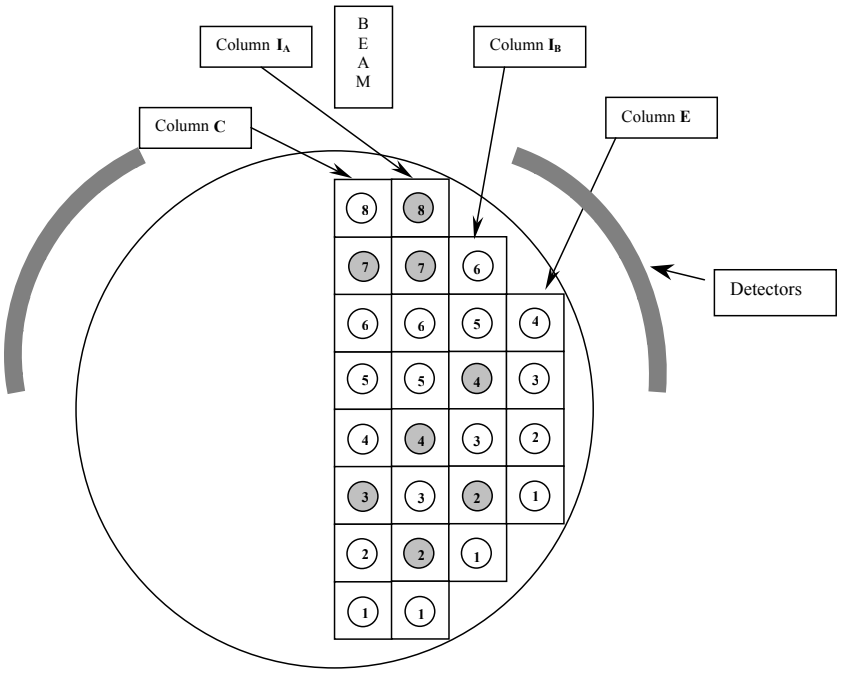

Figure 2.2.8 Schematic overview of the experimental device including legends (in grey the holes selected for polyethylene dummies)

After the experiments have been carried out in active as well in the passive mode (e.g. with and without beam from the accelerator). A series of Monte Carlo simulations have been set up in order

to validate the procedure and the results obtained, and to allow the extension of NDA measurement procedures to real situations.

2.2.4.3 Results

2.2.4.3.1 MDA determination

The determination of Minimum Detectable Activity (MDA) has been obtained applying the Statistic Theory of Hypothesis Testing [2]. The detection limit have been obtained establishing a critical level for which error of the first kind, α, and error of the second kind, β, both are assumed to be 10 %. The MDA for ^{238}U can then be assessed at 1.578 g. This value, considering the weight of the matrix (about 800 kg) gives a minimum detectable concentration of about 0.025 Bq/g of ^{238}U in the position C4 (see for the position Figure 2.2.8).

2.2.4.3.2 Neutron source position sensitivity

In Figure 2.2.9 the behaviour of the detection efficiency with respect to the spontaneous fission source position is reported. The blue line is related to the configuration with all concrete cylinders in place while the red one corresponds with the configuration in which concrete cylinders have been replace by PE-cylinders.

As can be easily seen, the detection efficiency is strongly dependent from the source location for both matrix configurations. The restricted available time didn't allow to try other intermediate source location but isn't worth noting that the slopes of the curves (all concrete and concrete plus polyethylene) differ less than 5 %.

2.2.4.3.3 Hydrogen content sensitivity

Figure 2.2.10 shows the behaviour of the total neutrons detected during the active measurements: the values obtained seem to demonstrate that when uranium is near to a more concentrated cluster of polyethylene dummies (^{238}U source in position C8), that there is a not negligible difference, almost equal to 20 %, between the measured values with and without polyethylene. The other locations of ^{238}U source are practically not affected by the presence of polyethylene (the differences between the measured values with and without polyethylene are less than 5 %).

2.2.4.4 MCNP simulations

In order to validate the measurements carried out in CEA Saclay and to extend the results to other real situations has been carried out a series of Monte Carlo simulations using the MCNP4A code [3]. The description of both the algorithm and the simulation procedure are given in [4].

2.2.4.4.1 MCNP determination of MDA

The MDA assessed applying the algorithm developed at ENEA was 1.456 ± 0.052 g of uranium: about 8 % less than the experimental value. This value is lower than the experimental and can be due to the fact that MCNP doesn't take into account dead time corrections and statistical fluctuation of the detection efficiency and electronic chain unevenness.

The good agreement between the experimental measurements and the code leads to a positive validation of the code itself, at least in terms of overall algorithm for MDA calculations.

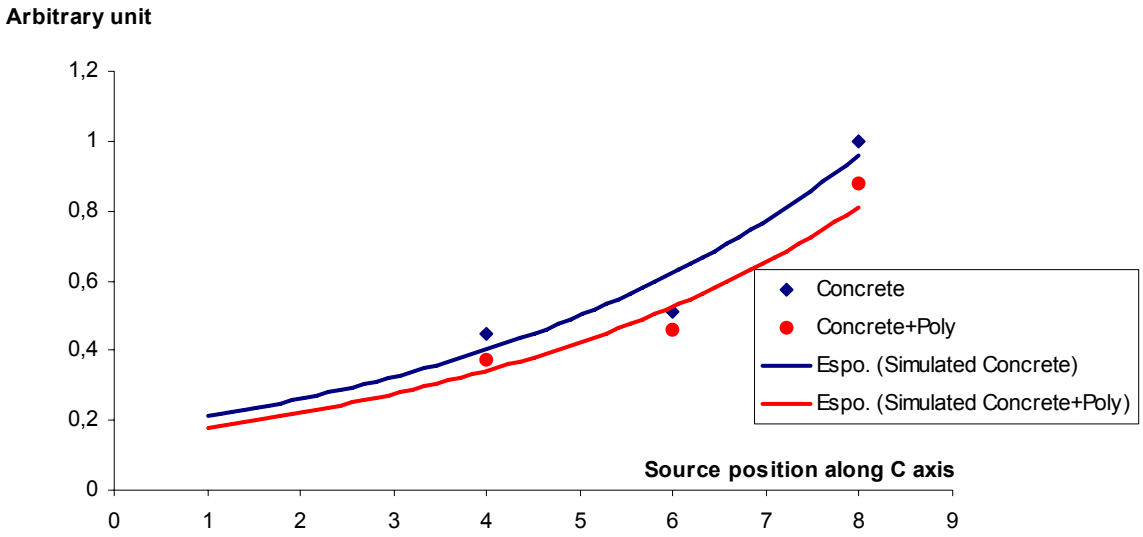

Figure 2.2.9 Passive measurements; system detection efficiency as function of the ^{252}Cf source position.

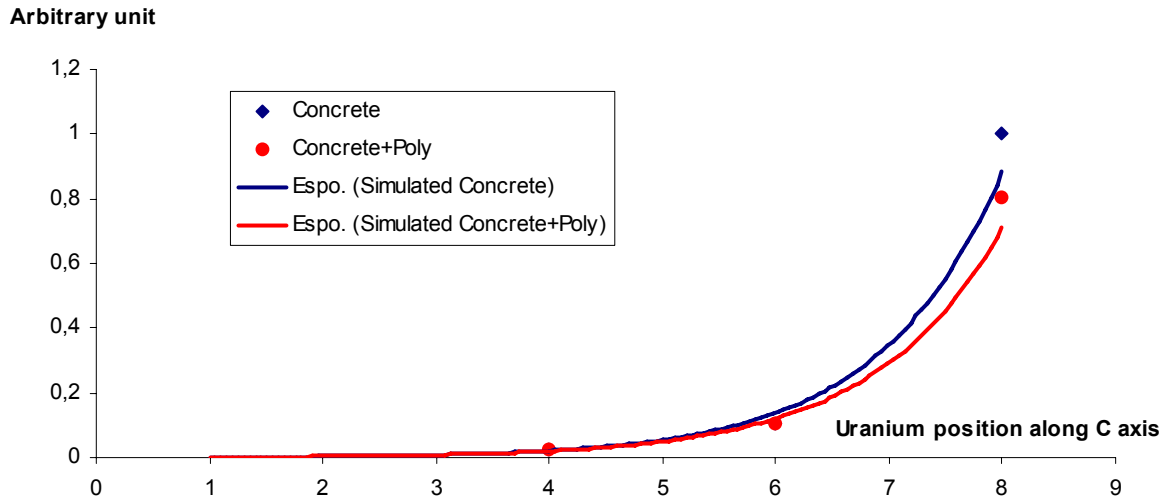

Figure 2.2.10 Active measurements; system detection efficiency as function of the ^{238}U source position including corrections for background.

2.2.4.4.2 Source position and hydrogen content sensitivity

To validate the code with respect to the source location effect and to the hydrogen content, the simulations were carried out inserting subsequently the ^{238}U source in all the holes of column C except C3 and C7 (see Figure 2.2.8), in both matrix configuration (all concrete cylinders and concrete plus polyethylene cylinders). The results are visualized in Figures 2.2.9 and 2.2.10.

Regarding the detection efficiency, the curve obtained by MCNP code is a good approximation of the behaviour of the experimental points: the difference is about 10 % higher for concrete and about 12 % for the concrete plus polyethylene configuration.

Looking at the totals for detection and prediction, and the curve obtained by the MCNP code, the approximation of the behaviour of the experimental points is quite good: the highest difference is about 8 % for concrete and 9 % for concrete plus polyethylene configuration.

2.2.4.4.3 Conclusions

The results show unfortunately a lack of experimental checks, but still lead to an acceptable validation of the code for both purposes, MDA calculation and localization effects, especially taking into account the dimension of the mock-up and the high grade of uncertainties involved.

2.2.5 Conclusions

The reported results show that suitable non-destructive techniques and procedures to control and characterize fissile material (actinides) present inside large-volume radioactive waste packages can be set up with the aid of a Mini Linatron electron accelerator. Photo-fission reactions produced in the large-volume waste package by the intense emitted Bremsstrahlung by the Mini Linatron are the most important reactions to detect eventually present fissile material. This high neutron intensity produced by such a machine is expected to be sufficient for neutron interrogation of large-volume waste packages.

It will be a necessity to perform neutron and photon dose rates calculations by MCNP to establish the most advantageous location of neutron and photon experimental setups to avoid (to minimize) radiation background effect on ^{3}H neutron counters that has to will deal with.
Research has shown that MCNP calculations can be used for MDA calculation and localization effects. It is evident, that models applied have to have a certain amount of details to be gain sufficient accuracy.

The results of a specific nuclear non-destructive measurements campaign on large concrete inactive package by using photons and neutrons produced by Mini Linatron as interrogating particles at ^{238}U established detection limits of 225g, 82g and 12g for respectively the centre (depth of 70 cm), the intermediate position (depth of 54 cm) and at the exenterate position (depth of 38 cm) of the concrete mock-up.

2.3 NDA characterisation of non-fissile material in large-volume waste packages

2.3.1 Introduction

In this section the performed research and development of non-destructive radiological characterization techniques for the non-fissile content in large-volumetric waste is described [5]. The objectives concerning this part of the project are defined as:

- Development of mobile NDA equipment and procedures for the non-destructive QA/QC characterization of the non-fissile content with special attention to source localisation.
- Validation of developed equipment and procedures for non-fissile radioactive large-volume waste.

These two objectives are reached by:

- Development of an “open/collimated NDA gamma system” able to measure 3 dimensional large-volume waste packages. This NDA system is classified as a *point-to-point-scanning-system* (PTP-system). The second system is a “3-dimensional NDA

image/cartography scan system for emitted photons that can be detected through the outline of a waste form" and is classified as a *3-dimensional automated scanning system* (3DAS system).

Figure 2.3.1 Heat exchanger

Figure 2.3.2 Concrete box and part of heat exchanger inside the testing area of the Olkiluoto NPP.

Figure 2.3.3 Waste bale inside the testing area of the Olkiluoto NPP.

Figure 2.3.4 The ISO container loaded with seventy 220 l drums on the transport platform at the WQCL site.

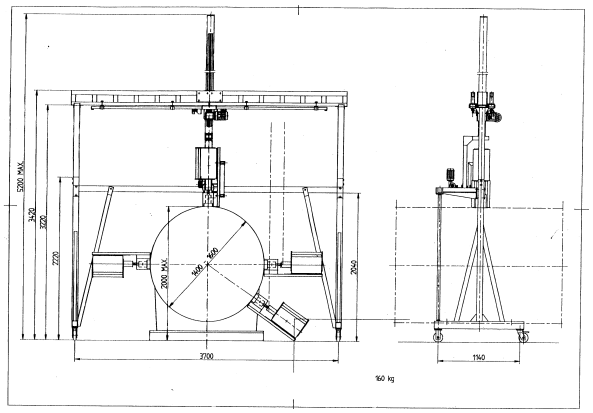

Figure 2.3.5 Left: technical drawing of the PTP system (dimensions in mm) – four different detector positions around a cylindrical object are indicated. The right-hand picture shows the PTP system during operation

    - Both systems are based on different measurement philosophies and are developed to operate under severe physical and radiological conditions.
    - Both systems are able to provide information for the assessment of locations with elevated or decreased radiation levels and nuclide specific activities.
    - Both systems are also mobile so that they can be transported to the site of the large waste component to be measured.
- Applying software tools to image scan results. These tools are developed in such a way that they can be used for the assessment of source locations with elevated radiation levels of non-fissile as well as from fissile material by NDA active and passive neutron detection systems as well for localization of areas with significant decreased radiation levels.
- Performing MCNP sensitivity simulations on important parameters like matrix effects:
    - To help/assist and to justify hardware and software developments
    - To test developed NDA-systems.
    - To verify image results and
    - To verify and to assist in activity calibrations.
- Validation of developed NDA-systems and procedures by means of two *in situ* validation experiments.

2.3.2 Selected large-volume waste packages for the *in situ* validation experiments

At the kick-off meeting of the project global definitions were set up, which large-volume waste packages have to fulfil. This global definition is mainly dealing with the volume of the waste package (at least 600 l) and secondary with the geometry in order not to be restricted in the selection. It is also evident that due to the fact that the NDA systems have to be transported, the site must have adequate provisions for hosting and testing areas for performing the *in situ* validation experiments.

The Olkiluoto NPP in Finland offered the possibility to investigate the following large waste packages:

- Heat exchanger; dimensions length 5.7 m, diameter 1.4 m, volume 8.7 m^3, mass 13100 kg (see Figure 2.3.1).
- Concrete box; dimensions side 2.7 m, height 1.0 m, volume 5.9 m^3, mass 8180 kg. This box contains radioactive and contaminated metal scrap (see Figure 2.3.2).
- Bale of soft waste; dimensions length 0.9 m, width 1.1 m, height 0.8 m, volume 0.75 m^3, mass 290 kg (see Figure 2.3.3).

The Waste Quality Checking Laboratory (WQCL) at United Kingdom offered an ISO sea-transport container loaded with seventy 220 l low-level waste drums, which are all radiological characterized according UK-regulations (see Figure 2.3.4). Dimensions -container length 6 m, width 2.5 m, height 2.5 m; load seventy 220 l drums, total weight of the radioactive waste 8388 kg, total activity 78.3 MBq of which ^{60}Co contributes with 41.1 MBq and ^{137}Cs with 5.08 MBq. In Annex 1 the actual loading scheme of the ISO-container is given.

2.3.3 Point-to-point scanning system (PTP system)

2.3.3.1 Design

The first mobile detector frame has been constructed by VTT and is specially designed for point-to-point scanning (PTP-system) and quantification of the activity of large horizontally lying cylindrical items (e.g. horizontal/vertical cylindrical, squares with or without folds) using a

collimated high purity germanium detector (HPGe). This PTP-system has to be operated manually. The number of spots varies per item, but a grid of 30 cm x 20 cm can be used for an item of dimensions of a few metres. In Figure 2.3.5 the technical drawing of the system and the system during a measurement campaign is presented.

2.3.3.2 First in situ validation experiment

2.3.3.2.1 Objectives and set-up

The aims of the first *in situ* validation test for the developed PTP-system are:

1. The set-up of procedures that makes full advantage of the properties of the PTP-system.
2. Testing of the PTP-system under real measuring conditions and to investigate if the developed hardware meets the requirements.
3. Testing of developed NDA PTP-assay-technique and procedures.

Three series of experiments had been set up for testing the developed PTP-system and validating the procedures. The first series of experiments at the Olkiluoto NPP was dealing with the radiological characterization of a heat exchanger, the second series with the characterization of a concrete box filled with radioactive scrap metal and the last series is dealing with a soft bale (see Section 2.3.1 for specifications of the large waste items).

2.3.3.2.2 Experimental and specific activity calculation procedures

Based on the existing experience of VTT, the following experimental procedure for the radiological characterization of large waste packages has been set up:

- Define and note the aim of the characterization including special remarks if needed, like detection limits of nuclides, total effort in man-hours, the minimum effort to spend in one complete measurement.
- Study the technical specifications of the large waste item especially the local changes of internal structures, densities and matrices.
- Assay the detector efficiency for the large waste item to investigate taking into account source-detector-distance and detector collimation if necessarily.
- Assay the minimum spectrum measurement live time to be able to reach required nuclide specific detection limits.
- Calculate the number of spectra (data points) that can be collected taking into account the total minimum effort to spend at measuring.
- Define the measurement grid, e.g. rectangular or triangular, and note the detector locations in a table.
- Assembly the PTP-system.
- Transport the PTP-system to a measurement location.
- Check if the free space around the PTP-system is sufficient especially the height has to be checked, note limiting parameters.
- Put on the main power of the PTP-system.
- Control the correct working of the electrical and manual detector adjustment systems of the PTP-system and the correct working of the gamma spectroscopy system.
- Adjust the gamma spectroscopy detector at the first data point to collect.
- Start the first data collection.

The procedure to assay the activity of the large waste item under investigation is:

- Select the most suitable detector efficiency curve (ε).

- Analyse the recorded gamma spectra with the aid of an appropriate gamma spectroscopy programme to report net counts of nuclides like ^{137}Cs and ^{60}Co.
- Create an image e.g. an iso-plot of a selected nuclide.
- Calculation procedure 1 applied for the heat exchanger:
  - Assess the activity components P_i calculated by MCNP simulation using formulas (9) and (12) of reference [5].
  - Calculate the nuclide specific activity of the waste package by summing the components as in equation (11) of reference [5].
  - Calculate the total activity by summing the activities of individual radionuclides.
- Calculation procedure 2 applied for the concrete box and soft bale:
  - Calculate the nuclide specific activity of the waste package using equations (10) and (13) of reference [5].
  - Calculate the total activity of waste package by summing the activities of individual radionuclides.
- Note the results of the reported nuclide specific activities and minimum detectable activities of important nuclides.

The collected PTP-data can be used to create an iso-plot for each nuclide. In these cases the data have to be accompanied with the measurement location at the large waste item.

To obtain suitable detector efficiency curves two possibilities exist. Efficiency curves can be obtained first by measuring or second by calculation. The second option is the preferable and more flexible one. This is due to the fact that the creation of an experimental calibration for one unique large waste item is costly and it creates additional waste.

A tool that is able to calculate with a sufficient accuracy such detector efficiency curves is MCNP.

2.3.3.2.3 MCNP simulations

The efficiency calibration for the contaminated heat exchanger was calculated using MCNP version 4C. The efficiency in this calibration can be defined as the number of particles emerging from the source and depositing essentially all their energy into the detector crystal. This corresponds to a complete photon interaction and charge collection in the detector crystal, i.e. contribution to a photo peak in a gamma spectrum.

The heat exchanger is modelled as a thick-walled steel cylinder containing a coaxial air cylinder of thickness equivalent to the spacing between the steel blanket and the pipe structure. The inner part of the heat exchanger, here considered as a large-diameter cylinder, is formed from 1600 U-shaped tubes, which have the contamination on their outer surfaces, and on support structures. The geometry formed by the heat exchanger tube structure is so complicated that it cannot be included in the simulations without some simplification. It was considered practical to homogenise the heat exchanger tubes and support structures into a mixture of iron-air with the density 1800 kg/m^3 and to specify the source as an equivalent homogenous volume source, see Figure 2.3.6.

MCNP simulations were performed for a real collimated detector and four different source descriptions, point source on tube batch surface (position z = 280), linear source on tube batch surface (position from z = 146 to z = 352), surface source on tube batch surface (position from z = 146 to z = 414) and volume source were used. All simulations were done for ^{60}Co. The results can be seen in Figure 2.3.7 for a longitudinal profile and in Figure 2.3.8 for an azimuthal profile of the heat exchanger.

2.3.3.2.4 Results

2.3.3.2.4.1 Heat exchanger

The surface dose rate of the heat exchanger was generally quite low about, 1 μSv/h, and the only nuclide found in normal five-minute gamma-spectrometric measurements was ^{60}Co. The ^{60}Co count rate was in some locations under the heat exchanger ten times higher than aside and above the heat exchanger – see Figure 2.3.9.

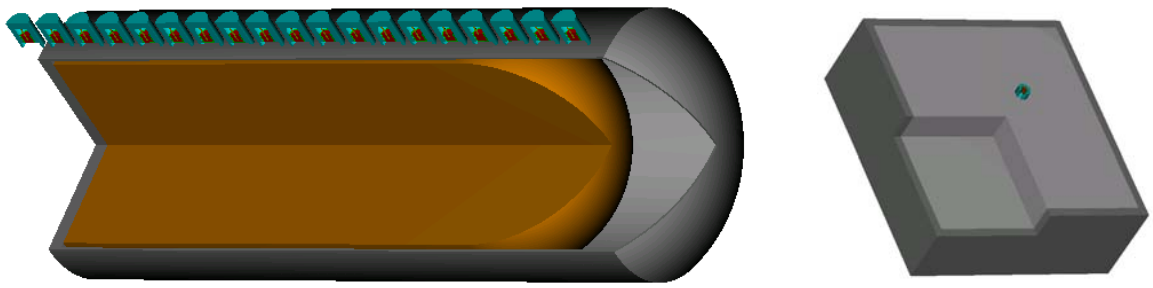

Figure 2.3.6 Visualisation of the MCNP simulation calibration geometry of the heat exchanger and of the concrete box filled with radioactive metal scrap.

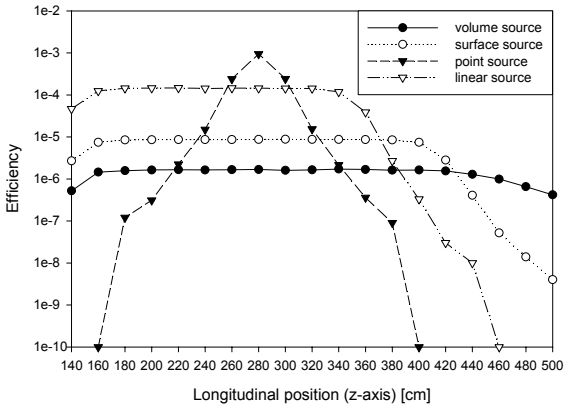

Figure 2.3.7 Calculated longitudinal efficiency profiles of ^{60}Co (1332.5 keV) in the heat exchanger.

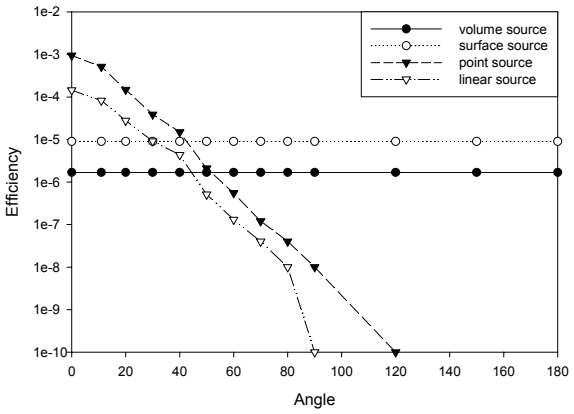

Figure 2.3.8 Calculated azimuthal efficiency profiles of ^{60}Co (1332.5 keV) in the heat exchanger.

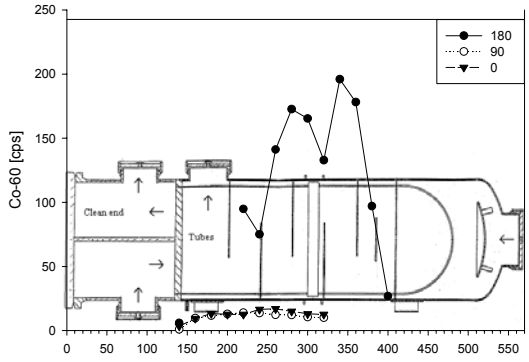

Figure 2.3.9 Count rate distribution of ^{60}Co under (φ = 180°), aside (φ = 90°) and above (φ = 0°) the heat exchanger.

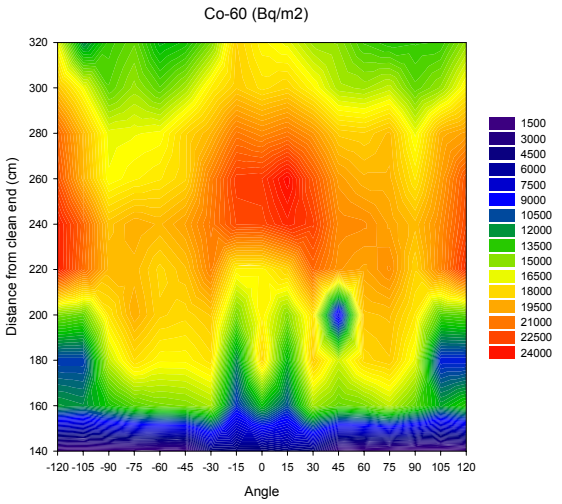

Figure 2.3.10 The measured ^{60}Co activity map of the heat exchanger by applying the volume source model calibration.

The cross-sectional view of the heat exchanger shows the correlation between the internal structures and the count rate profile measured from below. The count rate at the clean end (below

Z = 140 cm) is very low and also at the bottom. In two points (Z = 240 and 320 cm) the count rate drops seem to be due to internal walls in the heat exchanger.

The overall distribution of the activity of the bottom seems linear and to be limited between 140 cm < Z < 400 cm, with a total activity of about 1.4 MBq. The starting point coincides with the wall between the clean and contaminated zones and the ending point with the last support plate of the heat exchanger tubing.

The activity distribution of ^{60}Co obtained using the volume source model calibration can be seen in Figure 2.3.10. In the highest point the activity of the tubes were calculated to be about 30 kBq/m^2. One can see that the activity is higher above the heat exchanger, lower aside and higher again closer to the bottom.

The ^{60}Co activity for the heat exchanger is assessed at 6.2 ± 3 MBq and is based on the measurements in the area of 140-320 cm with data extrapolation for unmeasured surfaces taking into account the experimental results of the 3DAS-system.

2.3.3.2.4.2 Concrete box filled with radioactive metal scrap

The second target, the concrete box containing metal scrap, was measured above the centre of the box. The measurement time was 30 min and an extra collimator was used in order to suppress the dead time. The surface dose rate was quite high at the top surface of the full package, up to 2.6 mSv/h (see Figure 2.3.11 for the surface dose rate iso-plot). In the full box measurement the following nuclides were detected: ^{60}Co, ^{54}Mn, ^{58}Co and ^{124}Sb. The system dead time was 80 % and was caused by the high photon flux with ^{60}Co as the principal nuclide.

Table 2.3.1 displays the result of the PTP measurement using the calculated calibration efficiency and the TVO measurement done earlier. The discrepancy of those two measured activity inventories can be attributed to strict collimation due to high dead time of the PTP system.

Figure 2.3.11 shows that the activity of the box is peaked outside the centre of the box, which was under measurement. From this data it can be estimated that in the VTT measurement there is a bias of at least 20 %. However, even this obvious bias cannot fully explain the difference between the VTT and TVO measurements.

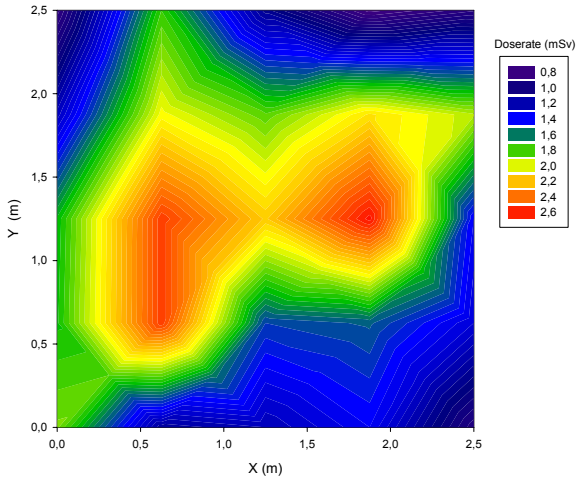

Figure 2.3.11 Surface dose rate iso-plot of the concrete box filled with radioactive scrap metal.

Table 2.3.1 Calculated ^{60}Co activity in the concrete box filled with metal scrap.

Nuclide	Activity GBq/box	
	TVO	VTT
^{60}Co	11.0	3.2

2.3.3.2.4.3 Soft bale

The third target, a bale of soft waste was measured at four sides. The measurement time was 30 minutes. The bale allowed also the determination of the matrix attenuation correction by a transmission measurement using a large-area transmission source. Table 2.3.2 displays the activity measured by TVO and by the VTT measurements on each of the four sides. During the TVO measurement the bale is rotated around the vertical axis to average out inhomogeneities and TVO uses a homogeneous reference plastic bale for calibration of their measurements.

The differences in the results of the VTT measurements reflect the true inhomogeneity of the bale. In general the activity inventories obtained are in a fair agreement with the value measured by Olkiluoto NPP.

Table 2.3.2 Comparison of the activity results obtained by TVO and VTT for the soft bale

	Activity Bq/bale					
Nuclide	**TVO**	**VTT side1**	**VTT side 2**	**VTT side 3**	**VTT side 4**	**VTT average**
^{58}Co	< 1.50E+04					
^{60}Co	7.23E+05	7.24E+05	4.78E+05	7.67E+05	2.52E+06	5.55E+05
^{137}Cs	9.77E+04	3.50E+04	2.72E+04	4.71E+04	1.27E+04	5.90E+04
^{54}Mn	4.21E+04	2.65E+04	1.76E+04	2.44E+04	1.06E+04	1.98E+04
^{95}Nb	1.36E+04					

For real waste packages the above conditions (uniform distribution of activity and matrix) are only fulfilled in rare cases. The method of attenuation correction is based on simple and fast transmission measurements through the object with an external transmission source.

2.3.3.2.5 Conclusions

The developed mobile detector frame to perform series of point measurements (*PTP system*) has fulfilled its expectations. The following conclusions can be made concerning the *PTP system*:

- Hardware: The system is designed for a collimated HPGe detector. This means that other detectors like NaI(Tl) or CdZnTe cannot be applied directly, but is possible after minor hardware modifications. The mobility of the system is good, dismantling and assembling to full operation is possible by 2 persons within 4 hours.
- Software: The applied commercial gamma spectroscopic software fulfils the requirements no special adoptions are needed. For imaging commercial software, like Microsoft Excel or SigmaPlot of SPSS Inc., has been applied and for this relative simple visualization application they fulfil the requirements.
- Procedures: The procedural set up by VTT to characterize large-volume waste packages fulfils the requirements, but is time consuming (about 7 days with 2 persons for a 100 % check of the heat exchanger [3]), and it has to be improved in user-friendliness to prevent errors. Further investigations are needed to establish a good procedure for the calibration efficiency (MCNP-simulation) with the main aim to improve the accuracy, while assuming homogeneity gives already in most cases reasonable results.
- Analysis results and accuracy: The analysed results and the accuracy “standard deviation of 50 %” are reasonable, taking into account the difficulties to establish good accurate calibration efficiency.

2.3.4 3-dimensional automated scanning system (3DAS system)

2.3.4.1 3DAS system design

The second mobile detector frame – see Figure 2.3.12 – has been developed at NRG and is called *3D Rise*, acronym for "3-dimensional radiation inspection equipment". It can be classified as a 3-dimensional automated scanning system (3DAS). The 3D Rise system is based on open detection of radiation, meaning that applied detectors and monitors are not shielded or not collimated.

The 3D Rise system can easily be equipped with a number of different detectors, like for:

- Detecting gamma photons as function of their energy with detectors like HPGe, NaI(Tl) and CdZnTe.
- Dose rate.
- Contamination.
- Neutron detectors or monitors.

These detectors and monitors have to be remotely controlled and have to be able to store collected data directly into a PC.

All detectors and monitors will be continuously moved during data collection (scanning). This means that the number of data points depends on the measurement sample frequency of the instrument. The sample frequency is normally adjusted between 1 and 25 s, resulting in a data amount between 1000 and 200 measurements for a 4 m^2 net scanning area, or expressed as one data point per 0.004-0.02 m^2.

2.3.4.2 Imaging and visualization of results

2.3.4.2.1 Imaging and visualization techniques applied with the 3DAS system

In literature a large number of graphical representations of data are reported and applied to present experimental results. Examples of data presentations are: text, bar graphs, scatter-plots, iso-plots etc. The following statement is therefore justified:

> *There exists no single general presentation technique that is always able to show unambiguous all information that is present but hidden in a data-set.*

It is evident that the selection of an existing presentation technique or the development of a new technique is strongly related to the information to be presented out of a data-set and has thus to fulfil a pre-defined aim. The data-set can be either measurements or calculations or gained in any other way. The aim that can be defined for the presentation technique to be applied by the non-destructive characterization of radioactive waste packages is:

> *The presentation technique to present radiological NDA characterization data has **to assist** operators in the interpretation of NDA waste characterization data so that a conclusion can be drawn that the characterized waste package is in accordance with the specified requirements.*

The operator, characterization specialist, waste producer but also governmental agencies can specify these requirements.

NRG has put R&D effort in searching *for a set* of analysing techniques in combination with presentations techniques that are able to show as much information as possible and that can be

applied in routine. This R&D effort has lead to the important conclusion: that presentation of *only* net quantitative data will never give a straight objective answer on the question:

Does the investigated radioactive waste package unambiguously fulfil the defined requirements?

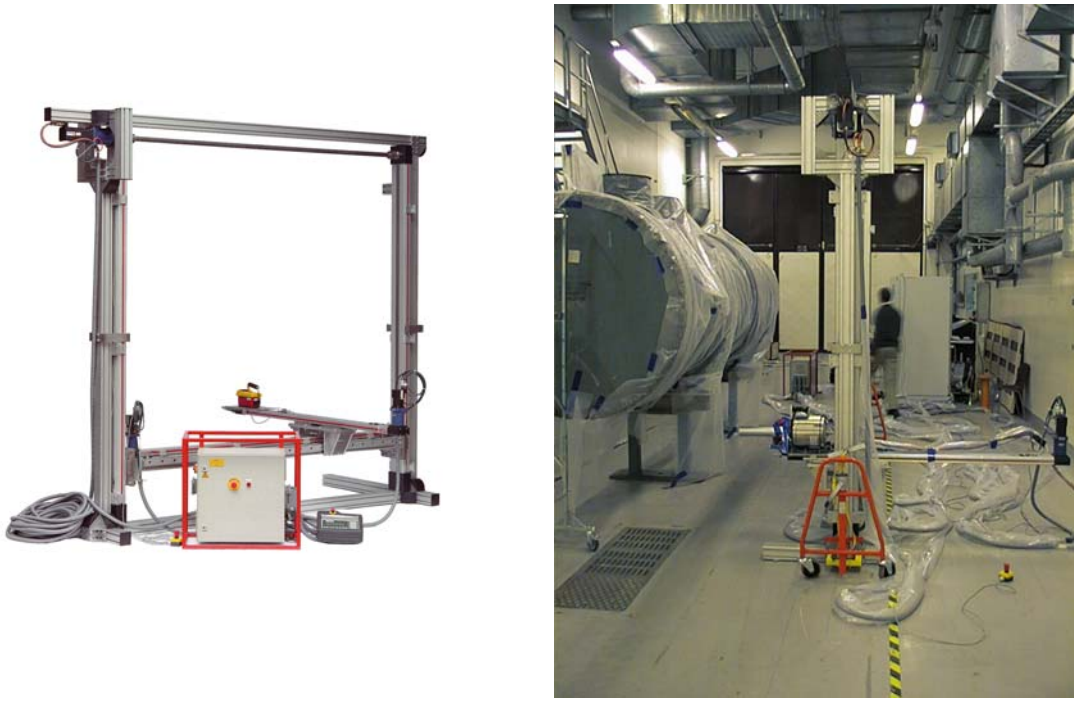

Figure 2.3.12 3*D Rise* system. Detector frame for 3-dimensional automatic scanning of large-volume radioactive waste packages developed by NRG including the cabinet with the process electronics and the EPIS controller to operate remotely the system (left-hand picture) and in operation during the measurement campaign at the Olkiluoto NPP (right-hand picture)

Table 2.3.3 Explanation of the colour bar for the interpretation of the iso-plots of the 3D Rise system

Colour	Meaning of colour bar in net data iso-plots [Based on the range of net collected data]	Meaning of colour bar in statistically[1] filtered net data iso-plots [Based on the statistical distribution of net data-set]	
Red	Net data value > 95 %	Net data value > (Average + $2\sigma_{population}$)	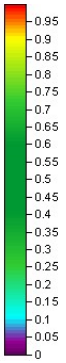
Yellow	85 % < Net data value < 95 %	(Average + $1\sigma_{population}$) < Net data value < (Average + $2\sigma_{population}$)	
Green	10 % < Net data value < 90%	(Average -$1\sigma_{population}$) < Net data value < (Average + $1\sigma_{population}$)	
Light blue	5 % < Net data < 15 %	(Average - $2\sigma_{population}$) < Net data value < (Average - $1\sigma_{population}$)	
Purple	Net data value < 5 %	Net data value < (Average - $2\sigma_{population}$)	

([1]) By the statistical filtering of the net data-set the type of statistical distribution and rejected outlier's are taken into account. This will result in the calculation of a unique average and standard deviation that describes the remaining data-set.

To obtain an objective answer as much as possible on the above question, the development of a filtering technique based on existing statistics had been started.

The aim of this statistical filtering technique is that the output has to give an objective and an unambiguous answer that **in** the collected NDA data-set no data is present that differs significantly e.g. on a confidence level of 2. This means that when all data is below this confidence level, the conclusion can be drawn that the waste package fulfils the specified requirements.

At this moment the following graphical presentations of a NDA data-set have been selected to report of each data-set measured by the 3DAS system:

- *Iso-plot of the net data-set*. The aim of this iso-plot is that the variations of the quantitative value in the net data-set can be observed and to assist by the conclusion if the quantitative values fulfil the defined requirements.
- *Iso-plot of the statistically filtered net data-set.* The aim of this iso-plot is that statistically significant deviations in the net data-set (positive and negative) can be observed and to assist in the conclusion that all significant levels fulfil the defined requirements.
- *Fractional plots of the net data-set.* The aim of these fractional plots is to observe if correlations and patterns are present in the quantitative data-set. Each individual fractional plot (one out of twenty) represents the data points in 5 % of the quantitative range of the data-set. E.g. the top left fractional plot contains the data points between 0 and 5 %; the second between 5 and 10 %, etc. Patterns give indications of the presence of unexpected radioactive sources, which may lead to miscalculation of the activity. Examples of correlations are: data points forming lines, clustering of data points, empty regions etc.
- *Fractional plots of statistically filtered net data*. The aim of these fractional plots is to observe if in the statistically filtered data-set correlations and patterns are present. Each individual fractional plot has to contain about 5 % of all data points. Patterns give

indications of the presence of unexpected radioactive sources and leading to a possible miscalculation of the activity.

To simplify the interpretation of the iso-plots of the "net data-set" and "statically filtered data-set" only colour bar has been applied to all iso-plots, see Table 2.1 for more details.

In Figures 2.3.15 and 2.3.16 (see Section 2.3.4.3.1.4.3) examples of iso-plots and fractional plots of *two net quantitative data-sets and two statistically filtered data-set* of the same waste item (heat exchanger) are presented as examples.

2.3.4.2.2 Tomographic imaging of large-volume waste

Analytical reconstruction methods for solving transmission tomography problems are fast, and well adapted to handle huge number of data (i.e. over-sampling and 3D tomography). However, these methods are the original basic of multiple artefact creation and provide a poor image quality when acquisition does not respect the principle of the inverse Fourier formula.

The main advantage of using algebraic methods by calculating images from projection is the capacity they provide for inverting the physical projection operator including detector response, and geometric dispositions (pre and post collimators). However, since the reconstruction problem is ill-posed, it is necessary to regularise this reconstruction. Several methods of regularisation can be applied, depending on the problems that have to be processed. Possible methods of regularisation include positivity, image-depending smoothness assumption (such as edge preservation smoother) and object support.

In this section an algebraic regularised method is proposed that deals with the problem of simultaneous penalising negative voxels, noise processing and missing data. This last problem can be due to a limited angle of view, or more simply the need of reducing the data that is directly proportional to the total acquisition time.
No attempt was made to correct for the spatial energy and angular dependency of the X-ray photon beam. Further, it is assumed that the transmission kernel can be viewed as a mathematical line.

Specific application of this method can be made to helical 3D- reconstruction over more classical waste, and more specifically, to an object containing sharp edges that have the bad habit to generate reconstruction artefacts.

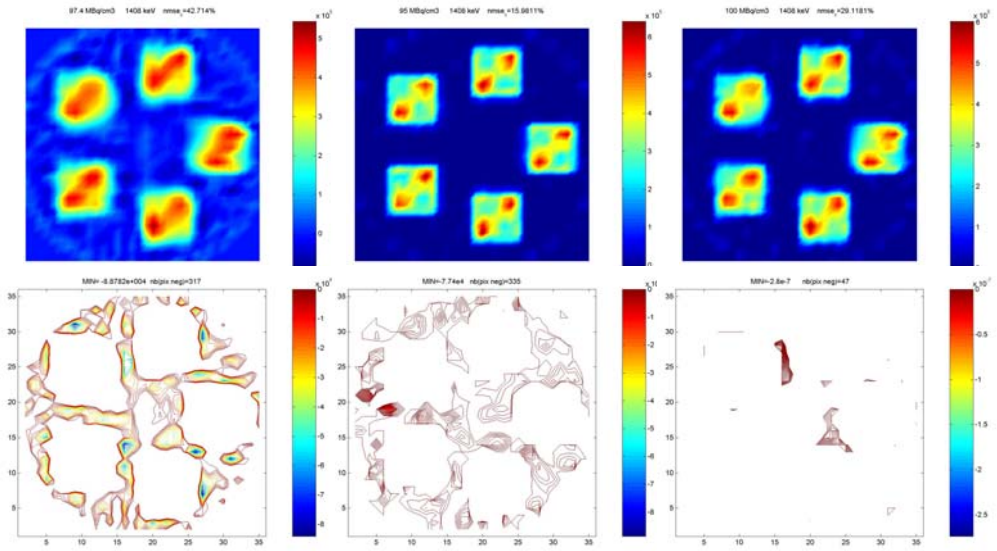

Figure 2.3.13 Effect of the positive-constraint on the image and negative pixels. Top-row: from left to the right: a) without constraint (CG-method); b) MAP-CG-HQ[1] $\beta_{pos} = 10^2$; c) MAP-CG-HQ $\beta_{pos} = 10^4$. Bottom row: location of negative pixels.

To handle simultaneously negative voxels, noise and missing data, and more generally to regularize the ill-posed problem, the following criterion [6] is proposed combining the corresponding constraints:

$$E(\mu) = \|H\mu - m\|^2 \quad \leftarrow \text{data consistency}$$
$$+ \beta_{noi} \sum_i \varphi_{noi}\left(\frac{\nabla \mu_i}{\delta_{noi}}\right) \leftarrow \text{noise processing}$$
$$+ \beta_{pos} \sum_i \varphi_{pos}(\mu_i) \leftarrow \text{positiveness}$$
$$+ \beta_{\text{sup}} \sum_i \varphi_{\text{sup}}\left(\frac{\mu_i}{\delta_{\text{sup}}}\right) \wp(\mu_i) \leftarrow \text{missing data}$$

The defined algorithm is called MAP-CG-HQ (Maximum a Posterior-Conjugate-Gradient-Half-Quadratic). The choice of the hyper-parameters βs and δs are of course crucial for the image quality. Estimation techniques do exist, but they are generally time consuming and remain tools for research laboratory. They are not fitted in applications for standard use and a more simple heuristic choice is proposed to deal with this problem.

In Figure 2.3.13 an example is presented of the effect of the positive-constraint on the image and the amount of negative pixels.

[1] MAP-CG-HQ stands for "Maximum a posteriori Gradient Conjugate Half Quadratic" – the name of the proposed regularised method.

2.3.4.3 In situ validation experiments

2.3.4.3.1 First *in situ* validation experiment

2.3.4.3.1.1 Objectives and set-up

The aims of the first *in situ* validation test for the developed 3DAS-system are:

1. The set-up of procedures that makes full advantage of the properties of the 3DAS-system.
2. Testing of the 3DAS-system under real measuring conditions and to investigate if the developed hardware meets the requirements.
3. Testing of developed NDA 3DAS scan-technique and procedures.

Three series of experiments have been set up at the Olkiluoto NPP for fulfilling the above aims. The first series of experiments had been set up for defining the detail set-up for two different continuous NDA scanning techniques, which are referred further in this report to as "slow" and "fast" scans. The experiments were at first carried out with a 5x4 inch NaI(Tl)-detector instead with the special HPGe-detector with extended end cap. This was to prevent that the HPGe-detector could accidentally be demolished during the tests.
After the specifications of the "slow" and "fast" scan procedures were set, they were tested in the second series of experiments as first under relative *simple* conditions during the radiological characterizing of the concrete box filled with radioactive scrap and secondary at an empty concrete box with a small radioactive source mounted at the outer wall of the box to simulate a contamination. Under *simple* conditions is meant the continuous movement of the detector in straight planes, while the radiological conditions were rather severe with dose rate levels up to 2.6 mSv/h.

The third and final test series of experiments had the aim to gain information about all aspects (hardware, software and procedures) of the developed 3DAS-system under real measuring conditions in routine. Therefore the goal was set to characterize 50 % (one complete side) of the heat exchanger with the defined "slow" and "fast" scan-procedure.

As this final test is of the highest interest, the test will be reported in detail and the former tests more generally.

2.3.4.3.1.2 Experimental and specific calculation procedures

Based on the experimental system testing at NRG and on the first serial of the *in situ* validation tests the following experimental procedure has been set up. This procedure as well as the procedure to prepare the data for the iso-contour and fractional plots have been described in detail in the topical report "Non-destructive assessment techniques of non-fissile radioactive material in large-volume waste packages by detection of emitted photons [5]. This procedure contains the following main items:

- General; registration of the waste package and the characterization test(s) to perform.
- Assembling of the 3DAS-system and adjusting the system next to large waste package and note limiting distances.
- Check the correct working of the mechanical system [7] e.g. reference position, automatic distance control, stability etc. and initialise the scan-parameters.
- Check the correct working of applied detectors and radiological monitors, e.g. HPGe-detector, dose rate etc., and initialise their data collecting sequence.
- Collection of radiological data.
- Data treatment to obtain *net-data* and *statistical* iso-contour and fractional plots.
- Procedure to assay the activity of the large waste package.

The procedure to assay the specific activity of the large waste item under investigation is:

- Select the most suitable detector efficiency curve (ε).
- Create a statistically filtered iso-plot of a selected nuclide e.g. ^{60}Co.
  - Assess the percentage of the surface ($P_{Surface\ i}$) of the waste package that has the following specific count rate:
    - $P_{Surface1}$: Greater then "Mean + 3* standard deviation".
    - $P_{Surface2}$: Between "Mean + 2* standard deviation and "Mean + 3* standard deviation".
    - $P_{Surface3}$: Between "Mean + 1* standard deviation" and "Mean + 2* standard deviation".
    - $P_{Surface4}$: Between "Mean + 1* standard deviation" and "Mean – 1* standard deviation".
    - $P_{Surface5}$: Between "Mean – 2* standard deviation" and "Mean – 1* standard deviation".
    - $P_{Surface6}$: Between "Mean – 3* standard deviation" and "Mean – 2* standard deviation".
    - $P_{Surface7}$: Less then "Mean – 3* standard deviation".
  - Calculate the average net count rate for the surfaces 1 to 7 for e.g. ^{60}Co as follows:
    - $N_{PSurface1}$: "Mean + 3.5* standard deviation".
    - $N_{Psurface2}$: "Mean + 2.5* standard deviation".
    - $N_{Psurface3}$: "Mean + 1.5* standard deviation".
    - $N_{Psurface4}$: "Mean".
    - $N_{Psurface5}$: "Mean – 1.5* standard deviation".
    - $N_{Psurface6}$: "Mean – 2.5* standard deviation".
    - $N_{Psurface7}$: "Mean – 3.5* standard deviation".
  - Calculate the nuclide specific activity of the waste package with:

$$A_{Co\text{-}60} = \Sigma \left(P_{Surface\ i} * \varepsilon_{Co\text{-}60} * N_{PSurface\ i;\ Co\text{-}60}\right)$$

$$A_{Waste\ Package} = \Sigma\ A_{All\ nuclides}$$

- Note the results of the reported nuclide specific activities and minimum detectable activities of important nuclides.

2.3.4.3.1.3 Results

2.3.4.3.1.3.1 Concrete box filled with radioactive metal scrap

The concrete box made available by the Olkiluoto NPP was filled with contaminated scrap metal. The dose rate at the top surface was between 0.8 and 2.6 mSv/h. It is evident that a non-collimated HPGe-detector will have 100 % dead time and is useless in this tough environment. Therefore the HPGe-detector was replaced by a non-collimated CdZnTe-detector (5.00 mm^3). CdZnTe-detector belongs also to the group of semiconductor-detectors, but can be operated at room temperature. The advantage of the CdZnTe-detector is that due to its small dimensions the detector can be applied directly in high radiation fields without any collimator. A disadvantage is the poorer energy resolution and peak-to-compton ratio in comparison with a HPGe-detector.

About 40 % of the upper surface of the concrete box has been scanned by the 3DAS-system in the slow and fast scanning mode. The localization of ^{60}Co by both scanning modes is in good agreement with results reported by the PTP-system (see Section 2.3.2.2.4.2). However, no assessment of the specific activity ^{60}Co has been performed due to the fact that not the complete surface of the box has been measured.

It has to be noted that the non-collimated CdZnTe-detector could easily handle the dose rate of 2.6 mSv/h and that recorded spectra contains good qualitative information about the specific nuclides responsible for the high dose rates.

2.3.4.3.1.3.2 Contamination experiment

A small closed source of NORM material (emitting beta particles and gamma photons) was fixed at the sidewall (position X = 1300 and Y = 500) of an empty concrete box and a to create an elevated radiation level a large-area ^{60}Co and ^{152}Eu transmission source was placed beneath the concrete box.

The applied contamination monitor was the dose rate monitor Inovision 451B. This monitor has been selected due to its properties to store its data once per second directly into the computer *and* that by opening a slide the monitor becomes also sensitive to β-radiation.

This means that by performing two scans, with the only difference *an open* or *closed* slide, experience can be gained about the applicability of a 3DAS-system to localize possible areas with surface contaminations in elevated background radiation fields.

In Figure 2.3.14 iso-plots are presented of the two experiments. The range of measured dose rate varies for the monitor with slide open and closed respectively from 0-15 µSv/h and from 0-13 µSv/h. The small red area is caused by the large-area transmission source. In Figure 2.3.14A at position X=1300 and Y=500 the characteristic pattern of a hot spot can be seen, while in Figure 2.3.14B at that position a more diffuse pattern is presented. This difference is caused by the small increase of the collected dose rate by detected β-radiation (observe and compare the colour bars).

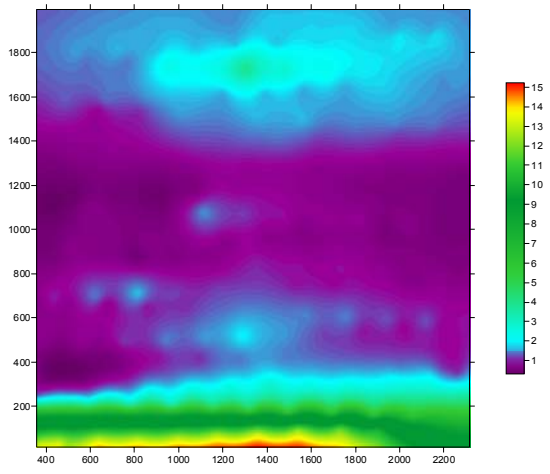

Figure 2.3.14A: **Fast** scan of the sidewall of an empty concrete box with an artificial contamination at position (X, Z; 1300, 500); Iso-data plot of *collected dose rate including contamination rate [micro Sv/h] with the Inovision 451B with slide open*

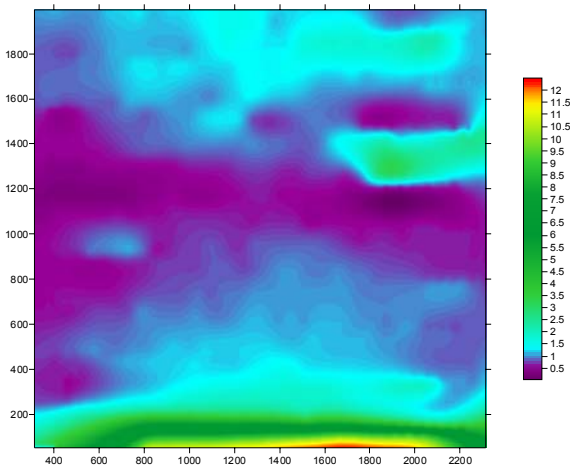

Figure 2.3.14B: **Fast** scan of the sidewall of an empty concrete box with an artificial contamination at position (X, Z; 1300, 500); Iso-data plot of *collected dose rate including contamination rate [micro Sv/h] with the Inovision 451B with slide closed*

The results of the contamination experiment prove that a 3DAS-system is capable to localize contaminations at the surface of a large waste item in elevated radiation fields. However, the applied monitor is far from the most suitable one, due to the fact that the monitor has a good sensitivity to gamma radiation. Therefore it is advised to select for this type of contamination scans a monitor with the highest beta/gamma sensitivity ratio.

2.3.4.3.1.3.3 Heat exchanger

The presented results are representative results of the performed NDA scans to characterize the heat exchanger. All results are reported in the topical report [5].

The following results are presented as examples:

- Slow continuous scan results of ^{40}K and dose rate.
- Slow and fast continuous scan results of $^{60}Co_{1332\ keV}$.

Slow continuous scan results of ^{40}K

This nuclide emits only one photon at an energy of 1461 keV and forms in general only part of the environmental background and is not emitted by the waste item under investigation like the heat exchanger. Therefore this photon can be used to prove the correct operation of the 3DAS-system during slow- and fast continuous scans of a waste package. ^{40}K analysis results are presented in iso-plots and fractional plots (see Figure 2.3.15 and 2.3.16). The following results are presented and discussed:

- Figure 2.3.15:
  - The *quantitative net iso-plot of ^{40}K* (see Figure 2.3.15B). It can be expected that these data will show no hot-spot, due that there are no elevated concentrations levels of ^{40}K in the environment and this is confirmed by the reported data.
  - In each quantitative net data-set there will be a *highest* and a *lowest net value*. These values will be responsible for the automatic scaling of the range and thus also of the colour bar of the iso-plot. Due to the automatic scaling no information can be extracted of significantly elevated or decreased levels.
  - The scattered data points in *each individual fractional plot* may not show any correlation with each other, while the number of data points has to increase first till a maximum has been reached and then has to decrease again. In the case that no correlation is present the increase-decrease-pattern of data points in subsequent fractional plots will be normally distributed according to a normal- or lognormal-statistical distribution and this pattern can be observed in Figure 2.3.15D. The Y- and X-axis of each of the fractional plots are respectively equal to 2 meter and to 7 meter, thus covering the total heat exchanger. Each detail plot contains the measurements lying in 5 % window.
- Figure 2.3.16:
  - The *statistically filtered iso-plot of ^{40}K* (see Figure 2.3.16B). It can be expected for ^{40}K that no pattern can be discovered and the *yellow and light blue spots* has to be randomly distributed over the complete iso-plot. The yellow and light blue spots are corresponding to data that have respectively a value between +1 and +2, and –1 and –2 standard deviations. It can be concluded that the presented iso-plot is in accordance with the expectations.
  - In the unique *statistically filtered fractional plots* (see Figure 2.3.16D) no patters exist. Most of the data points seem randomly distributed and also the number of the data points in each fractional plot seems equal. These conclusions are not completely true, because this conclusion can only correctly be drawn when the data-set contains more than 2500 independent data points. However this ^{40}K data-set contains only about 600 independent data points.

Figure 2.3.15 Examples of quantitative iso-plots one without and the other with a significant pattern. Slow continuous scan (measuring time 20s per spectrum and 1s per dose rate data)

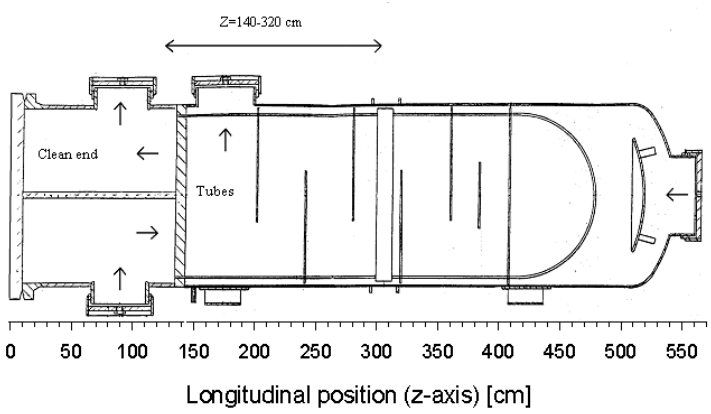

Figure 2.3.15A Internal structure of the heat exchanger. The arrows show the water flow.

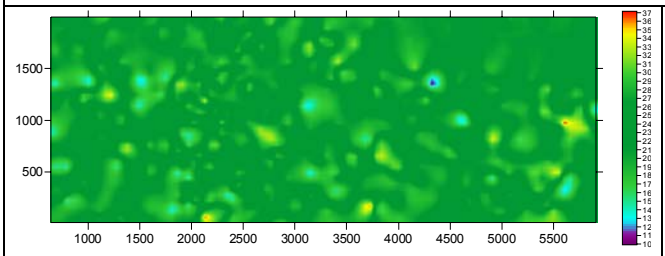

Figure 2.3.15B Iso-plot of the net area of the ^{40}K, 1461 keV.

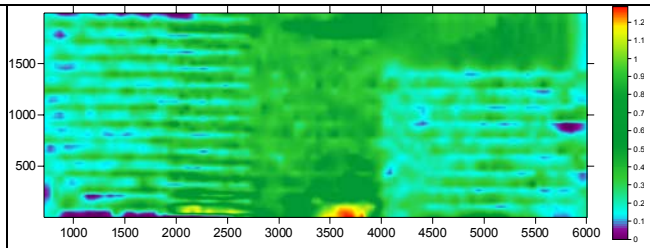

Figure 2.3.15C Iso-plot of the collected dose rate measured with the Inovision 451P.

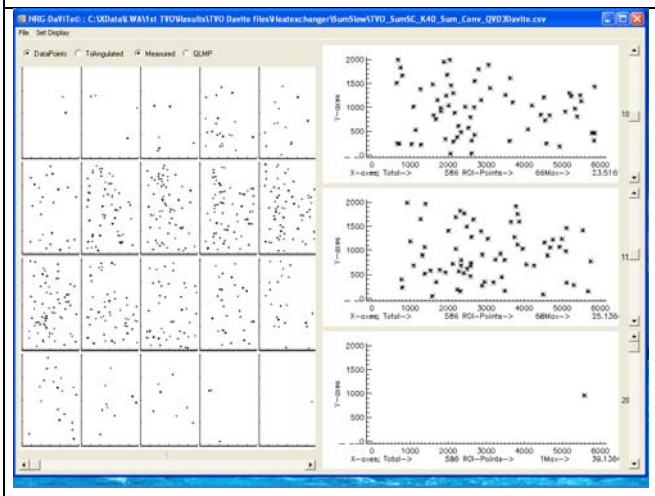

Figure 2.3.15D Fractional net area data of ^{40}K 1461 keV; details 10, 11 and 20.

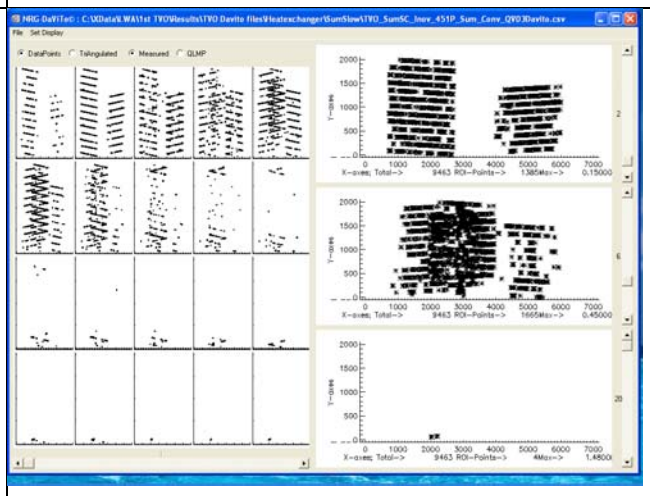

Figure 2.3.15E Fractional net area dose rate data of the Inovision 451P; details 2, 6 and 20.

Figure 2.3.16 Examples of statistically filtered iso-plots one without and the other with a significant pattern. Slow continuous scan (measuring time 20s per spectrum and 1s per dose rate data)

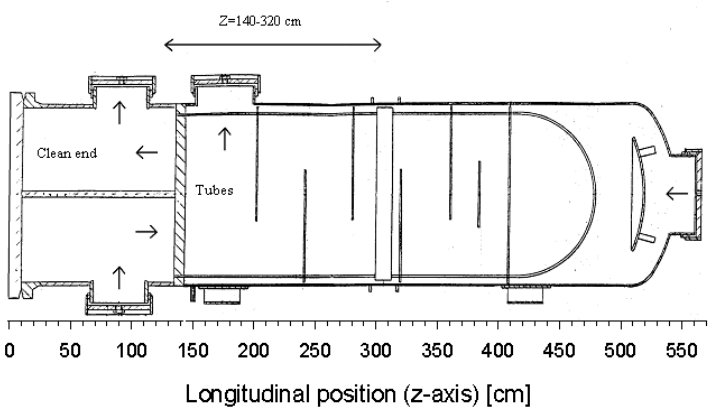

Figure 2.3.16A Internal structure of the heat exchanger. The arrows show the water flow

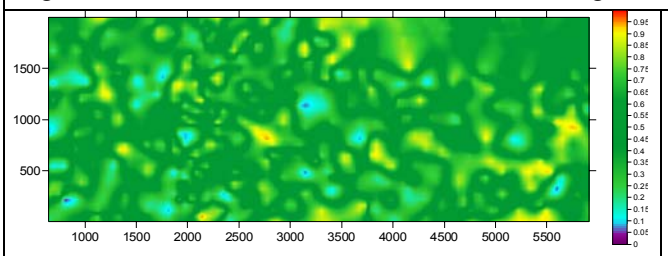

Figure 2.3.16B Iso-plot of the statistically filtered net data of ^{40}K, 1461 keV.

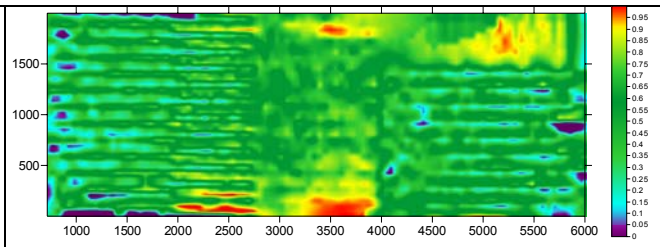

Figure 2.3.16C Iso-plot of the statistically filtered dose rate measured with the Inovision 451P.

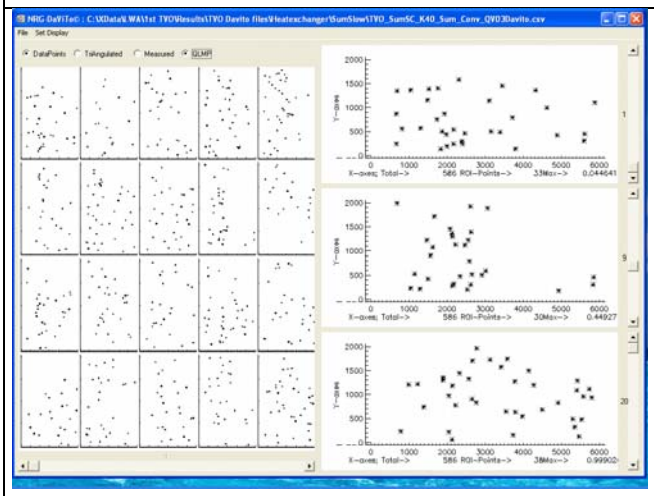

Figure 2.3.16D Fractional the statistically filtered net data of ^{40}K 1461 keV; details 1, 9 and 20.

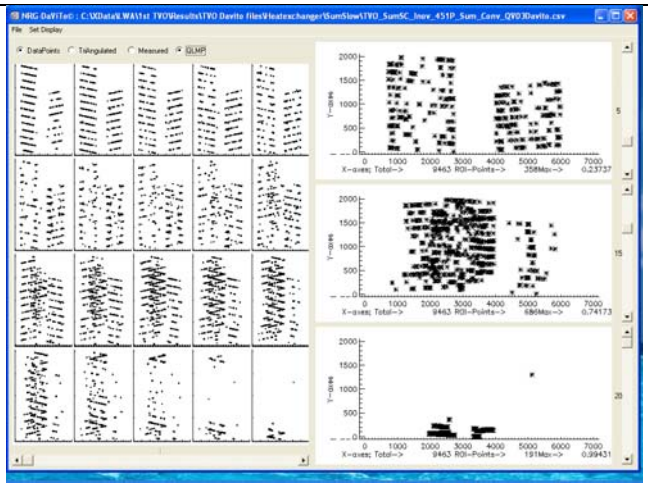

Figure 2.3.16E Fractional the statistically filtered dose rate data of the Inovision 451P; details 2, 6 and 20.

- In the first (top left) and the last (bottom right) statistically fractional plot all data points are visualized that corresponds to data that lie respectively beneath and above two standard deviations cq. a confidence level of 95 %.

Slow continuous scan results of the dose rate
It is evident that the measured dose rate is the sum of the local background and the local dose rate caused by the photons emitted by the heat exchanger.

The following analysis results are presented and discussed:

- Figure 2.3.15:
  - The *quantitative net iso-plot of the dose rate* (see Figure 2.3.15C). First, the green patterns that are visible are corresponding to the performed scan. Second, in the iso-plot the location with the highest dose rate is at location (3750,0) and some spots with decreased radiation levels like at locations between (400,0 and 1750,50).
  - In the *quantitative fractional plots* patterns are unambiguously visible (see Figure 2.3.15E and also the three detailed expanded fractional plots). It is evident that these patterns have consequences for an eventual activity calculation. The fractional plots are compared with the internal drawing of the heat exchanger (see Figure 2.3.15A). Out of this comparison it can be understood why the patterns are reported. However these individual fractional plots contain no information about locations with significant increased or decreased radiation levels.
- Figure 2.3.16:
  - In the *statistically filtered iso-plot of the dose rate data* (see Figure 2.3.16C) more areas have been marked in red and purple corresponding to elevated and decreased levels at a significant level of at least 95 %, meaning that these areas contain a radiation level that significantly differs from the population of measured dose rates.
  - In the unique *statistically fractional plots* (see Figure 2.3.16E) patterns are reported and sometimes in such a detail that they can be directly linked to the internal structure of the heat exchanger. In the first detail (top left) and the last (bottom right) fractional plot all data points are visualized that correspond to dose rates that lie beneath respectively above two standard deviations.
  - In the highest fractional plot (bottom right) all significant dose rates are visualised and localised.

Slow and fast continuous scan results of $^{60}Co_{1332\ keV}$
Both scans are recorded with a non-collimated HPGe detector. The distance between the detector end-cap till the wall of the heat exchanger was set to 30 cm, so that during both fully automatic scans the HPGe detector respectively with speeds of 15 mm and 60 mm is able to follow all the curves and edges of the heat exchanger. The results that are being discussed are presented in Figure 2.3.17. The wrinkle lines in the plots are caused by the performed scan and by the non-optimised software linking between locations and collected data. This was corrected before the later experiments.

By comparing the results of the slow (Figures 2.3.17A-D) and fast scan (Figures 2.3.17E-H) it is unambiguous that the slow and fast scan results give identical results and patterns. It is evident and could be expected that the visualisation of the results and patterns of the slow scan are more significant, due to the larger range of the collected data. However, the comparison of the fractions that have been calculated according to the procedure given in Section 2.3.4.3.1.2 (see Table 2.3.4) no significant differences can be observed.

The determined ^{60}Co activities with the slow and fast NDA scan are in good agreement. The difference in the ^{60}Co activity is caused by the scan method.

Figure 2.3.17 Analyse results of $^{60}Co_{1332\ keV}$ of the slow and fast NDA scan of the heat exchanger.

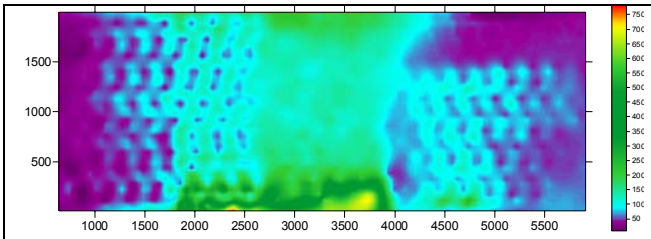

Figure 2.3.17A ISO-plot of the net data of $^{60}Co_{1332\ keV}$ of the slow NDA scan.

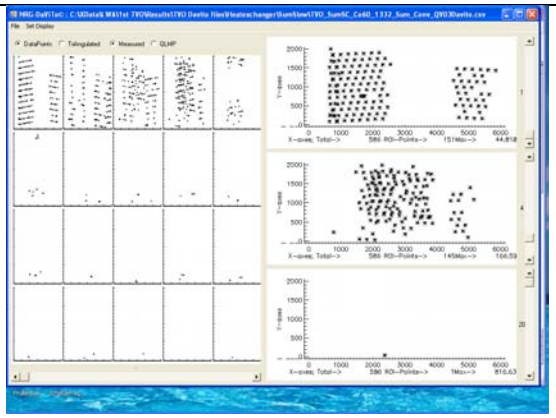

Figure 2.3.17B Fractional plots of the net area data of $^{60}Co_{1332\ keV}$ of the slow NDA scan; details 1, 4 and 20.

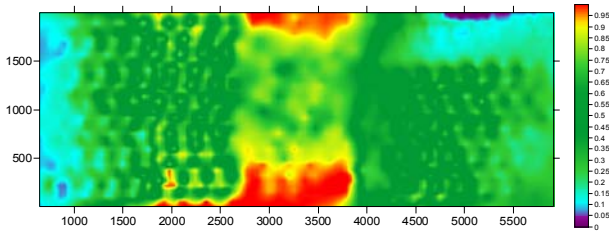

Figure 2.3.17C Iso-plot of the statistically filtered net data of $^{60}Co_{1332\ keV}$ of the slow NDA scan

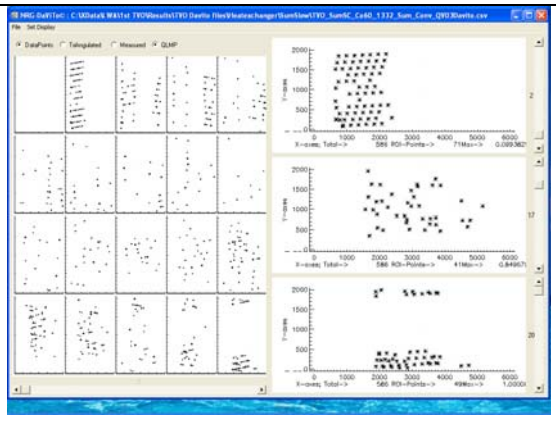

Figure 2.3.17D Fractional plots of the statistically filtered net area data of $^{60}Co_{1332\ keV}$ of the slow NDA scan; details 1, 4 and 20.

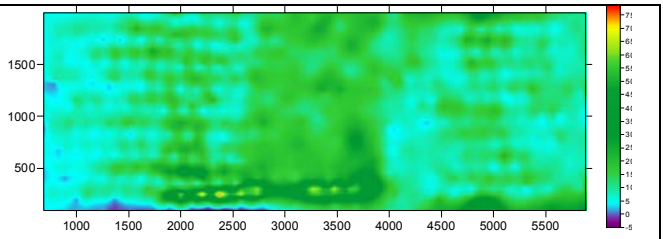

Figure 2.3.17E ISO-plot of the net data of $^{60}Co_{1332\ keV}$ of the fast NDA scan.

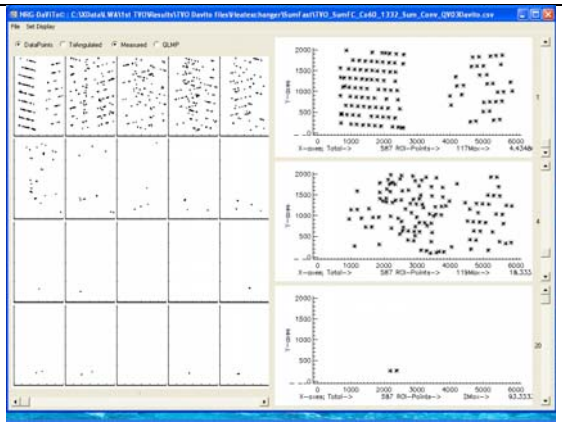

Figure 2.3.17F Fractional plots of the net area data of $^{60}Co_{1332\ keV}$ of the fast NDA scan; details 1, 4 and 20.

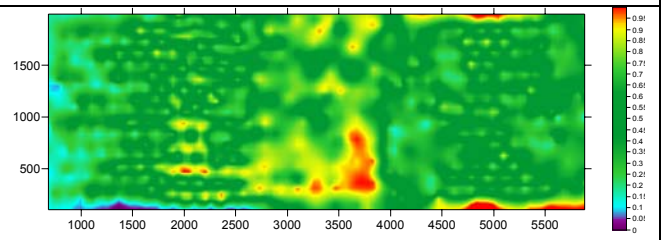

Figure 2.3.17G Iso-plot of the statistically filtered net data of $^{60}Co_{1332\ keV}$ of the slow NDA scan

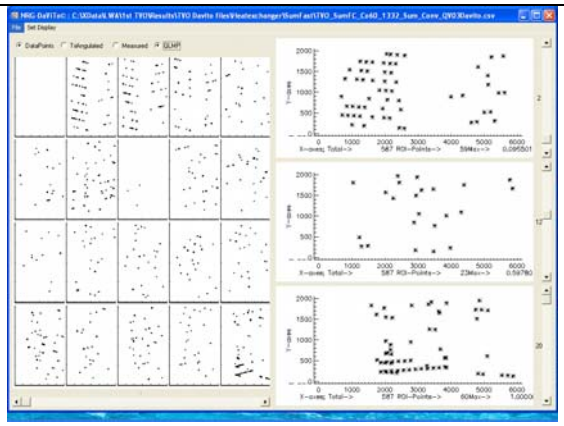

Figure 2.3.17H Fractional plots of the statistically filtered net area data of $^{60}Co_{1332\ keV}$ of the slow NDA scan; details 2, 12 and 20.

Table 2.3.4 Overview of the calculated surface fractions for the heat exchanger according to the procedure presented for the *slow scan* (measuring time per gamma spectrum 20 s with a total scan time of 4 hours for the heat exchanger) and for the *fast scan* (measuring time per gamma spectrum 2 s with a total scan time of 1 hour for the heat exchanger) and of the calculated specific ^{60}Co activity.

Fraction	Slow scan	Fast scan
Net data value > (Average +3$\sigma_{population}$)	0.0017	0.000
(Average +2$\sigma_{population}$) < Net data value < (Average + 3$\sigma_{population}$)	0.000	0.000
(Average + 1$\sigma_{population}$) < Net data value < (Average + 2$\sigma_{population}$)	0.216	0.199
(Average -1$\sigma_{population}$) < Net data value < (Average + 1$\sigma_{population}$)	0.588	0.584
(Average - 2$\sigma_{population}$) < Net data value < (Average - 1$\sigma_{population}$)	0.129	0.155
(Average - 2$\sigma_{population}$) < Net data value < (Average - 3$\sigma_{population}$)	0.187	0.017
(Average - 3$\sigma_{population}$) < Net data	0.046	0.044
Specific ^{60}Co activity	4.2 ± 2.1 MBq	5.6 ± 2.8 MBq

By the fast NDA scan the distance between detector and heat exchanger is often smaller than the defined 30 cm, resulting in higher detection efficiencies that are not taken into account in the activity calculation. These smaller distances are due to limitations of the automatic process control to follow accurately the curves of the heat exchanger.

2.3.4.3.2 Second *in situ* validation experiment

2.3.4.3.2.1 Objectives and set-up

The main aims of the second *in situ* validation experiment are to gain information and to get more experience about:

- Sensitivity of applied NDA-3DAS-scan-procedures.
- Reproducibility of NDA-3DAS-scans.
- Effect of detector collimation by NDA-3DAS-scans.

To be able to fulfil the above-stated aims, the experimental programme had to contain scans that provide sufficient data for these aims and this could be performed by the following three series of experiments on an ISO container loaded with seventy 220-l drums that are fully characterized.

The follow series of experiments have been performed:

1. Sensitivity of applied NDA-scan-procedures; a calibration drum that contains a ^{137}Cs source will replace one of the 220-liter drums. The calibration drum will be shifted between experiments from directly next to the wall of the ISO container to its centre. After each shift of the calibration drum the total side surface of the ISO container is scanned.

2. Reproducibility; by placing a drum with a ^{60}Co source directly next to one of the walls of the ISO container and taking care that the drum doesn't have to be replaced by any handling of the calibration drum.
3. Effect of collimation; by performing identical scans with and without collimation. A special collimator had been developed that could be mounted on the Y-axis of the 3DAS-system. The developed collimator shielded the HPGe-detector from the side, but leaves the front entrance of the detector open.

This second *in situ* validation experiment was carried out at the *Waste Quality Checking Laboratory* (WQCL) of the United Kingdom operated by NNC Ltd.

2.3.4.3.2.2 Experimental and specific calculation procedures

The experimental procedure is equal as described in the topical report [5]. During this second *in situ* experiment no additional tests were performed to optimise the established slow- and fast scan procedure. Therefore all scans are performed with the same scan speed settings (see Table 2.3.5) for a net area of "2 m * 2 m".

Table 2.3.5 Overview of resulting axes speeds and net scanning times over a 2 m* 2 m area applied in the 2nd *in situ* validation experiment.

Description		Slow scan	Fast scan[1]
X-axis speed	[mm/s]	7.5	60
Y-axis speed	[mm/s]	0.5	3.0
Axes speed ratio	[ ]	25	20
Endurance time	[s]	4000	667
Spectrum repeating time	[s]	21 (20+1)	3 (2+1)
Number of collected spectra	[ ]	190	222
Source-detector-distance	[cm]	10	10

([1]) Applied with and without a collimator.

2.3.4.3.2.3 MCNP calculations

The MCNP calculations can be divided into two parts:

- The first part deals with the validation of developed techniques by means of controlling if the images based on collected data with the 3DAS-system are comparable with images based on the MCNP calculations.
- The second part deals with the validation of the developed guideline (see Annex 7). MCNP is used to assess a suitable detector calibration efficiency.

Validation of developed NDA-techniques

This second *in situ* validation experiment has as aim to perform a NDA radiological characterisation of an ISO container loaded with seventy characterised 220 l low level radioactive waste drums (see paragraph 2.3.1 and topical report [5] for the technical specifications). It is evident that simplifications have to be made in order to model such an ISO container with a large variety of densities, chemical matrices and radioactivity distributions.

The ISO container was simplified for the *MCNP simulation* as follows:

- By applying a single steel layer for the walls with an average thickness.
- By applying a concrete slab with thickness of 40 cm as floor beneath the ISO container.

- Only the "validation part" of the container is taken into account in the model. The "validation part" of the container is the region in which the calibration drum is situated.
- 220 l drums are simplified by a assuming a single layer steel cylindrical wall and lids.
- The average elemental composition of the waste packages was calculated according to container consignment data.
- The drums have been divided into 5 groups as function of the waste density and average densities for individual groups were determined and used.
- The empty calibration drum was described as a sixth type of drum.
- The individual drums were placed in their real positions according to the container consignment description.
- The real radionuclides inventory of the individual drums was considered.
- Outer borders of the model space are created by the floor concrete slab complement by an air sphere.
- The empty calibration drum with the ^{137}Cs point calibration source in the centre of the drum was specified as a part of the model description.
- The photon energy cut-off was set at 10 keV.

Two types of MCNP output files were created. First, energy distributions of air kerma rates for point detectors for several sets of detectors at a distance of 10 cm from the ISO container walls are calculated (see an example of this output in Figure 2.3.18). Second output contains calculated coordinates of intersection points of photons at the container outer surfaces (see Figure 2.3.19). These intersection points are used for the creation of iso-plots of photon fluxes at the container outer-surface. Both models have been set up in a flexible way, so that any other detections systems can be added to the models as needed.

To study the possibility to identify a drum depending on its activity content and position a special series of MCNP simulation has been performed. The calibration drum (an empty 220 l drum with a ^{137}Cs source placed at its centre) was chosen as representative of a "hot" drum. This calibration drum replaced virtually original drums of the consignment.

The calculated air kerma values per emitted photon are processed into 2D-bar graphs:

- First, to visualize an eventual relation between the air kerma and the "hot" drum position
- And second to obtain by performing NDA measurements along the surface of the ISO container the possibility to identify and when possible to locate a "hot" drum against the signals background caused by the other drums of the consignment and the environment.

The best results are achieved by subtraction of the contribution of the ^{137}Cs primary photons collected when no calibration drum was applied from the data series containing contributions of the calibration drum.

The simulations without calibration drum can be seen as a kind of *background*. This *background* series has been labelled with "000" in Figure 2.3.20. In Figure 2.3.20 also the other calculated series are presented including the *background*. The results obtained after subtraction of the background of each series are presented in Figure 2.3.21.

The results presented in Figure 2.3.21 allow the following conclusions:

- It is apparent that unambiguously identifiable "hot drum" positions are present in the consignment and sixth data group for the calibration drum positions 223, 233, 243, 123, 133 and 143 it can be seen that these drums are less shielded by the forth row of drums (counting from left to right) and this is due to the shift of this forth row of drums. See Annex 1 and the topical report [5] for the overview of the actual loading scheme of the ISO container.

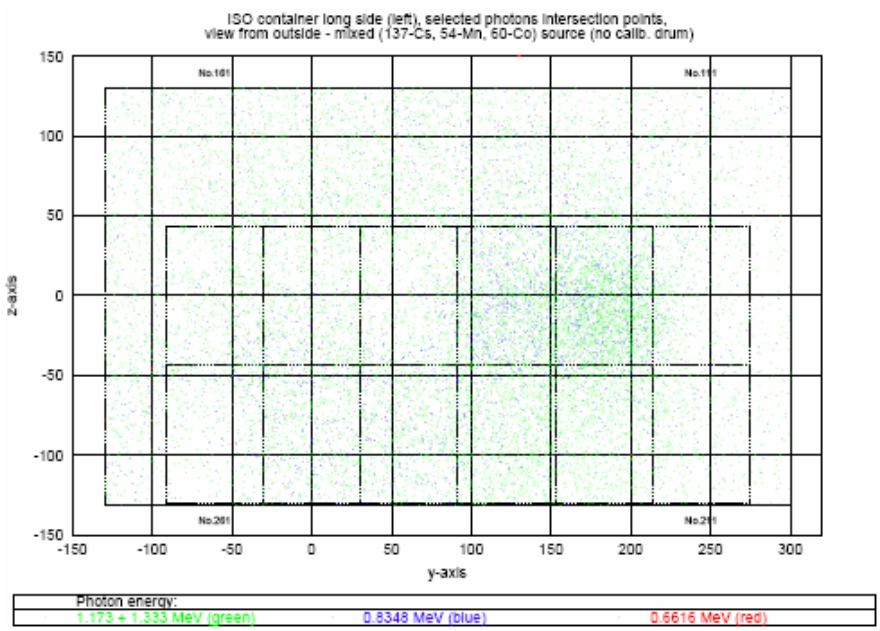

Figure 2.3.18
Calculated air kerma distribution at the left long side of the ISO container.

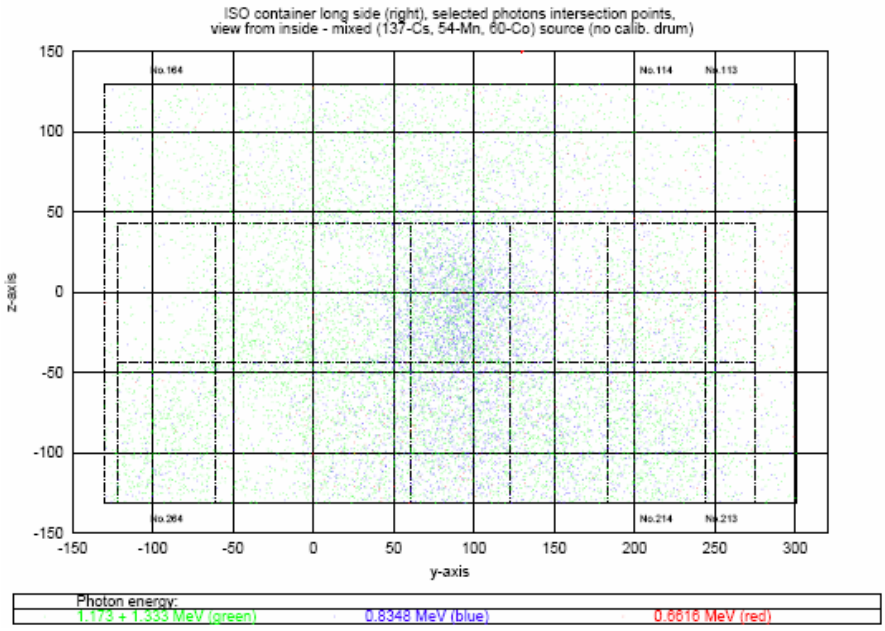

Figure 2.3.19
Calculated intersection points of selected photons at the right long side of the ISO container.

- Positive indications are present about the presence of a “hot drum” in the consignment corresponding to positions 222, 232, 242, 122, 132 and 142 of the calibration drum. In the overview of the loading scheme of the ISO container (see Annex1) it can be seen that these drums are completely shielded by the first column of drums. This explains also the less pronounced detector response. However, the interpretation of this data is not unambiguous.
- It is also visible – see the last data group – that a “hot drum” in the bottom layer cannot be identified by a NDA measurement from top side of the ISO container.
- Calibration drum positions in the top layer are represented by wide elevated levels with a local maximum, see positions 122 and 123. In the detector response profiles are present that offers the possibility to identify the approximate position of the calibration drum. The widening of elevated levels in responses profiles are caused by longer distances between the drums in top layer and the detector positions.

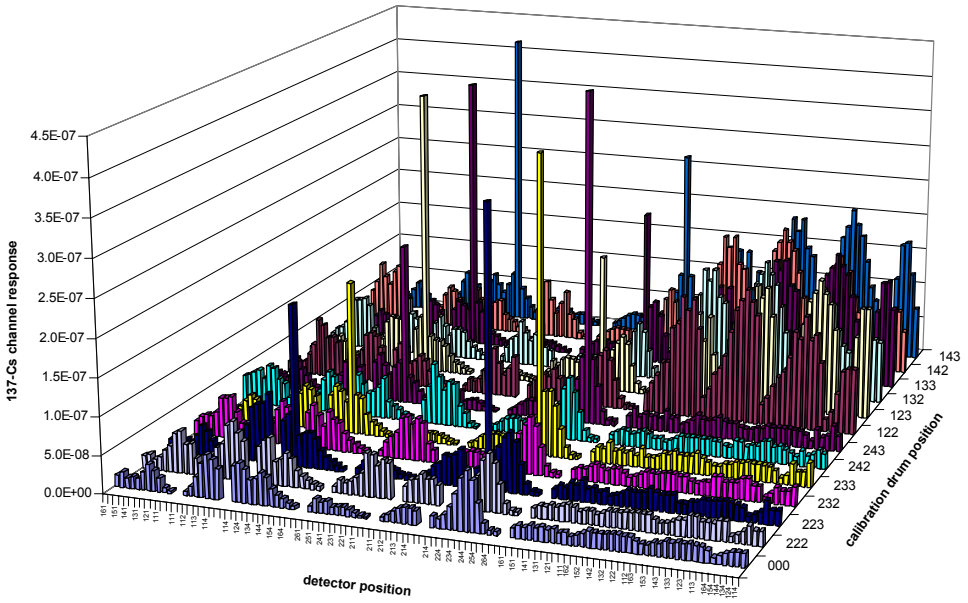

Figure 2.3.20 Calculated detector responses for different calibration drum positions; air kerma, contribution from ^{137}Cs primary photons (0.662 keV).

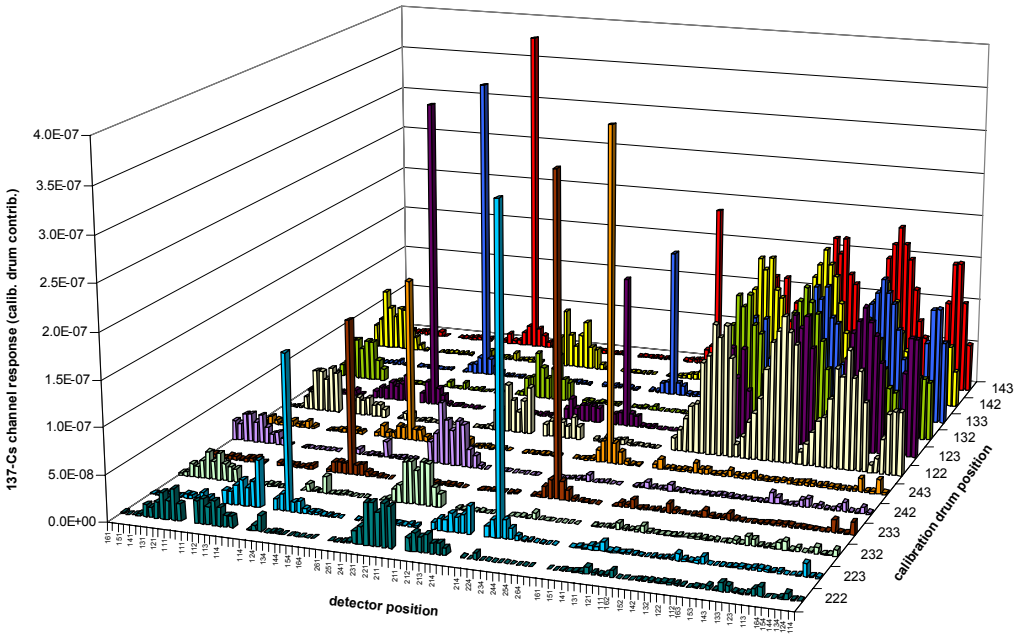

Figure 2.3.21 Calculated detector responses for different calibration drum positions; air kerma, contribution from ^{137}Cs primary photons minus the ^{137}Cs *background* defined by "000" configuration (see "000" in Figure 2.3.20).

In Figure 2.3.22 the contour map is shown of the calculated contribution of ^{60}Co photons (1.332 MeV) to the air kerma distribution 10 cm from the container's right side. The hot spot in this map is corresponding to the ^{60}Co activity present in the drum located at position 134 (see Annex 1 for details of this drum).

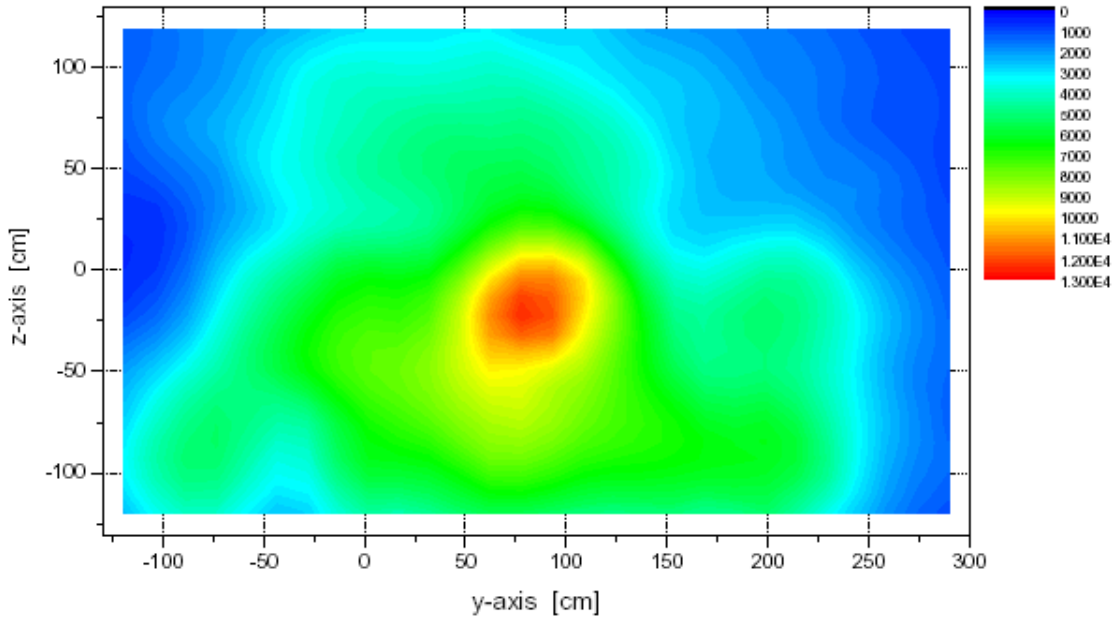

Figure 2.3.22 Contour plot of ^{60}Co (1.332 MeV) photon flux [$^{-1}$s] passing through a virtual rectangular detector of size 0.227 m * 0.238 at the right side of the ISO container. The average density of the drums has been applied. The entrance doors has the Y-axis coordinate of 300.

Validation of the developed guideline

To validate the developed guideline the following MCNP detector calibration efficiency calculations have been performed for the ISO container:

- Divide the waste object in a maximum of four zones of which each zone can be assumed to have a homogenous density but different from the adjacent zone.
- Divide each zone in a maximum of four equal layers with a uniform activity distribution of the nuclide of interest. For each layer the efficiency has to be calculated taking into account the shielding effects of the other layers. The sum of the four calibration coefficients of the different layers of one zone is of course equal to the calibration coefficient of the zone when this is not split-up in different layers. The aim of this subdivision in layers is that when it can be proved or assessed that an elevated radiation level is caused by an activity present at a greater depth this can be taken into account in the activity calculation of a specific nuclide.
- The simulated calibration factors have to be expressed in the dimension "Bequerel per outer surface of the waste object zone [Bq/m^2]". The sum of the individual surface zones is equal to the total outer surface of the waste object.

In this way a maximum of 16 calibration factors can be obtained (4 representing the uniform activity distribution of each zone, and 4*4 factors for the four layers of the four individual zones).

For the ISO container the four zones has been setup with the same properties e.g. a density of about 320 kg/m^3 and uniform activity distributions for ^{137}Cs and ^{60}Co. Due to this set-up parts of the ISO container can be assumed to have identical geometries and there through only the detector efficiencies of a small part (half of the long side) of the ISO container need to be simulated.

In Figure 2.3.23 results of the MCNP calculations are presented of the air kerma per emitted photon as function of the four defined zones for respectively ^{137}Cs and for ^{60}Co. This Figure allows making the conclusion that the contribution of the fourth zone (shielded by zones 1, 2 and 3) is

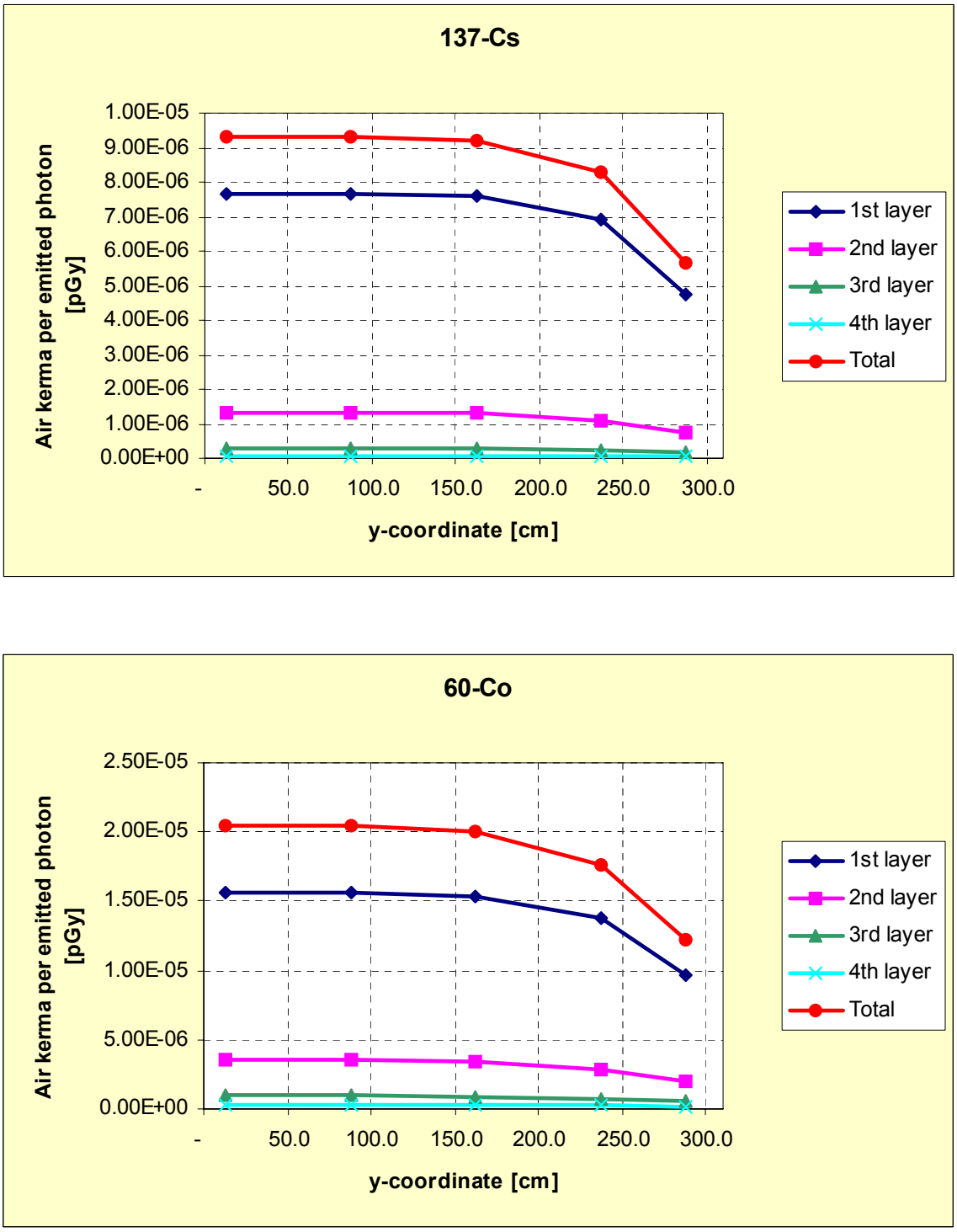

Figure 2.3.23 Results of MCNP calculations of the air kerma per emitted photon and as function of the four zones for respectively ^{137}Cs and for ^{60}Co. The y-coordinate (0.0) is corresponding with the middle at the long side of the ISO container.

Negligible and elevated radiation levels caused by activities in this zone will thus normally not be detected.

In Figure 2.3.24 the results of these MCNP detector efficiency calculations are presented for respectively ^{137}Cs (661 keV) and for ^{60}Co (1173 and 1332 keV).

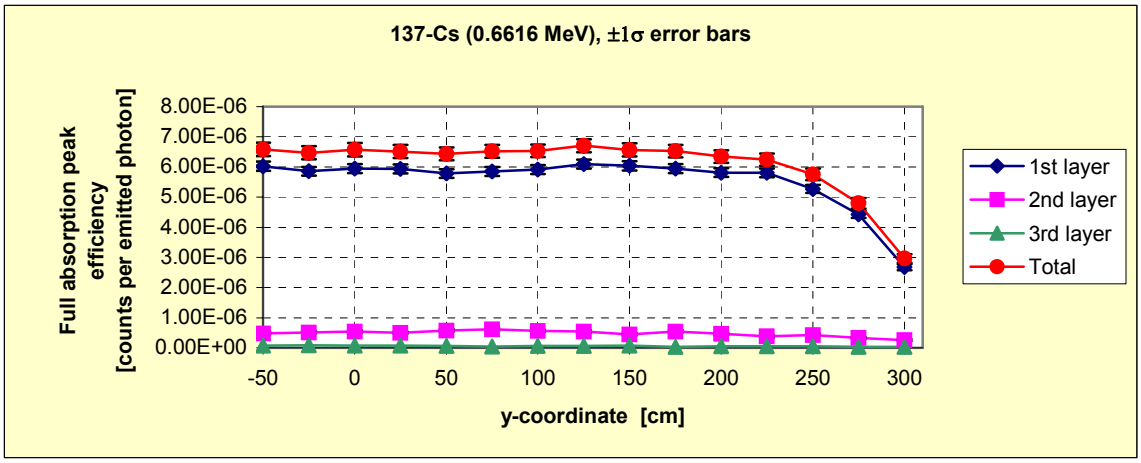

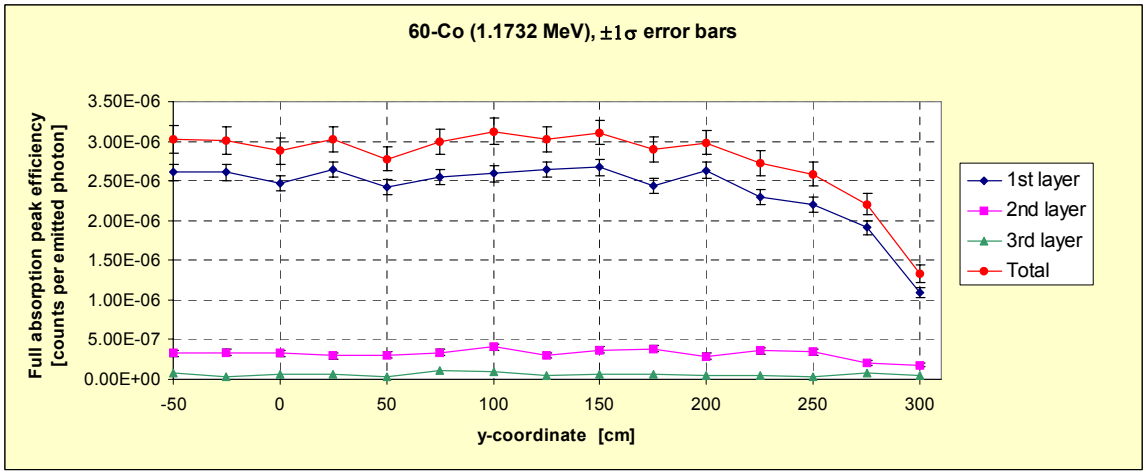

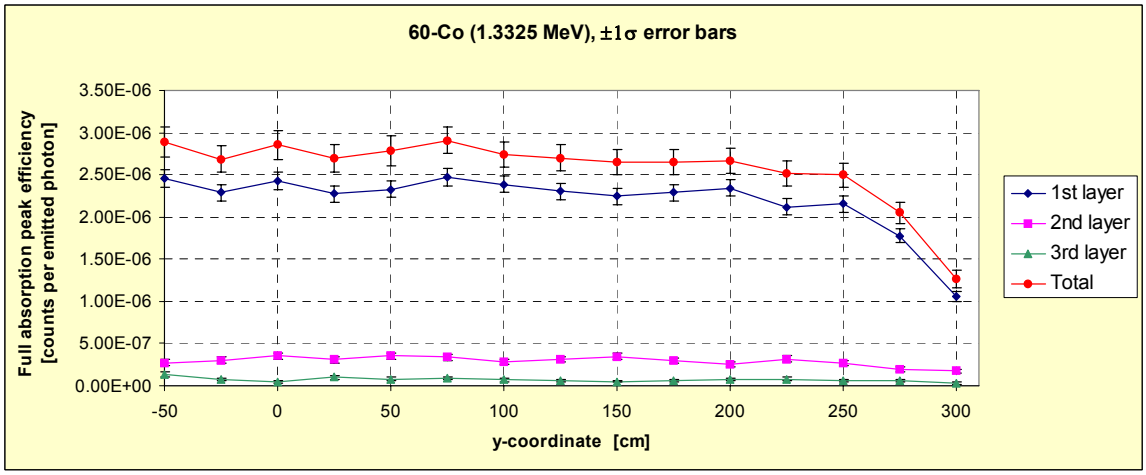

Figure 2.3.24 Results of MCNP detector efficiency calculations per emitted photon and as function of the four zones for respectively ^{137}Cs (661 keV) and for ^{60}Co (1173 keV and 1332 keV). The y-coordinate (0.0) is corresponding with the middle at the long side of the ISO container.

Based on the above MCNP results, a calculation procedure analogous as applied for the PTP-system for the specific activity calculation of the heat exchanger (see Section 2.3.3.2.2) and the collected data as presented in the Figures A4.2 and A5.2 (see Annex 4 and Annex 5) the activity in the ISO container can be assessed at 66 ± 33 MBq for ^{60}Co and at 7.2 ± 3.6 MBq for ^{137}Cs.

These calculated values are in a good agreement with the total nuclide specific activities of the consignment, consisting of seventy 220 l drums including the applied calibration drum, reported by WQCL -Waste Quality Checking Laboratory-UK. The reported activities are respectively of 41 MBq for ^{60}Co and 6.3 MBq for ^{137}Cs.

2.3.4.3.2.4 Results

Sensitivity of slow and fast NDA procedures

The results of analysed slow and fast scans show that results of the slow and fast scan methods are comparable. Both methods provide enough indications about the presence of hot-spots, elevated areas and areas with decreased levels. In Figure 2.3.25 and 2.3.26 the iso-plots are given from the slow and fast scan in which drum 123 have been replaced by calibration drum WQCL-13 (see Annex 1 for the actual loading scheme), note the differences in counts (see colour bars).

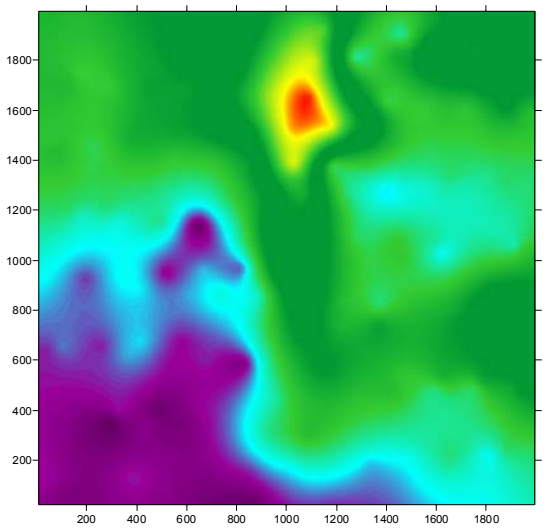

Figure 2.3.25 Iso-plot of the ^{137}Cs net data of the "slow scan, run ISO-0047" at position "right side 1 (close to doors)".

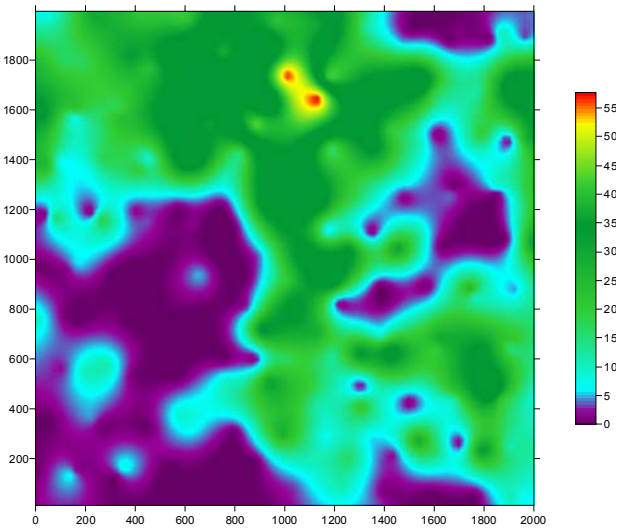

Figure 2.3.26 Iso-plot of the ^{137}Cs net data of the "fast scan, run ISO-0045" at position "right side 1 (close to doors)".

In general it can be concluded that circular patterns (see Figure 2.3.22) are caused by point-source-like activities close to the surface e.g. activities in the drum close to the sidewall, while patterns that look like line-sources as can be seen in Figure 2.3.25 are probably caused by activities in the next row or column of drums e.g. activities that are partially shielded by other waste.

In Annexes 2 and 3, examples of full analysis reports are presented for respectively ^{60}Co and ^{137}Cs. The reports are from the scan of the whole ISO container, in which the WQCL calibration drum replaced drum 123. The report consists out of the following plots:

- Iso-plots of individual scans but normalized at the *maximum value* of all collected net data of the total surface of the nuclide under investigation. Aim: to visualise the locations and areas with the most elevated and decreased radiation levels *at the walls of the ISO container*.
- Iso-plots of the net data per individual scan. Aim: visualisation of detailed information from locations and areas with the elevated and decreased radiation levels *per individual scan*.

- Iso-plots of statistically filtered net data per individual scan. Aim: visualisation of detailed information from locations and areas with *statistically significant* elevated and decreased radiation levels per individual scan.
- Fractional plots of the net data per individual scan. Aim: visualisation of possible existing patterns in the net data-set (the scale of the X and Y axes is 2 m).
- Fractional plots of statistically filtered net data per individual scan. Aim: visualisation of possible existing patterns in the statistically filtered net data-set (the scale of the X and Y axes is 2 m).

Comparing the figures in these two annexes, the completely different distributions of ^{60}Co and ^{137}Cs in the ISO container is clearly shown, but also the advantage of the different visualizations. Compare the changeovers from Figures A4.2 to A4.3 for ^{60}Co (see Annex 4) and A5.2 to A5.3 for ^{137}Cs (see Annex 5). The conclusions that can be drawn are that the detected ^{60}Co hot spots are significant, while the detected ^{137}Cs hot spots can still fall within the statistical variation. However, looking at the fractional plots (see Figures A5.4G-H and A5.5G-H) it is clear that some significant patters are present. This means of course that the activity is not homogenously distributed.

In Figures A4.4G-H and A4.5G-H nice examples can be seen of patterns created by a hot-spot.

A conclusion can also now be drawn that the combination of applied presentation techniques iso-plots of quantitative and statistically filtered both complemented with fractional plots fulfils the aim that: *The techniques applied for presenting characterization data of radioactive waste packages have to assist in the interpretation of NDA waste characterization data and must be able to show unambiguously information that is present (but hidden) in a data-set, so that the conclusion can be drawn that the characterized waste package is in accordance or is not in accordance with the predefined specified requirements.*

By comparing results of the *in situ* validation experiments in Annex 4 of ^{60}Co and presented MCNP modelling results in Figure 2.3.22 one has to take into account some differences present in the pictures like:

- The Y-axis (height) of the analysis report is in the MCNP-results referred as *Z-axis*.
- The X-axis (position at the right side of the ISO container) of the analyze report is in the MCNP-results referred as *Y-axis*.
- The positon (0,0) of the analysis report is equal to the lower left corner of the ISO container, and corresponds to the position (-50,-120) in the MCNP-results.

The conclusion that can be drawn out of this comparison is that the MCNP simulations are able to produce a good representation of an actual situation.

In general it can be concluded that the MCNP modelling results of the ISO container are in a much better agreement than the MCNP modelling results of the heat exchanger. This can be mainly due to the amount of details and better justified simplifications that are taken into account in the model of the ISO container.

Reproducibility

The reproducibility of slow and fast NDA scans are assessed with the aid of collected ^{60}Co scan data. The reported iso-plots of the statistically filtered data is used for this purpose, because this type of iso-plots show small differences more significantly than net data iso-plots. The ^{60}Co data has been collected at the same time as the data was collected for the sensitivity analyses.

Therefore differences caused by the replacement of the WQCL calibration drum have to be taken into account by the interpretation of these plots.

In Figures 2.3.27 and 2.3.28 two of the analyzed statistically filtered iso-plots of ^{60}Co are given. Those iso-plots have been constructed and analyzed for the slow and for the fast scans. As can be expected the iso-plots of the fast scans show more differences due to the smaller range of the collected data.

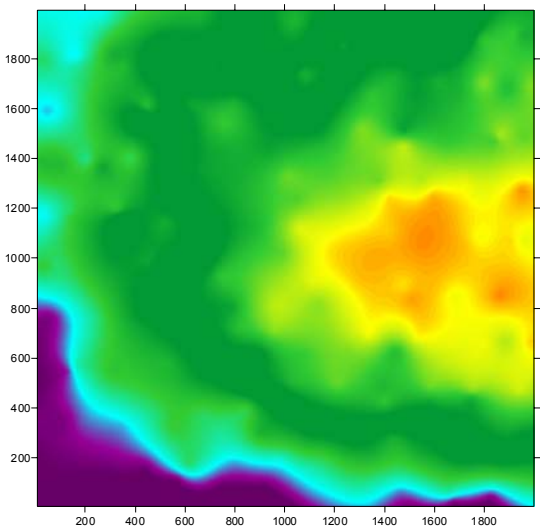

Figure 2.3.27 Iso-plot of the statistically filtered data of ^{60}Co (1.332 keV) coming from the *first* fast scan of the background at position "right side 1(close to doors)".

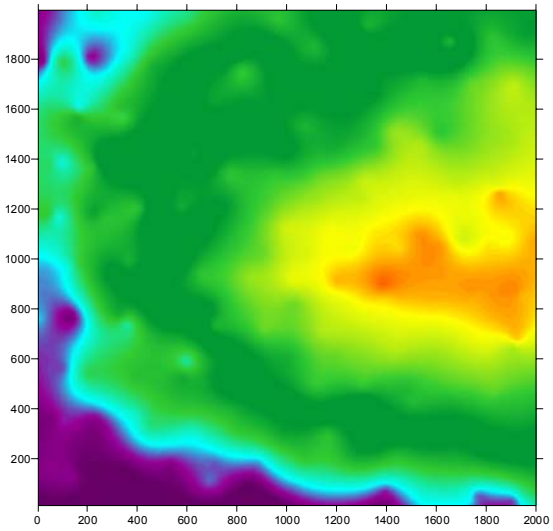

Figure 2.3.28 Iso-plot of the statistically filtered data of ^{60}Co (1.332 keV) coming from the *last* fast scan at position "right side 1(close to doors)". The calibration drum WQCL 13 has replaced drum 123.

In general it can be concluded that the differences for both scan methods are minor and that the reproducibility of scans is good for both nuclides ^{137}Cs and ^{60}Co.

Effect of detector collimation

The effect of collimation is clearly visible in the reported results. Collimated detectors give *sharper profiles* of hot-spots and elevated areas when they are located at the surface or near surface (see Figures 2.3.29 and 2.3.30). This effect has been noticed by analyzed scans of ^{137}Cs and ^{60}Co. The differences become less visible in the statistically filtered iso-plots.

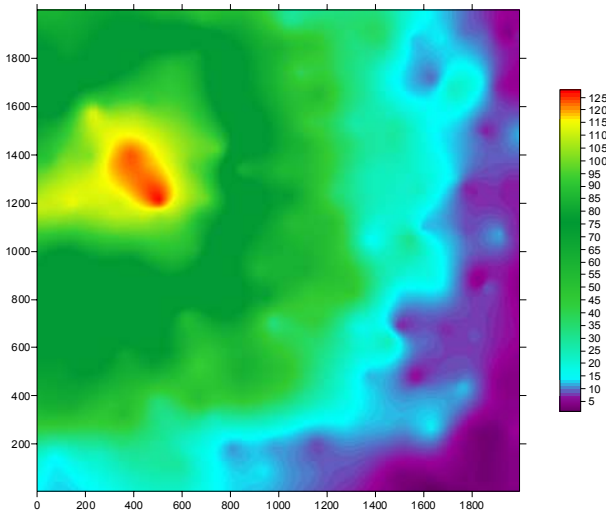

Figure 2.3.29 Iso-plot of ^{60}Co (1.332 keV) net data of the "fast scan run ISO-0033", performed *without* a collimated detector at position "left side 1".

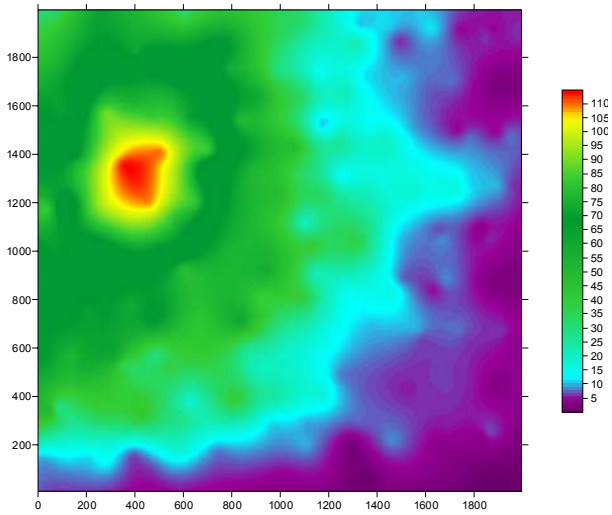

Figure 2.3.30 Iso-plot of ^{60}Co (1.332 keV) net data of the "fast scan run ISO-0032", performed *with* a collimated detector at position "left side 1".

Collimation can also be a disadvantage for a 3DAS system and especially in those cases when photons can mainly enter the detector through its sidewall. The activity is then partly shielded by more dens material than present in the waste package. In such a situation the possibility exists that the collimated detector will not detect an elevated radiation level and it will thus also not be reported and taken into account in the activity calculations.

The results of an open geometry system can be further improved by improving the signal-to-noise ratio. It should be possible to develop and apply a *collimator* that would reduce the background (meaning the environmental background and the increase of the background by the waste package under investigation, scattering of photons from walls, etc.), but still having such an aperture that the detector sensitivity for photons entering through the sidewall of the detector would not be reduced too much.

Important differences that can be observed between a collimated and an open detector system are:

- Collimation gives a better signal-to-noise ratio for hot-spots and elevated areas emitting photons that are able to enter the detector through the aperture of the collimator.
- Collimation and especially small apertures, will not give any indication of hot-spots or elevated areas that can only be measured when the detector is placed not at a right angle to the scanned surface, see the iso-plots of the validation area at observe the patterns that are referred to as *a kind of line source*.

2.3.4.3.3 Conclusions

The developed mobile detector frame *3D Rise*, acronym for "3-dimensional radiation inspection equipment" and classified as a 3-dimensional automated scanning system (3DAS), has fulfilled its expectations. The following conclusions can be made concerning the 3D Rise system:

- Hardware: The system can be equipped with non-collimated detectors like HPGe, NaI(Tl) and CdZnTe, and dose rate and contamination monitors so that it can handle radiation levels from 10 nSv/h up to 500 mSv/h. The mobility of the system is good, dismantling and assembling to full operation is possible by 2 persons within 4 hours.

- Software: Applied commercial gamma spectroscopic software will in general fulfil the requirements for this type of systems, but the software has to have the ability to perform a scan (record multiple spectra series). The software to operate and to program automatic scans for the *3D Rise* system is user-friendly and simple to handle, while the statistical filtering application (application in Excel) has to be improved in execution time and user-friendliness. Finally the imaging application (application programmed in the IDL environment) fulfils the requirements.
- Procedures: The procedure to characterize a large waste package by NRG fulfils the requirements. The estimated time needed to characterize large objects is of course dependent on the size and structure of the object, but can be assessed at about 20 minutes per scan-area of 2 m* 2 m including re-positioning by 2 persons. E.g. a 100 % check of the TVO's heat exchanger and ISO container can be performed in fewer then 3 hours.
- Analysis results and accuracy: The overall accuracy of the calculated activities is assessed at about 50 %. This Figure is reasonable taking into account the difficulties to establish correct detector efficiencies. One advantage of scanning is the increased number of collected data points, so that by applying advanced graphical (imaging) data presentation algorithms and statistical filtering methods spots and areas can be directly located that have significant *elevated* or *decreased* radiation levels in relation to the average level of the data of the scan.

2.3.5 Conclusions

The main goal for this work-package was the development of a NDA procedure for the QA/QC characterization of non-fissile material in large-volume waste packages.

The results achieved by the PTP-system and the 3DAS-system in the NDA characterization of the heat-exchanger and the ISO container [5] have lead to the set-up of a general guideline, see Annex 7.

Both developed systems, the PTP system and the 3DAS system, can in principle be applied. However, the developed 3DAS system is preferable. This is mainly due to the quality and cost-savings for a NDA characterisation and reporting of results of the 3DAS system over the PTP system.

An important point of interest, and this is equal for both systems, is how to determine the detector efficiency calibration to be applied. The gained experience in this project is that MCNP is able to provide these efficiency calibrations by simplification of the large-volume waste package and the measurement geometry. It is evident that the adopted simplifications in the MCNP models have to be justified.

2.4 Multi-energy transmission technique for large-volume waste packages

2.4.1 Introduction

The radiation emitted within a radioactive waste package may be moderated within the waste package through interactions with the waste matrix. This result in a difference between the spectrum of the radiation emitted from the waste package and the spectrum of the radiation emitted within the waste package. Thus, in order to quantify the true radioactivity of a waste package, through its non-destructive assay (NDA), a correction for its matrix effects needs to be applied. Such a correction requires knowledge of the properties of the waste package.

Various matrix correction methods exist for the techniques routinely employed for the non-destructive assay of radioactive waste packages. Like for gamma spectroscopic assays: based on the mass and volume; differential peak absorption from emitted photons and with the aid of a transmission source and for neutron assays: add-a-source technique and count ratio techniques.

If the matrix of a waste package is well characterized, its matrix effects may be covered by instrument calibration. It is evident that waste packages generally have varying matrices and, even if the matrix of every waste package needing to be assayed is well defined, it is not practical to recalibrate an instrument for every assay.

The attenuation of the flux of a type of radiation at a given energy passing through a waste package is dependent on three factors:

- The energy of the incident radiation. The higher the energy of the radiation, the less chance there is of interaction with the waste matrix and, therefore, moderation.
- The constituents of the waste matrix (moderators/absorbers). Heavier elements attenuate gamma-rays more than light elements, whereas light elements moderate neutron fluxes. Also, certain elements have high neutron absorption cross-sections like chlorine.
- The density of the waste matrix. The denser the matrix, the more chance of interaction and, therefore, moderation.

Additionally, for neutron assays, induced fissions and (α-n) reactions within the waste matrix may contribute to the signals observed.

The aim of this paragraph is to report on the research performed on the development / formulating of a matrix characterization technique for applications in the non-destructive assay of large-volume waste packages.

This paragraph is a summary of the topical report on transmission correction techniques [8].

2.4.2 Matrix characterization of waste packages

With the exception of the ratio techniques for neutron assays, the matrix correction techniques outlined above require prior knowledge of the waste matrix. This information can be obtained from the attenuation of gamma rays passing through a waste package.

The attenuated intensity of a beam of photons of energy E, $I_1(E)$, passing through an attenuating material is given by the relation

$$I_1(E) = I_0(E)e^{-d\rho[\mu/\rho](E)} \qquad (1)$$

where $I_0(E)$ is the un-attenuated photon intensity at energy E, d is the distance travelled by the photons in the attenuating material, ρ is the density of the attenuating material and $[\mu/\rho]$ (E) the mass attenuation coefficient of the attenuating material at energy E. Furthermore, the mass attenuation coefficient of a material is the weighted sum of the mass attenuation coefficients of the material's constituent elements,

$$[\mu/\rho](E) = \sum w_i [\mu/\rho](E) \qquad (2)$$

where w_i is the fraction by weight of element i. Therefore, if the constituent elements of a waste package are known, the attenuation of gamma-rays of differing energies, from external sources, can be used to determine the mass attenuation coefficients of the waste package at the differing

energies and then the percentage weights of the constituent elements. This is achieved by setting up simultaneous equations of the form of Equation 2 for every energy and solving for each w_i. This requires measurements at as much energies as there are constituent elements. However, if the mass attenuation coefficients of some of the constituent elements are similar within the energy range used, one of these elements can be taken as a representative for the group, thus reducing the number of measurements needed.

Figure 2.4.1 shows the documented mass attenuation coefficients of some of the light elements, up to and including Copper [9]. It can clearly be seen that in the energy range 400-3000 keV all of the featured elements, with the exception of hydrogen and beryllium, are very similar. Thus, any elements within this group present within a waste package may be represented by only one of these elements. Alternatively, if the constituent elements of a waste package are not known, the above procedure can be used to infer the resemblance of a waste package to a set of reference elements. Matrix characterization constitutes the first step in a procedure for a matrix correction technique for large-volume waste packages.

2.4.3 Matrix characterization of large-volume waste packages

The characterization methodology described above requires the use of external sources of gamma-rays to determine the percentage weights of the constituent elements, or representatives thereof, of the waste packages. These sources must therefore be strong enough to allow reasonable transmission through the waste packages. Naturally, one expects that as the shielding properties of the waste package increases, the specific activity and the emitted photon energy of applied sources needed for its characterization will also increase. For large-volume waste packages, the activity of the sources needed for their characterization could soon become too large to use practically.

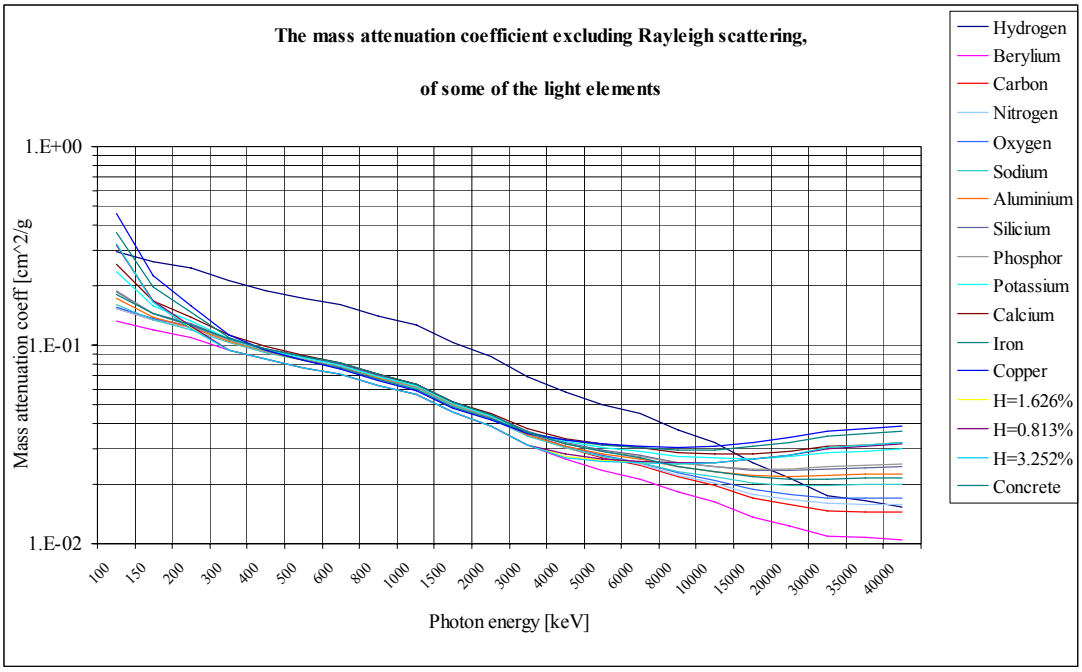

Figure 2.4.1: Mass attenuation coefficients of some of the light elements [9]

A solution to this problem could be the use of a Linac (linear electron accelerator) to produce the necessary photons. Photons produced in this manner, called Bremsstrahlung radiation, have the possibility to possess photon energies and intensities required for the characterization of large-volume waste packages whist the process of creating them remains practical in the sense of health

physics. Portable Linacs are commercially available and the portability of equipment for the assay of large-volume waste packages is greatly desirable.

Matrix characterization and correction techniques need to factor in the effects of the attenuated gamma rays of high energies affecting the measurements of the gamma rays of lower energies. Gamma rays of one energy may be in-elastically scattered within a waste package may exit the waste package with the energy of one of the other gamma rays used for the matrix characterization of the waste package. Detection of these scattered gamma rays will interfere with the measurement of the true attenuated signal of the gamma rays of the external source of the lower energy.
One solution is only to measure the highest energy gamma rays of various external sources and to measure the sources independently. This, however, is not very practical.

A Bremsstrahlung radiation spectrum is continuous up to a maximum energy. An energy dispersive photon detector could then be employed to measure only the photons at this maximum energy.

For non-energy dispersive detectors, a solution could be to use different maximum energies of a Linac(s) and only measure the signals from the gamma rays within small windows at the high-energy ends of the Bremsstrahlung spectrum. A weighted average of the mass attenuation coefficients of the energy ranges could then be used in the subsequent simulations, with a weighting depending on the Bremsstrahlung radiation spectrum.

2.4.3.1 Original multi-energy-transmission methodology

The original methodology proposes using MCNP simulations to test the methodology by determining the contributions to the total measured signal of a non-energy dispersive detector from various energy ranges [10].

Also, the mass coefficients at the midpoints of the selected energy ranges are used instead of weighted averages and the density of the waste is equated to the density of a reference element through a transmission measurement and use of equation 1.

This approach is desirable for large-volume waste packages whose densities are unknown and are difficult to calculate by other means. However, the method will give in the case of an abundance of hydrogen respectively beryllium an over-estimation or an under-estimation of the waste density.

MCNP simulations on a cubic concrete mock-up waste package (side 1.2 m, density 2.05 kg/m^3) with varying mass amounts of hydrogen were performed [11] to investigate the above effect. The maximum energy of the Linac was set at 6 MeV and the energy range at 5-6 MeV. Oxygen and calcium are the main constituent elements in the concrete mock-up. The results are presented in Table 2.4.1 and show clearly the expected trend.

All calculations have been performed with Excel in which the methodology and models have been programmed.

Table 2.4.1 Results of MCNP simulations to study the effect of the abundance of hydrogen on calculated effective densities [kg/m^3] of a concrete mock-up with a density of 2.05 kg/m^3.

Hydrogen mass fraction (%)	Calculated effective density [kg/m^3]	
	Reference element oxygen	Reference element calcium
0.813	2.14	1.84
1.626	2.15	1.85
3.253	2.18	1.87

After having determined the density of the waste package, the specific mass attenuation of the waste package has to be assayed. The method applies for these calculations three selected reference elements and three transmission measurements.
The mass attenuation curves of two of the three reference elements need to sufficiently overlap in the lowest selected energy range to be able to compute the mass attenuation of the third reference element.

Further MCNP simulations were performed on the above described concrete mock-up, using the true density and those computed in the prior MCNP simulations. The maximum Linac energy is set at 11 MeV, in order to calculate according to the methodology the mass fractions of the reference elements [12]. It was intended and planned to apply a Linac with this maximum energy to validate experimentally the developed multi-energy-transmission technique. As reference elements were chosen hydrogen, oxygen and calcium and applied energy ranges 6-7 MeV, 7-8 MeV and 10-11 MeV. The results are reported in rows 1-14 in Table A6.1 of Annex 6.

The simulation results showed that there appears no correspondence between calculated and true hydrogen mass fractions and the results also appear to depend on the density used and also on which reference element is applied in the calculation of the Hydrogen mass fraction. The conclusion can be made that the proposed methodology needs refining.

2.4.3.2 Revised methodology

The proposed methodology (see Section 2.4.3.1) assumes that the mass attenuation coefficients of oxygen and calcium are equal for the energy range 6-7 MeV. However they are not e.g. at 6.5 MeV the mass coefficients are for oxygen and calcium respectively 0.024775 cm^{2}g^{-1} and 0.029950 cm^{2}g^{-1}.

Therefore, as a first refinement, the necessity for the mass attenuation curves of two of the reference elements to overlap at 6.5 MeV is removed. This refinement offers a greater flexibility in the choosing of reference elements. The measured mass attenuation coefficients are then be used to set up and solve simultaneous equations of the form (3).

$$[\mu/\rho]_M (E_j) = \sum w_i [\mu/\rho]_{Pi} (E_j) \quad (3)$$

The results are presented in rows 15-22 of Table A6.1 of Annex 6 under *"revised methodology 1"*. These results appear also to depend on the applied density. However, more of interest is the negative signs appearing in the results. This can be due to the attribution of inelastic scattered photons in the energy ranges 6-7 MeV and 7-8 MeV coming from primarily higher energies (e.g. range 8-11 MeV) in the mock-up. Unfortunately the MCNP programme cannot produce an output that quantifies the attribution of these inelastic scattered photons in the defined energy ranges.

The mass fractions of the mock-up can be calculated by applying two reference elements and two energy ranges i.e. 5-6 MeV and 10-11 MeV. One of the reference elements has to be always hydrogen, due to its unique mass attenuation properties (see Figure A6.1 of Annex 6) and oxygen or calcium as the other.

The results of these calculations are presented in Table A6.1 of Annex 6, rows 22-35, under *"revised methodology 2"*. The following conclusions can be made:

- The values for the hydrogen mass fractions listed do not quantitatively agree with the true values of hydrogen mass fractions.
- The differences between the calculated hydrogen mass fractions agree with the differences between the true hydrogen mass fractions, with the exception of those calculated with the Oxygen effective density and Oxygen as 2nd reference element.
- The differences calculated using Calcium as 2nd reference element agree better with the true values than with Oxygen as 2nd reference element.
- The best agreement between the true and calculated differences is obtained by applying the true densities.

and finally

- Exploiting this correspondence, the above methodology may be used to calculate the true values for the mass fractions of waste packages by reference to those calculated for calibration waste packages.

2.4.3.3 Constraints on mass fractions

The constraint that the mass fractions should sum to unity has not been enforced. This can be clearly seen from the calculated mass fractions presented in Table A6.1 of Annex 6. For *n* reference elements *n* equations are needed to determine their mass fraction. To enforce the constraint *n-1* transmission measurements, giving *n-1* equations are needed. The final equation is given by the constraint.

$$1 = w_1 + w_2 + w_3 \qquad (4)$$

The results of the mass fractions of hydrogen, oxygen and calcium calculations are presented in Table 2.4.2. The energy ranges 5-6 MeV and 10-11 MeV are applied.

Table 2.4.2 Overview of the results of MCNP simulations and calculations according to the "revised methodology 2 with constraints". Specifications: maximum Linac energy 11 MeV

	Calculation methodology					True hydrogen mass fraction (%)								
Nr.	Density [kg/m^3] true/computed			Reference element		0.813 Computed mass fractions (%)			1.626 Computed mass fractions (%)			3.252 Computed mass fractions (%)		
	True	O	Ca	O	Ca	H	O	Ca	H	O	Ca	H	O	Ca
	Revised methodology 2 with constraints													
1		2.14				-9.228	64.47	44.76						
2		2.15							-8.904	-65.72	43.19			
3		2.18										-8.213	68.38	39.84
	Difference between calculated H fractions of 0.813 and ….					**0.0**			**0.324**			**1.015**		
4	2.05					-5.145	52.82	52.32	-4.259	52.58	51.68	-2.557	52.66	49.89
	Difference between calculated H fractions of 0.813 and ….					**0.0**			**0.886**			**2.588**		
5			1.84			5.692	21.92	72.39						
6			1.85						6.070	23.37	70.56			
7			1.87									6.873	26.47	66.66
	Difference between calculated H fractions of 0.813 and ….					**0.0**			**0.925**			**1.728**		

Again, the differences between the calculated hydrogen mass fractions using true densities agree with the differences between the true hydrogen mass fractions. However this is not the case for the other calculations e.g. quantitative values.

This leads to the recommendation that if the density of a waste package can be determined more accurately through other means than through a transmission measurement, then this density should be used in preference.

2.4.4 Third *in situ* validation experiment

2.4.4.1 Objectives and set-up

The aim of this validation experiment was to collect data to validate developed multi-energy transmission models. This validation experiment took place with the Saphir Linac at CEA Saclay, France with a maximum energy range between 15-35 MeV. The specifications of this Linac differ significantly from the originally proposed mobile Linac with maximum energies of 6, 9 and 11 MeV.

As mock-up of a large-volume waste package a concrete dummy with a diameter of 1.08 m and a height of 0.3 m was available (see Figure 2.4.2). In the mock-up rows of removable cylinders are present (see Figure 2.4.3). These cylinders were replaced during experiments by cylinders of polyethylene (PE), NaCl or KCl to simulate different mass fractions of hydrogen and chlorine in a waste package. Cylinders of concrete, PE, NaCl and KCl were not mixed.

An Inovision pressurized ion chamber monitor type 451P-DE-SI is used to measure the photon flux that passed through the object. To minimize the detection of in-elastically scattered photons a

2 cm wide with a length of approximately 20 cm was placed in front of the monitor (see Figure 2.4.3).

Figure 2.4.2 Experimental set-up of the third *in situ* validation test at the Saphir linear accelerator location of CEA Saclay, France. The concrete mock-up is situated at the conveyor, while the instruments will be placed on the platform of the 3Drise system (see also Figure 2.4.3), so that can be positioned and exactly adjusted behind the mock-up.

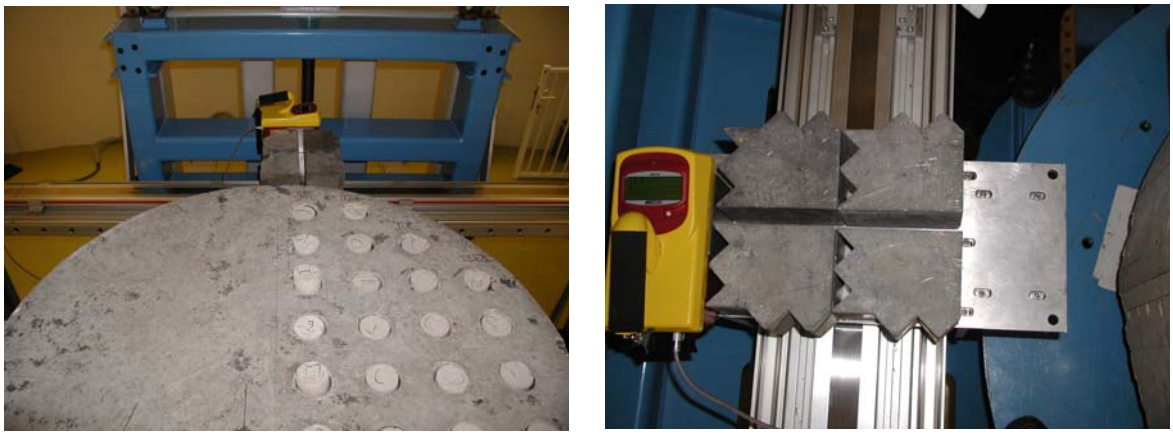

Figure 2.4.3 Overview of the concrete mock-up with the removable cylinders and the adjusted Inovision pressurized ion chamber type 451P-DE-SI. Also details are showed of the 20 cm Pb collimator in front of the Inovision monitor.

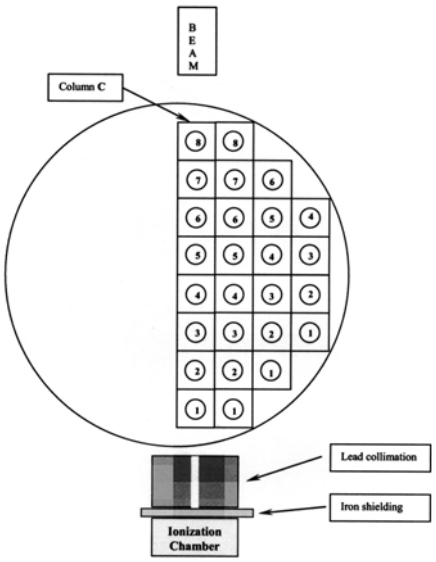

Figure 2.4.4 Schematic overview of the MCNP model applied for the simulations in which the concrete cylinders have been replaced by PE cylinders (column C).

2.4.4.2 Experimental and calculation procedures

Four series of measurements were defined as function of the removable cylinders:

- Cylinders of concrete: the cylinders are randomly removed out of the mock-up.
- Cylinders of concrete and PE: PE cylinders randomly displace the concrete cylinders.
- Cylinders of concrete and NaCl: NaCl cylinders randomly displace the concrete cylinders.
- Cylinders of concrete and KCl: KCl cylinders randomly displace the concrete cylinders.

The Linac was adjusted at three maximum energies respectively 15 MeV, 20 MeV and 30 MeV. The dose rate was sampled at one-second intervals and all data was digitally recorded. This allowed the average dose rate over a period of time to be calculated, thus reducing experimental uncertainty. The measurements were also randomly repeated in order to prove reproducibility.

As stated above the original aim of this validation experiment was to determine the amounts of the neutron poison elements e.g. hydrogen and chlorine present in a mock-up, with a less powerful Linac. Unfortunately the developed constraint transmission methodology (see Section 2.4.3.3) could not be adjusted for these new maximum Linac energies in the due remaining time of this project.

2.4.4.3 MCNP calculations

The scope of the MCNP simulations was to reconstruct the energy distributions of the dose rates stored in the ionization chamber used during the measurement campaign carried out with the Saphir at CEA Saclay [13]. The number of histories for each MCNP run was selected choosing a maximum statistical uncertainty to a single energy interval of 2.5 %.

In Figure 2.4.4 the schematic set-up of the MCNP model representing the experimental set-up is given.

In Figure 2.4.5 it can be seen that the main differences due to the increasing number op PE-cylinders in the mock-up is in the energy range of 1.25 and 6.25 MeV with a maximum around 3 MeV. At higher energies the differences stay in a band between +5 % and –5 %. This can also be explained with the aid of Figure 2.4.1:

- The region between 1.25 MeV and 6.25 MeV is exactly the region in which hydrogen has the most influence on the mass attenuation.
- Above 6.25 MeV the mass attenuation coefficient of hydrogen becomes rapidly less significant and disappears in the noise.
- The *noise* band e.g. between + 5 % and – 5 %, is accordance with the defined errors of the MCNP simulation.

Comparing the results abstracted from Figure 2.4.5 the conclusion can be made that the simulated influence of hydrogen is in good agreement with expectations.

Further, in Figure 2.4.6 the simulated dose rate results are given in arbitrary units of the "Concrete PE" experiment, so that they can easily be compared by the experimental measured dose rate values.

2.4.4.4 Results

The non-attenuated dose rates (e.g. Inovision monitor direct in a non-attenuated beam of the Linac) are too intensive to be measured, thus forbidding the calculation of the mass fractions of the constituent reference elements of the test object. However the measurement on eight empty cylinders (voids) could be used as the non-attenuated measurement. Eight is the maximum number of cylinders that can be removed out of the mock-up. This calculation would also then allow the determination of the mass fractions of the constituents of the cylinders used in the other measurements.

The aim of the experiment has then to be defined as: Assay small changes in the composition of the mock-up by means of collected collimated dose rates and test of the assumption that no in-elastically scattered photons are detected due to the collimation used.

Unfortunately, the experiment was dogged with problems. The NaCl and KCl cylinders became activated; therefore invalidating the data collected using them.

Also the Linac did not function properly at the higher maximum energy settings during some parts of the experiments, restricting the collection of data using these energies.

The results of the experiments with randomly removed concrete cylinders, leaving voids behind, are presented in Figure 2.4.6. Due to the removal of the concrete cylinders the density of the mock-up over the Linac beam is decreasing. The measurement with all 8 concrete cylinders present is assumed to be "I_0". The differences between the reported ratios are small but significant.

In Figure 2.4.7 the results are presented of the experiments by which the concrete cylinders were replaced by polyethylene cylinders. The dose rate increases as function of the number of polyethylene cylinders and it can be seen that these differences between cylinders are significant. The curve is a function of the *density* due to the replacement of concrete by polyethylene and to the increase of the *mass fraction of hydrogen*. To assay the contribution of the mass fraction of hydrogen the data is also presented in Figure 2.4.8 as function of density of the mock-up.

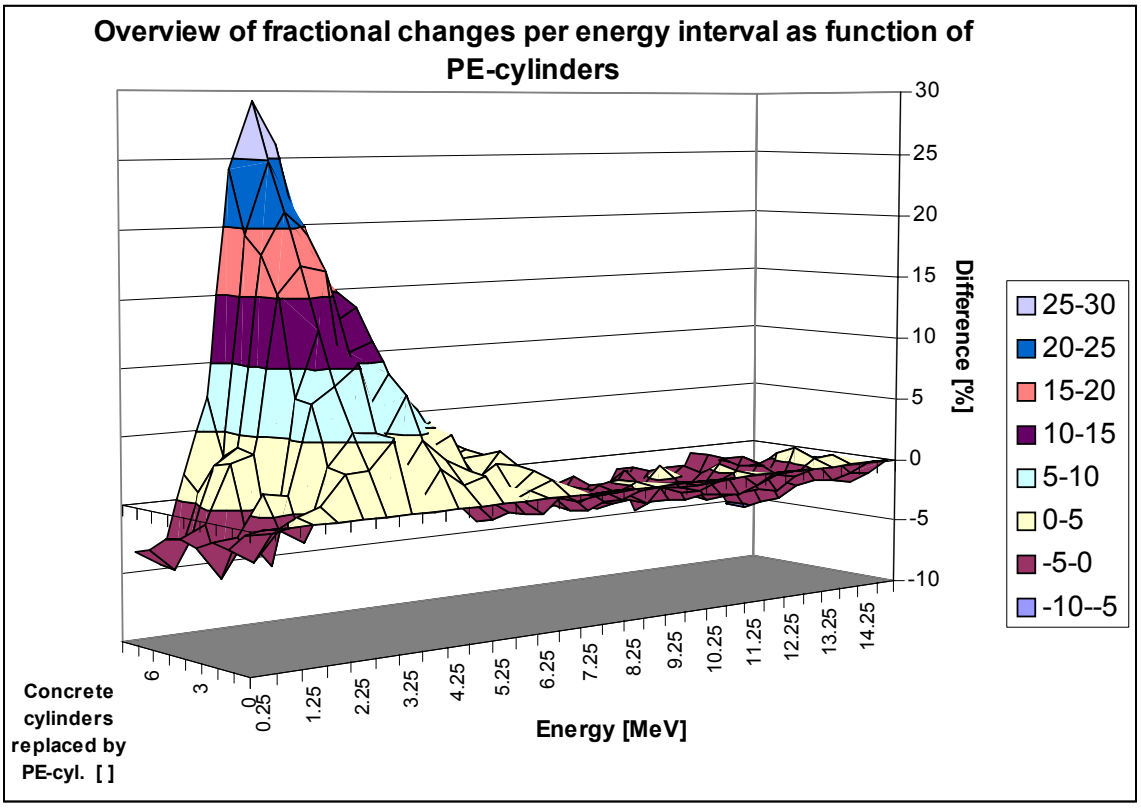

Figure 2.4.5 Overview of the fractional changes per energy interval as a function of the PE cylinders that have replaced concrete cylinders. The changes are expressed as percentage of the begin situation, e.g. no PE cylinders are present in the concrete mock-up.

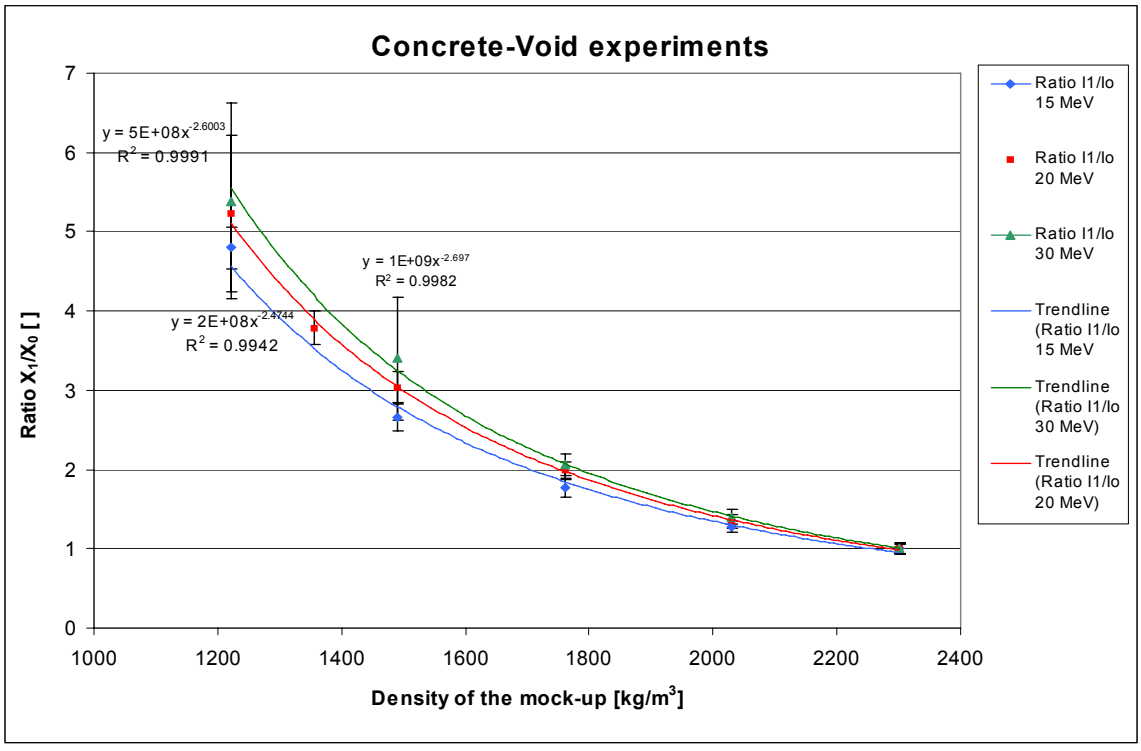

Figure 2.4.6 Overview of the experimental results in which the concrete cylinders have randomly been removed out of the mock-up and leaving voids.

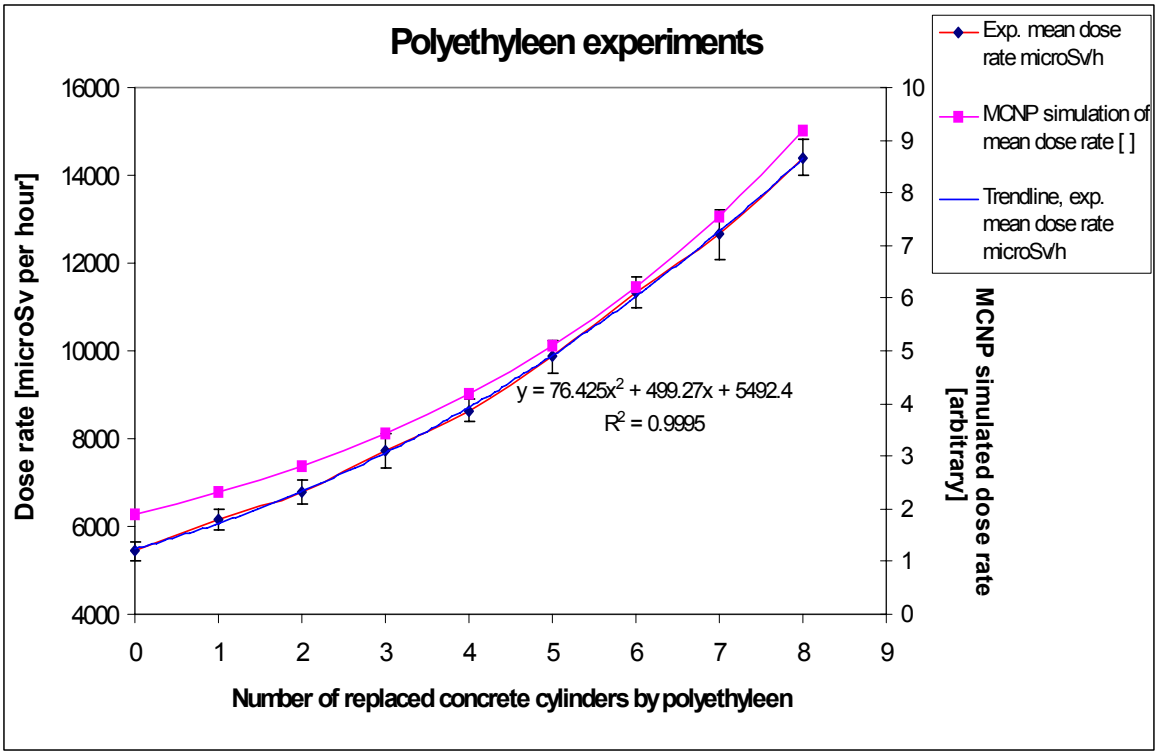

Figure 2.4.7 Overview of experimental and MCNP-simulations of the experiment in which the concrete cylinders have randomly been replaced by PE cylinders in the mock-up.

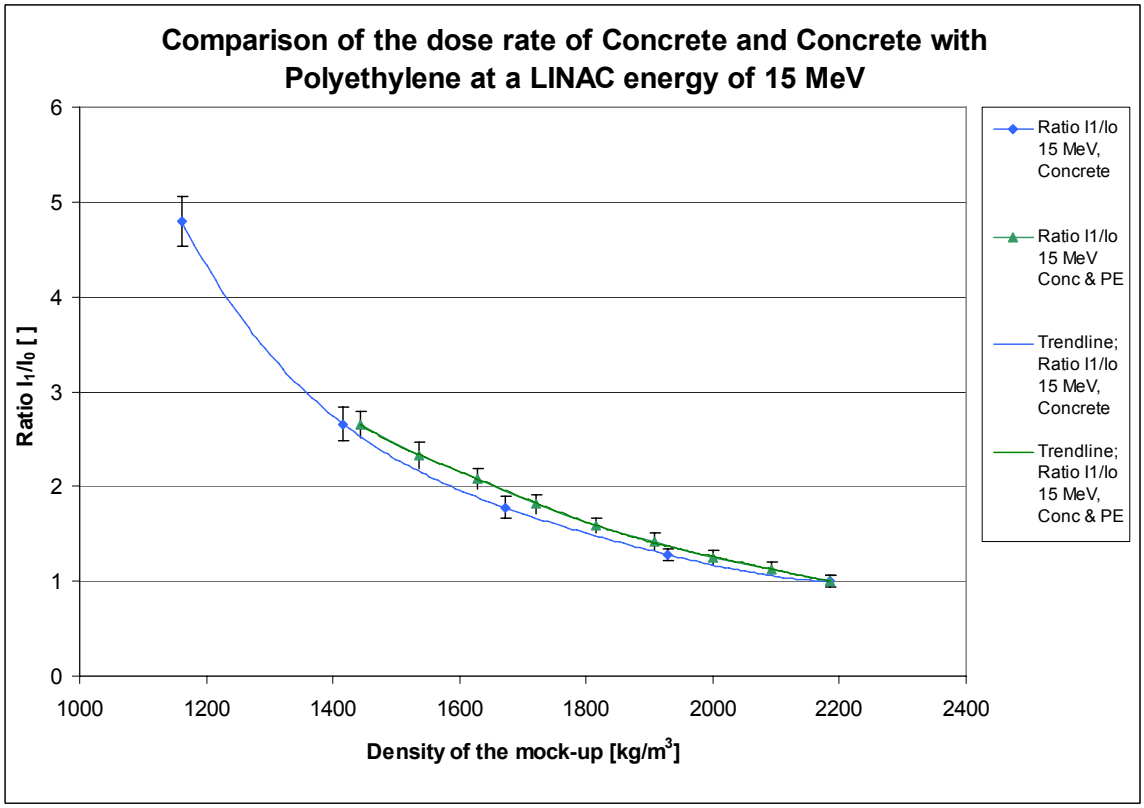

Figure 2.4.8 Comparison of the measured dose rates between concrete & voids and concrete & polyethylene

In Figure 2.4.8 differences are present between the two curves. However, at this moment it is difficult to quantify the absolute value and therefore also the differences between the curves. This is mainly due that the Saphir installation was not stable during both series of experiments. The quantitative values of I_0 (concrete mock-up with all 8 cylinders of concrete) differs about 25 % and the effect on the other experiments of the series could not be estimated.

It can be expected that due to the increase of the mass fraction of hydrogen, the curve of the PE ratios lies be below the curve of the concrete ratios. However, by replacing the concrete by PE cylinders the matrix of the cylinders changes from "Silicon" to a "carbon-hydrogen". Taking into account the information about the mass attenuation coefficients in Figure 2.4.1 it can be concluded that the decrease of the mass attenuation coefficient of the mock-up had a much greater effect than the increase in hydrogen fraction.

2.4.4.5 Conclusions

Due to time constraints, only the series of measurements at 15 MeV maximum energy were simulated. Therefore, the developed algorithm (Section 2.4.3.3) could not be tested. However, the following conclusions, based on the results of the validation experiment and MCNP simulations were reached:

- The applicability of the ionization chamber detector. The applied detector is energy independent, a detector that can discriminate between these energies will be needed for more optimum results.
- MCNP simulations can be used to reconstruct the energy distributions of ionization chamber signals.

2.4.5 Conclusions

A theory for a technique for the characterization of a large-volume waste package using the transmission of Bremsstrahlung photons through the waste package has been presented. The validation experiments have confirmed that differences in the composition of waste packages can be detected and measuring using high-energy photons up to and including 30 MeV. However, the method for measuring the dose rates of photons within defined energy windows needs to be addressed. This may be best achieved using mathematical modeling and computer simulations. Alternatively, energy dispersive detectors will be needed for. Furthermore, mass attenuation coefficients are only documented for certain energies, forcing interpolation if mass attenuation coefficients needed in the matrix characterization of a waste package are not documented.

In conclusion, more research needs to be performed on this topic before a working method for the matrix characterization of large-volume waste packages can be established.

3 Assessment of results and conclusions

The objective of this R&D project was the development of NDA procedures for the QA/QC characterization of large-volume radioactive waste packages, for fissile as well as for non-fissile material present in the waste.

Therefore the performed R&D had to deal with all facets of NDA QA/QC characterization. In Table 3.1 an overview of the work carried out in this project and presented in this report is given, which reflects the complexity of the topics that have been dealt with.

The R&D on the development of suitable nuclear non-destructive technique and procedures to control and characterize fissile material (actinides) have been focused on neutron detection following neutron and photon interrogation by using both a mobile electron linear accelerator called Mini Linatron and a fixed accelerator called Saphir. These R&D investigations have lead to nuclear non-destructive methods that on the one hand permit specifying radiological and emission rays provided by electron linear accelerators and on the other hand localising and quantifying fissile masses inside concrete large waste packages by measuring neutron emission rate produced in the contaminant content following photons and neutrons irradiation provided by electron linear accelerators – the transportable one and the fixed one.

Bremsstrahlung calculations and specifications of the applied Linac are essential to the prediction of the photon transmission assay.

Furthermore, neutron and photon dose rates calculations by MCNP permit establishing the most advantageous location of neutron and photon experimental set-ups to minimize radiation background effect on ^{3}H neutron counters which has to be handled.

The assayed neutron intensity of about 10^{10} $n.s^{-1}$ produced by a Mini Linatron at a maximum energy of 11 MeV is expected to enhance performances for neutron interrogation of some large-volume waste packages. The results of a specific nuclear non-destructive measurement campaign on large concrete inactive packages by using photons and neutrons produced by Mini Linatron as interrogating particles established ^{238}U detection limits of 225, 82 and 12 g for respectively a depth of 0.70, 0.54 and 0.38 m in concrete.

Experiments performed with a fixed Linac and an adjusted maximum energy of 15 MeV resulted in a minimum detectable activity for ^{238}U of about 1.58 g at a depth of 0.48 m in concrete.

Other experiments confirmed the expectation that when ^{238}U is near a more concentrated cluster of hydrogen (simulated by a cluster of polyethylene) there is a non-negligible difference of about 20 % in the response as compared to without a cluster. This means that clusters of hydrogen have to be known in order to decrease the uncertainty in the activity calculations of actinides.

Table 3.1 Overview of work carried out and reported

Topic	Developments		Calculations		Experiments	
	Theory	Measuring devices	MCNP	Others	Tests	Validation
Fissile material						
Passive background	●	●		●	●	
Active background	●	●		●	●	
Active photon interrogation	●	●	●	●	●	●
Active neutron interrogation	●	●	●	●	●	●
Non-fissile material						
Photons		●	●	●	●	●
Tomography	●			●		
Contamination		●			●	
Transmission						
Linear accelerator	●	●	●	●	●	●

To assay the non-fissile content of large-volume waste packages, two measuring devices have been designed. The first system can be classified as point-to-point system (PTP system) and is able to measure accurately with the aid of a collimated HPGe detector the photon flux emitted through the surface at a well-defined location. The second system is classified as a 3-dimensional automatic scanning system (3DAS system) and is able to scan the surface of large-volume waste packages. The 3DAS system can be equipped with multiple detectors and hand monitors and all are in principle non-collimated.

The results achieved by the PTP system and the 3DAS system by the NDA characterization of a heat exchanger were in good agreement. The reported specific activity for ^{60}Co was respectively for the PTP and 3DAS system 6.2 ± 3 MBq, 4.2 ± 2.1 MBq (slow scan) and 5.6 ± 2.8 MBq (fast scan). The uncertainties for both systems are assessed at 50 %.

The activity of the ISO container is assessed at 66 ± 33 MBq for ^{60}Co and at 7.2 ± 3.6 MBq for ^{137}Cs. These calculated values are in a good agreement with the total nuclide specific activities of the ISO container, filled with a consignment consisting of seventy 220-l drums including the applied calibration drum, reported by WQCL (Waste Quality Checking Laboratory, UK). The reported activities are respectively of 41 MBq for ^{60}Co and 6.3 MBq for ^{137}Cs.

The above experience combined with the experience gained by NDA characterization of an ISO container has lead to the set-up of a general guideline – see Annex 7.

Both developed systems, the PTP system and the 3DAS system, can in principle be applied. However the developed 3DAS-system is preferable. This is mainly due to the quality and cost savings for a NDA characterisation and reporting of results of the 3DAS system over the PTP system.

An important point of interest, and this applies to both systems, is how to determine the detector efficiency calibration to be applied. The gained experience in this project is that MCNP is able to provide these efficiency calibrations by simplification of the large-volume waste package and the measurement geometry. It is evident that the adopted simplifications have to be justified.

To support the simplifications, prior knowledge e.g. from accompanying documents will help, but it will often be the case that this information will not be detailed enough, especially for the activity calculation of actinides. Therefore investigations have been set up to study transmission correction techniques for large-volume waste packages, focused on the use of a linear accelerator.

A multi-energy transmission model has been developed, tested and improved by artificial data provided by MCNP calculations. The results showed that with the improved model the differences between hydrogen mass fractions could be calculated within 10 %, however not the true values of the hydrogen mass fractions. Experiments were performed with a fixed Linac at different maximum energies in order to investigate if a non-energy dependent detector could be used to measure the differences in the transmission signal through a concrete mock-up with a diameter of 1.08 m. Results showed that differences could be measured and were reproducible, but extracting properties of the waste matrix could not yet be obtained due to occurrence at the same time of the following effects and problems:

- scattering of Brehmsstrahlung photons in the waste matrix entering the detector with a lower energy
- increase of the mass fraction of hydrogen
- decrease of the mass attenuation coefficient due to matrix changes from concrete to polyethylene
- stability of the Linac between the different series of experiments not good enough.

In conclusion, more research needs to be performed on this topic before a working method for the matrix characterization of large-volume waste packages can be established.

Finally, it can be concluded that a guideline for NDA QA/QC characterization for non-fissile material in large-volume waste packages has been established. Such a guideline for fissile material (actinides) to be applied in routine could not be established, while at laboratory scale such a characterization can be performed for waste packages up to 1000 l.

Concerning matrix characterization and assaying the mass fractions of hydrogen by multi-energy transmission techniques, more research is needed.

4 Acknowledgements

As always, it is a great pleasure to acknowledge the contribution of the many people and institutes involved, directly and indirectly, in this project. The project has benefited enormously from the permissions to perform *in situ* validation experiments at different locations in Europe: at the Olkiluoto nuclear power plant in Finland, in the WQCL laboratory in the United Kingdom, and at the Saphir facility of CEA Saclay in France. Furthermore, the partners in this project team wish to thank the European Commission for its financial support and technical assistance.

5 References

1 A. Lyoussi, A. Dodaro, N. Cherubini; Non-destructive measurement techniques and methodologies for fissile mass detection in frame of the Large Waste Package project; CEA report NT/CEA/DEN/SMTM_LMN : NT 2004-91.

2 L.A. Currie; Limits for qualitative detection and quantitative determination; Analytical Chemistry 40, 586-593 (1968).

3 MCNP; A General Monte Carlo N-Particle Transport Code", LA-12625-M Version 4B, J.F.Briesmeister, Ed., November 1993.

4 N. Cherubini, A. Dodaro; ENEA Mid-term Report - EC Contract FIKW-CT-2000-00027- Development of NDA procedures for the QA/QC characterization of large-volume radioactive waste packages; May 2002, RAD-CAT-NDA(02)03.

5 A. Tiitta, T. Kekki, L.P.M. van Velzen, K. Svoboda, J. Kluson, T. Ćechák, R. Thierry; Non-destructive assessment techniques of non-fissile radioactive material in large-volume waste packages by detection of emitted photons; Topical report of project FIKW-CT-2000-00027; Project Report PRO1/P7017/04, VTT Processes, Finland October 2004.

6 I. Laurette; Reconstruction en géométrie conique: application à l'imagerie d'émission tridimensionnelle (in French); PhD thesis; Université de Nice – Sophia Antipolis, 1997.

7 User manual of the 3D Rise system; TEVEL Technique, June 2003.

8 R. Strange, N. Cherubini, A. Dodaro, A. Lyoussi, F. Laine, G. Mhedi, K. Svoboda, L.P. M. van Velzen: Topical report: Transmission correction techniques for large-volume waste packages; NNC report 11191/TR/011, 2004

9 R.G. Jaeger et al.: Engineering compendium on radiation shielding; Springer-Verlag; 1968.

10 L.P.M. van Velzen; Multi-energy Transmission Correction Technique for large-volume waste packages; NRG report P20606/01.55160/C, 2003

11 N. Cherubini, A. Dodaro; Simulated 5-6 MeV transmission data – EC contract FIKW-CT-2000-00027; Development of NDA procedures for the QA/QC characterization of large-volume radioactive waste packages; Additional Information.

12 N. Cherubini, A. Dodaro; ENEA report on Multi-transmission technique - EC Contract FIKW-CT-2000-00027-; Development of NDA procedures for the QA/QC characterization of large-volume radioactive waste packages; Nov 2002. RAD-CAT-NDA (02)08.

13 A. Lyoussi, J. Romeyer Dherbey, F. Jallu, E. Payan, A. Buisson, G. Nurdin, J. Allano; "Transuranic waste assay detection by photon interrogation and on-line delayed neutron counting"; Nuclear Instruments and Methods in Physics Research B 160 (2000) pp 280-289.

Annexes

A1 Technical characteristics and physical properties of the Mini Linatron

A2 Technical characteristics and physical properties of the Saphir facility

A3 Actual loading scheme of the ISO container in the second *in situ* validation experiment

A4 Fast scan of the total ISO container with a *non-collimated* HPGe detector; cobalt-60

A5 Fast scan of the total ISO container with a *non-collimated* HPGe detector; caesium-137

A6 Transmissions correction techniques for large-volume radioactive waste packages; calculation results

A7 NDA procedure for the QA/QC characterization of non-fissile material in large-volume waste packages

A1 Technical characteristics and physical properties of the Mini Linatron

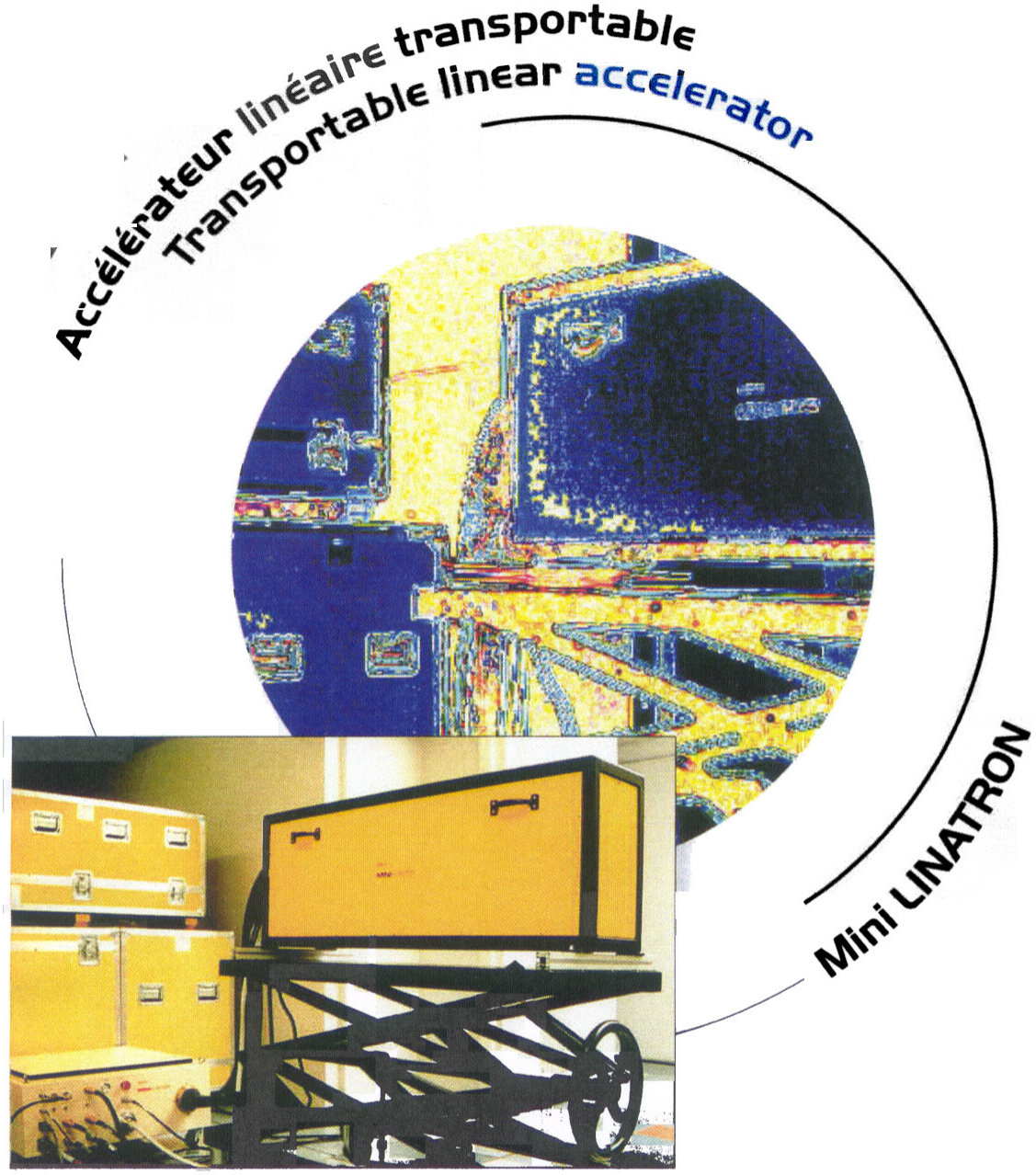

CEB

DÉPARTEMENT DÉTECTION ET PROTECTION NUCLÉAIRE

SERVICE MOYENS D'ESSAIS ET CONTRÔLES

Energie des électrons accélérés : 6, 9 ou 11 MeV

Energy of accelerated electrons : 6, 9 or 11 MeV

Le Mini LINATRON est un moyen utilisé pour répondre aux besoins suivants :

The Mini LINATRON is used for :

- Evaluation des effets des rayonnements nucléaires,
- Evaluation des facteurs de protection gamma des véhicules blindés,
- Calibration des systèmes dosimétriques,
- Méthodes d'interrogation nucléaire photonique,
- Aide à l'expertise pour radiographie industrielle.

- The evaluation of nuclear radiation effects,
- The evaluation of gamma protection factors of armored fighting vehicles,
- The calibration of dosimetric systems,
- The photonuclear interrogation methods,
- The appraisal help for industrial radiography.

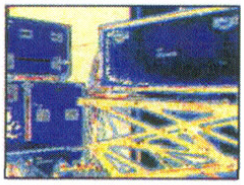

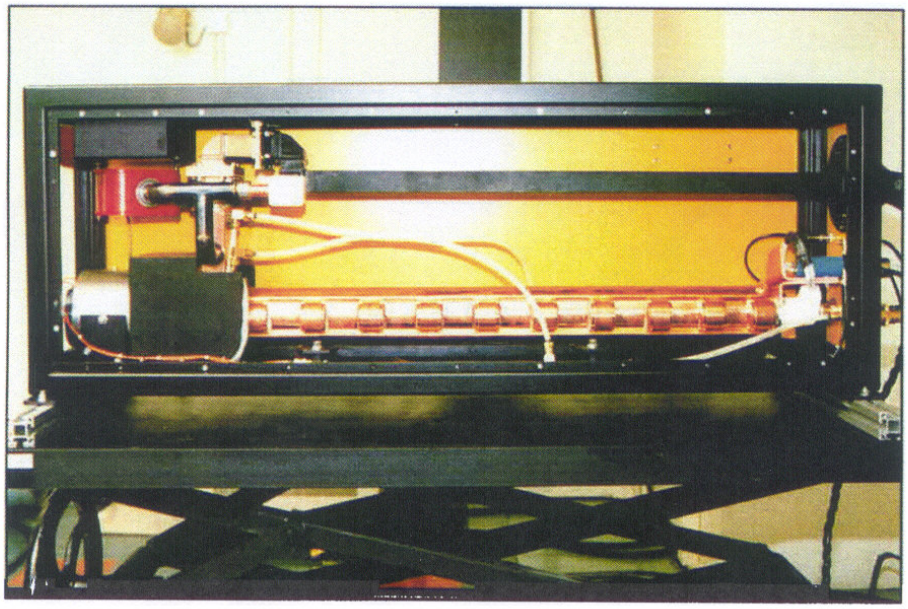

ACCÉLÉRATEUR ACCELERATOR

Caractéristiques principales :

Main specifications :

- Niveaux d'énergie (MeV) : 6, 9 et 11
- Durée de l'impulsion (µs) : 4,5
- Récurrence des impulsions (Hz) : 10 à 300
- Cible de rayonnement de freinage : 1,8 mm W+2,54 mm Cu
- Débit de dose gamma maximum (Gy/mn à 1m) : 23

- Energy levels (MeV) : 6, 9 and 11
- Pulse duration (µs) : 4.5
- Pulse rate (Hz) : 10 to 300
- Bremsstrahlung target : 1.8 mm W+2.54 mm Cu
- Gamma maximum dose rate (Gy/mn at 1m) : 23

MINI LINATRON DANS L'ESPACE SEPTANT À VIROULOU (46)

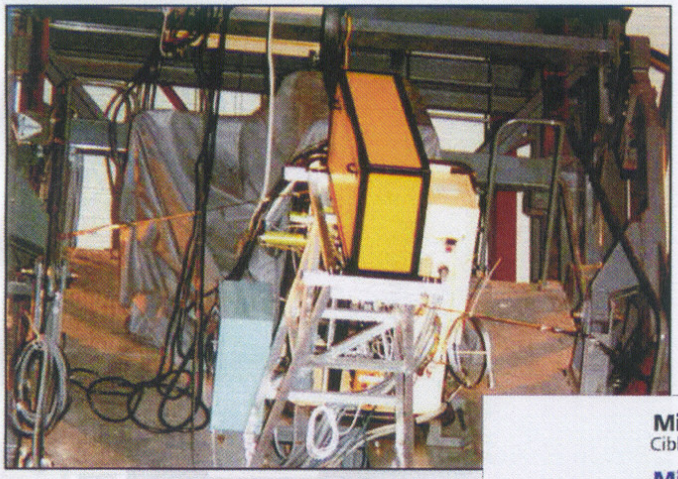

MINI LINATRON IN VIROULOU (46) ROOM

Points particuliers :

Particular points :

- Commande à distance jusqu'à 200 m,
- Collimateur 30°.
- Control from a distance up to 200 m
- Collimator of 30°

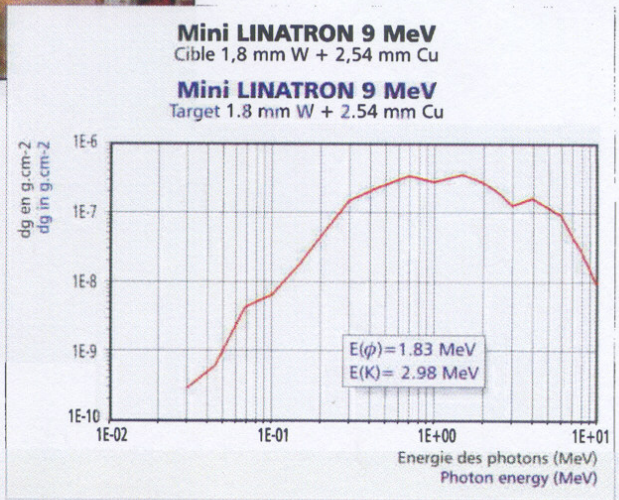

SPECTRE ISSU DE LA CIBLE

BREMSSTRAHLUNG SPECTRUM

A2 Technical characteristics and physical properties of the Saphir facility

Geometrical description of Saphir facility

Figure A2.1 gives an overview of the Saphir facility. The height (from ground floor to ceiling) is about 3.5 m.

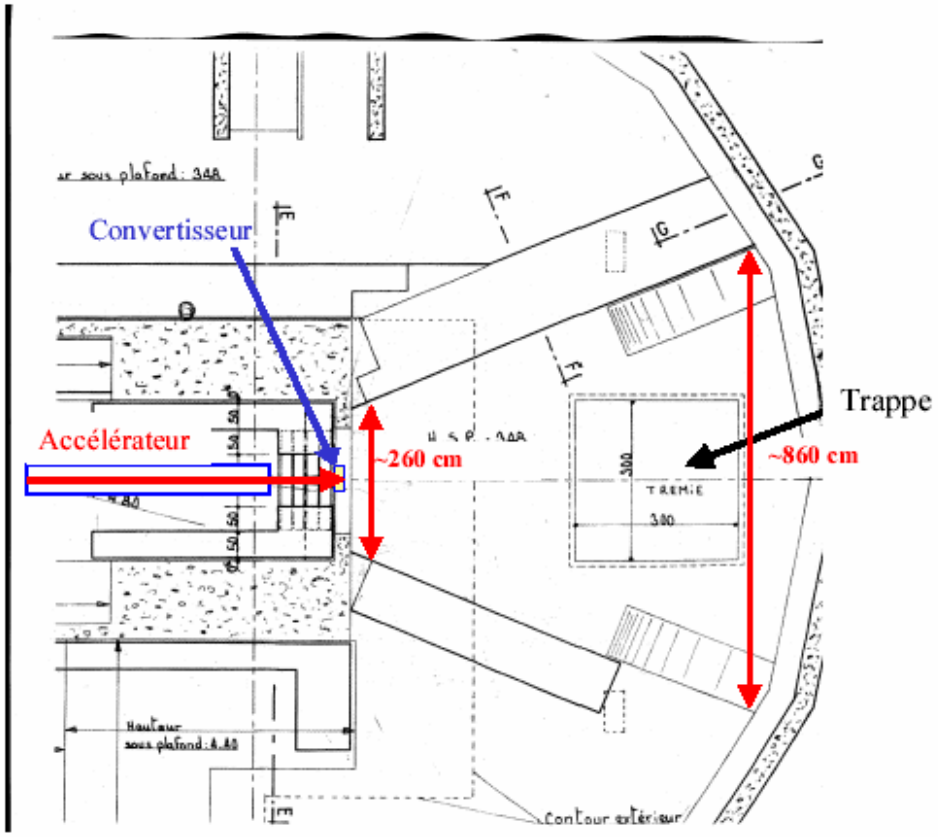

Figure A2.1 Overview of the Saphir facility

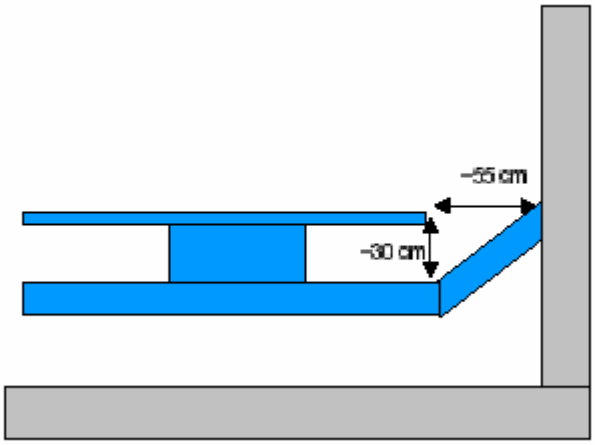

Figure A2.2 Conveyor description

Photons and neutrons flux estimation

Photons and neutrons transport calculations have been carried out by using specific CEA programs. Results are given for the position located 1 m forward from the tungsten (W) braking target. The thickness of the tungsten target is 0.02 m. The Linac pulse duration is constant and adjusted to 2.5 µs, pulse rate constant to 6.25 Hz and pulse current intensity constant to 100 mA for these calculations. The applied electron energy was 15 MeV.

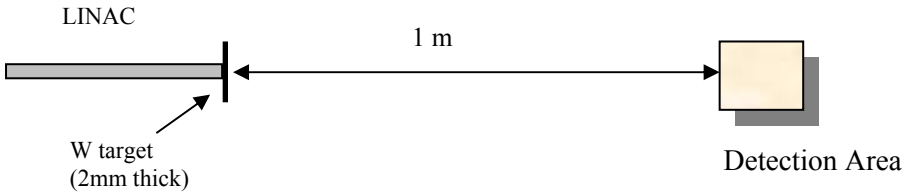

Three specific layout configurations have been considered in the framework of these photon and neutron flux calculations:

1. Target of W.
2. Target of W + lead collimator (as shown below).

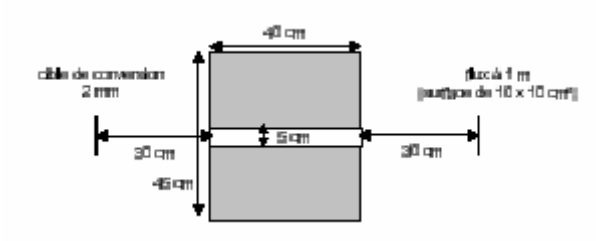

3. Target of W + lead collimator embedded with borates polyethylene ($(CH_2)_n$ + 5 % of boron)

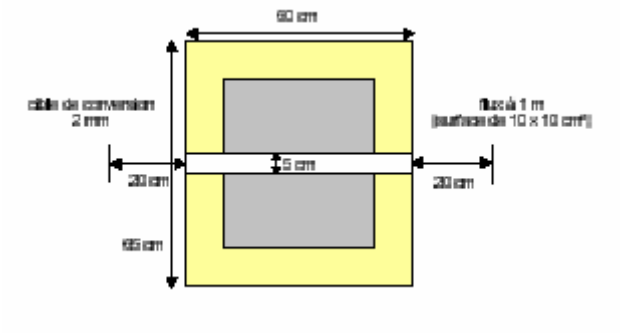

Neutron fluxes

Table A2.1 gives calculated neutrons flux for the three configurations as described above.

Configuration	Neutron flux at 1 m ($s^{-1}.cm^{-2}$)
W + Pb +CH2	$9{,}70.10^{3}$
W + Pb	$1{,}64.10^{4}$
W	$1{,}35.10^{4}$

Table A2.1: Neutron flux

It is important to notice that there is an other neutron component due to (γ,n) reaction on waste and it matrix.

Photon fluxes

Table A2.2 gives calculated photon fluxes for the three configurations as described above.

Energy (MeV)	**Photon flux at 1 m ($s^{-1}.cm^{-2}$)**		
	W + Pb +CH2	W + Pb	W
1	$6{,}78.10^{8}$	$7{,}28.10^{8}$	$1{,}22.10^{8}$
2	$3{,}90.10^{8}$	$4{,}23.10^{8}$	$6{,}87.10^{8}$
3	$2{,}14.10^{8}$	$2{,}47.10^{8}$	$4{,}35.10^{8}$
4	$1{,}26.10^{8}$	$1{,}20.10^{8}$	$2{,}29.10^{8}$
5	$1{,}06.10^{8}$	$1{,}14.10^{8}$	$1{,}86.10^{8}$
6	$8{,}59.10^{7}$	$8{,}80.10^{7}$	$1{,}46.10^{8}$
7	$5{,}96.10^{7}$	$6{,}12.10^{7}$	$1{,}11.10^{8}$
8	$4{,}53.10^{7}$	$5{,}00.10^{7}$	$8{,}71.10^{7}$
9	$4{,}17.10^{7}$	$4{,}27.10^{7}$	$7{,}06.10^{7}$
10	$3{,}55.10^{7}$	$3{,}56.10^{7}$	$6{,}27.10^{7}$
11	$2{,}75.10^{7}$	$2{,}86.10^{7}$	$4{,}83.10^{7}$
12	$2{,}35.10^{7}$	$2{,}46.10^{7}$	$4{,}32.10^{7}$
13	$1{,}73.10^{7}$	$1{,}62.10^{7}$	$2{,}74.10^{7}$
14	$1{,}15.10^{7}$	$1{,}20.10^{7}$	$2{,}22.10^{7}$
15	$7{,}57.10^{6}$	$8{,}75.10^{6}$	$1{,}41.10^{7}$
Total	$\mathbf{1{,}87.10^{9}}$	$\mathbf{2{,}00.10^{9}}$	$\mathbf{3{,}39.10^{9}}$

Table A2.2: Photon flux

A3 Actual loading scheme of the ISO container in the second *in situ* validation experiment

Bottom layer of ISO container

Top layer of ISO container

Figure A1.1 Overview of the actual loading scheme of the ISO container

A4 Fast scan of the ISO container with a *non-collimated* HPGe detector; cobalt-60

Drum 123 has been replaced by
WQCL calibration drum number 13

Iso-, statistically filtered data plots and
fractional plots of collected and statistically filtered data

Measuring time 2 seconds per spectrum

Cobalt-60 (1332 keV)

Figure A4.1 Iso-plots of normalised at the maximum of collected data.

Figure A4.2 Iso-plots of collected data.

Figure A4.3 Iso-plots of statistically filtered data.

Figure A4.4 Fractional plots of net data.

Figure A4.5 Fractional plots of statistically filtered data.

Figure A4.1	Iso-plots; normalised at maximum of collected data of ^{60}Co (fast scan *without collimator* and measuring time 2 s per spectrum).

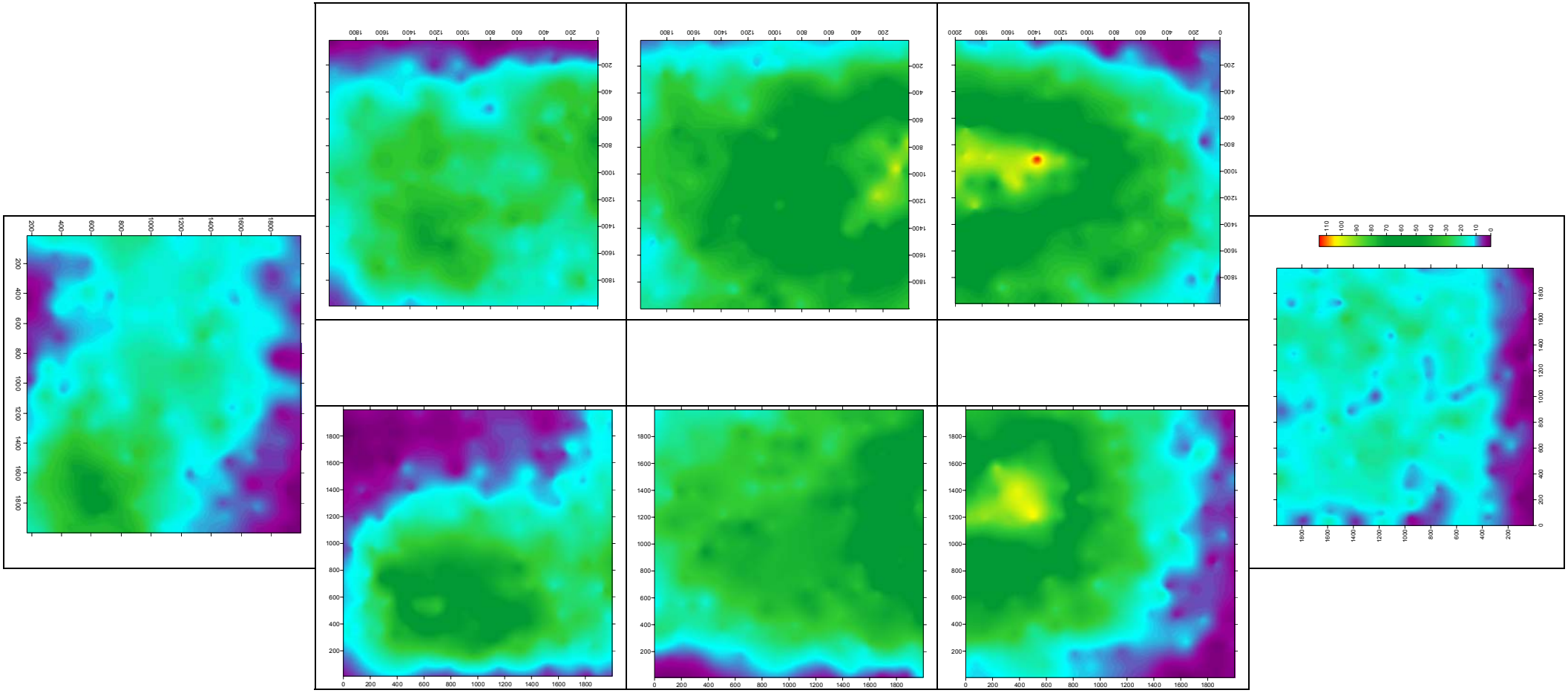

Scan results of ISO-0039 at the front side.	Scan results of ISO-0042 (top) and ISO-0038 (bottom).	Scan results of ISO-0043 (top) and ISO-0035 (bottom).	Scan results of ISO-0045 (top) and ISO-0033 (bottom).	Scan results of ISO-0030 at the backside (doors).

Figure A4.2	Iso-plots of collected data of ^{60}Co (not normalized; fast scan *without collimator* and measuring time 2 s per spectrum).

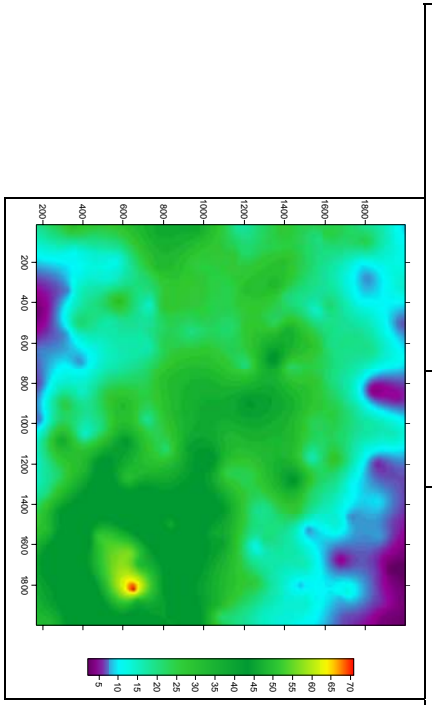

Scan results of ISO-0039 at the front side.

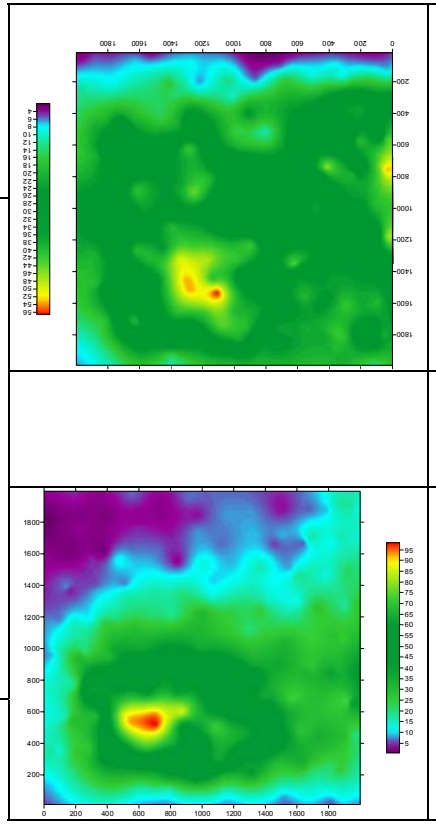

Scan results of ISO-0042 (top) and ISO-0038 (bottom).

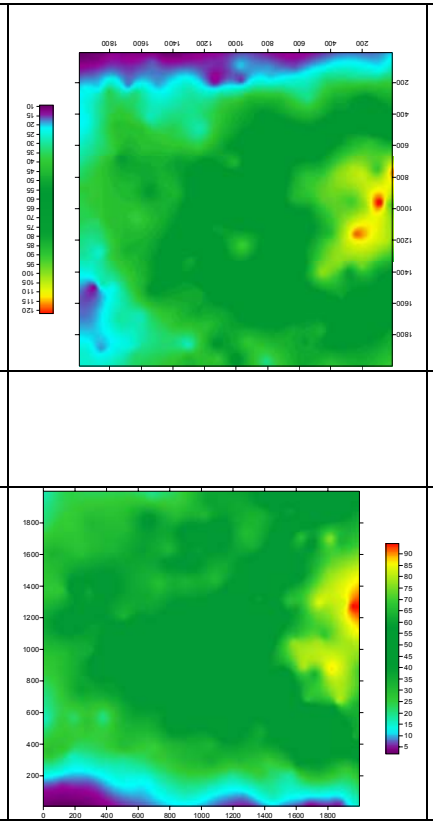

Scan results of ISO-0043 (top) and ISO-0035 (bottom).

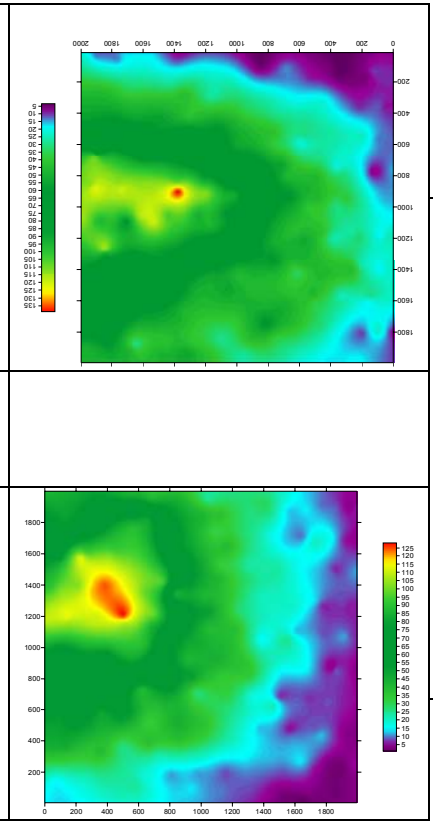

Scan results of ISO-0045 (top) and ISO-0033 (bottom).

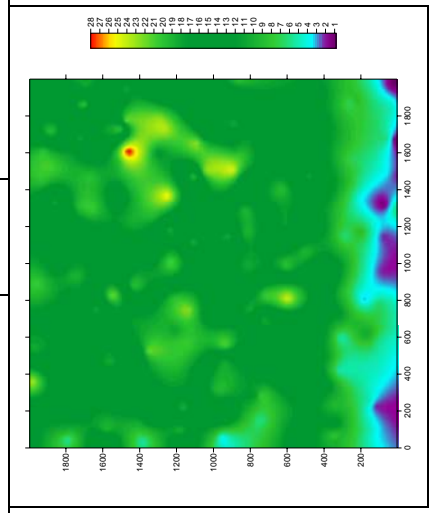

Scan results of ISO-0030 at the backside (doors).

Figure A4.3	Iso-plots of statistically filtered data of ^{60}Co (fast scan *without collimator* and measuring time 2 s per spectrum).

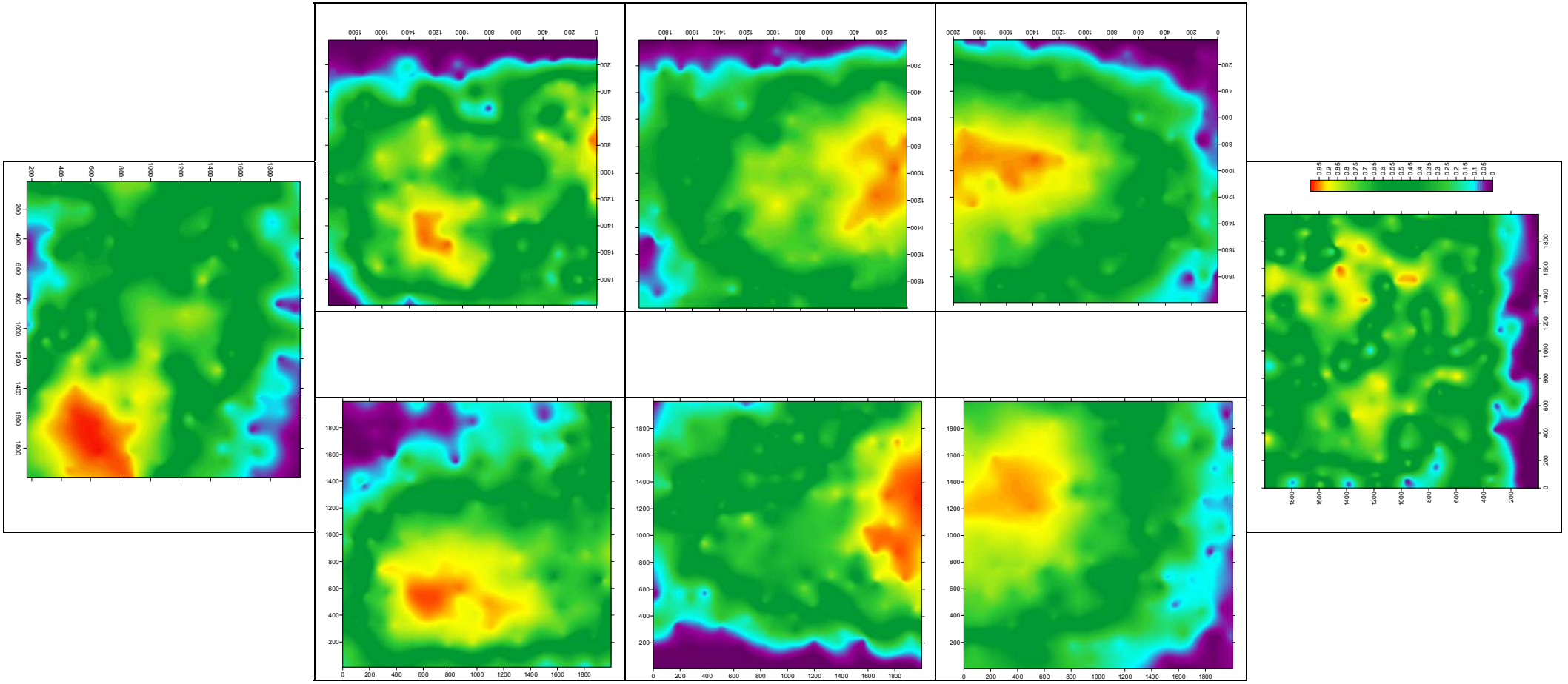

Scan results of ISO-0039 at the front side.	Scan results of ISO-0042 (top) and ISO-0038 (bottom).	Scan results of ISO-0043 (top) and ISO-0035 (bottom).	Scan results of ISO-0045 (top) and ISO-0033 (bottom).	Scan results of ISO-0030 at the backside (doors).

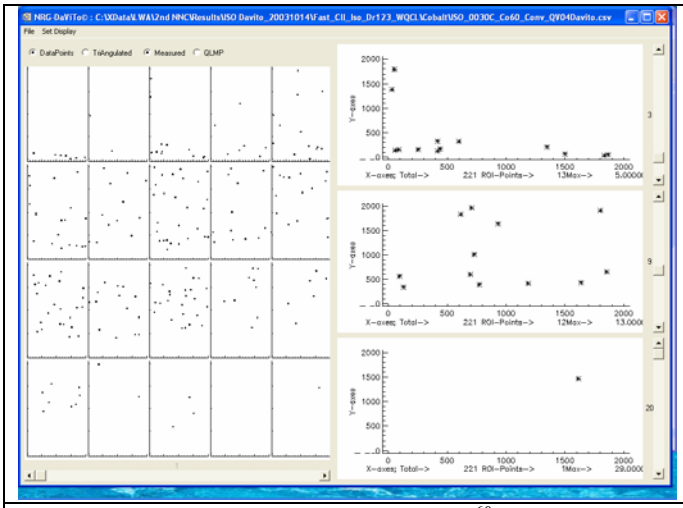

Figure A4.4 A Fractional net area data of ^{60}Co 1332 keV, run IS0-0031; details 2, 7 and 20.

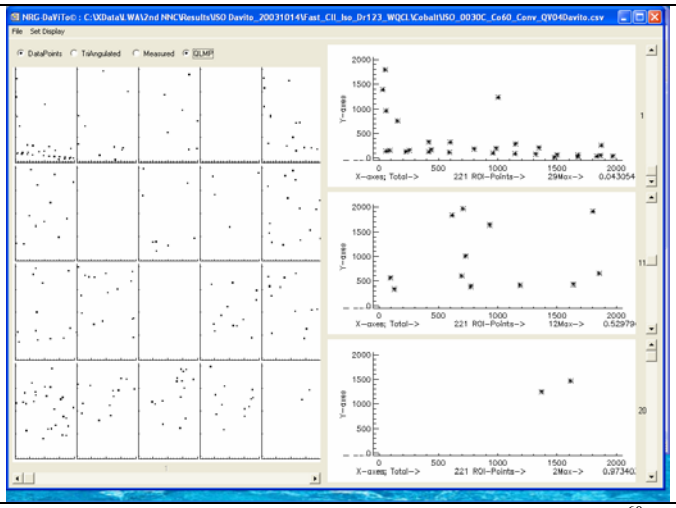

Figure A4.5 A Fractional statistically filtered data of ^{60}Co 1332 keV, run IS0-0030; details 1, 16 and 19.

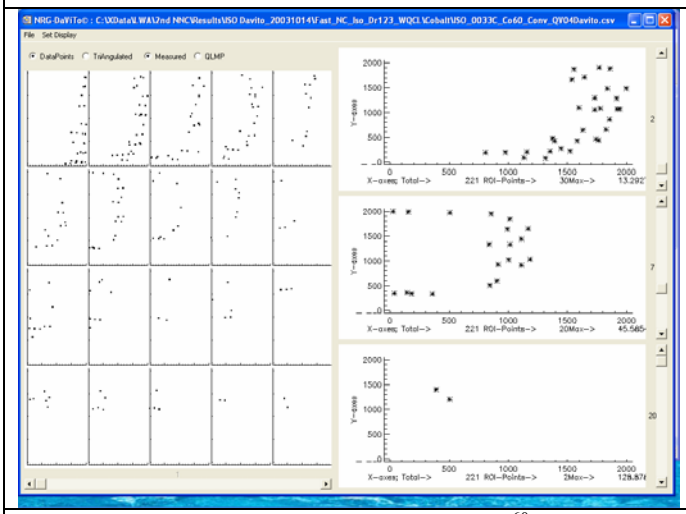

Figure A4.4 B Fractional net area data of ^{60}Co 1332 keV, IS0-0033; details 2, 7 and 20.

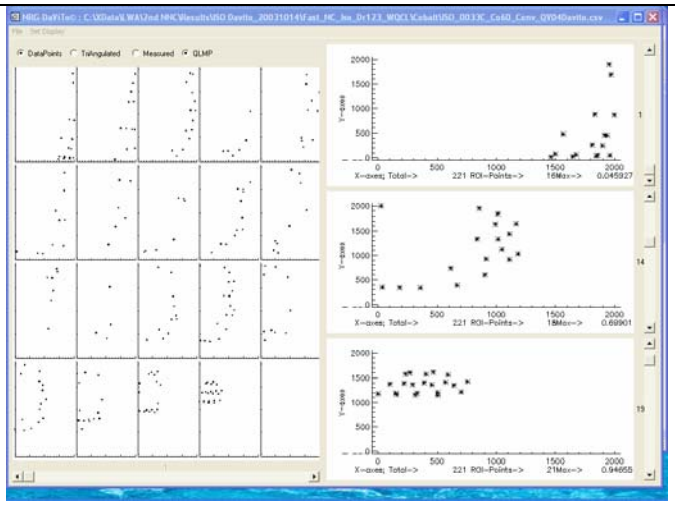

Figure A4.5 B Fractional statistically filtered data of ^{60}Co 1332 keV, run IS0-0033; details 1, 14 and 19.

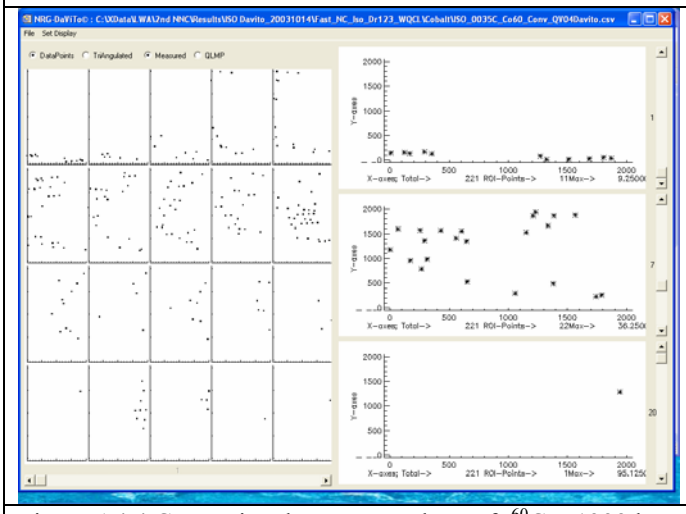

Figure A4.4 C Fractional net area data of ^{60}Co 1332 keV, IS0-0035; details 1, 7 and 20.

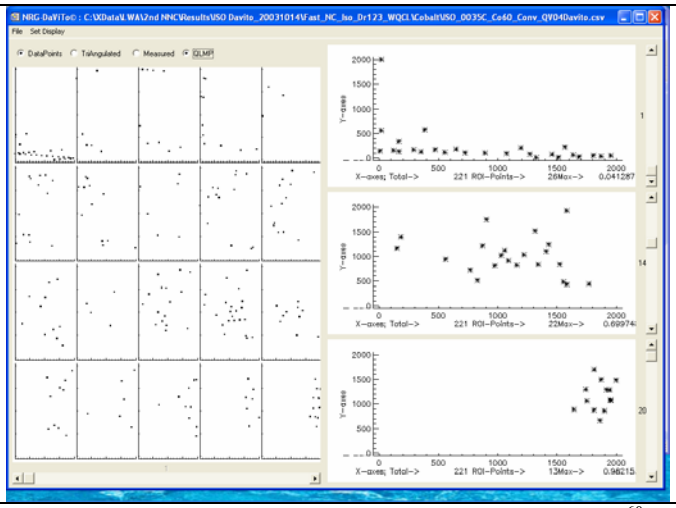

Figure A4.5 C Fractional statistically filtered data of ^{60}Co 1332 keV, run IS0-0035; details 1, 14 and 20.

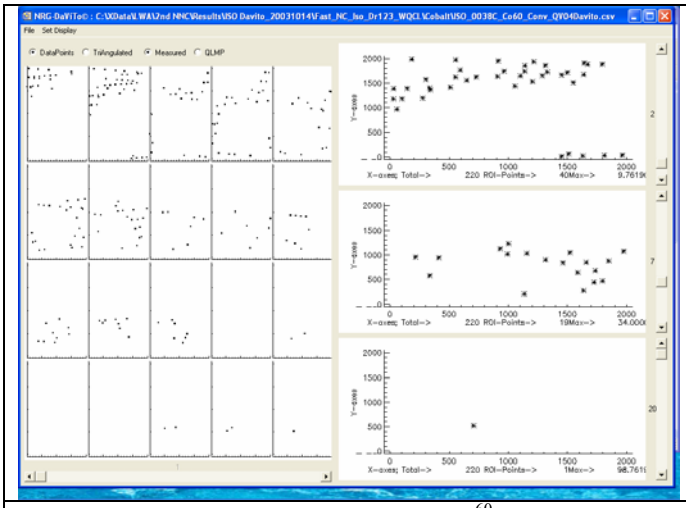

Figure A4.4 D Fractional net area data of ^{60}Co 1332 keV, run IS0-0038; details 2, 7 and 20.

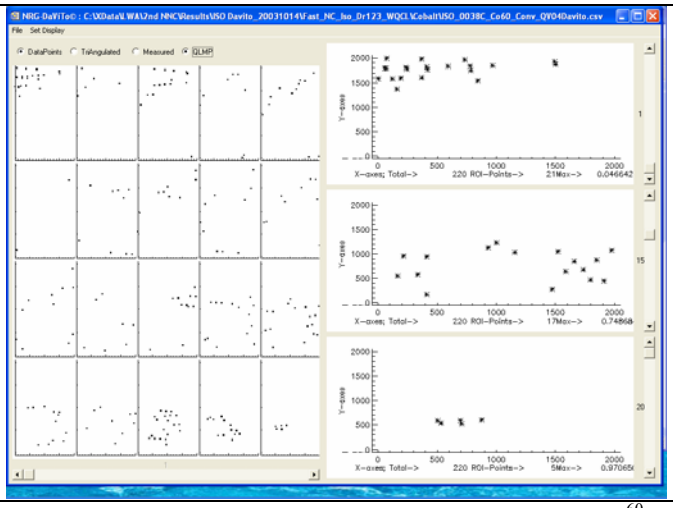

Figure A4.5 D Fractional statistically filtered data of ^{60}Co 1332 keV, run IS0-0038; details 1, 15 and 20.

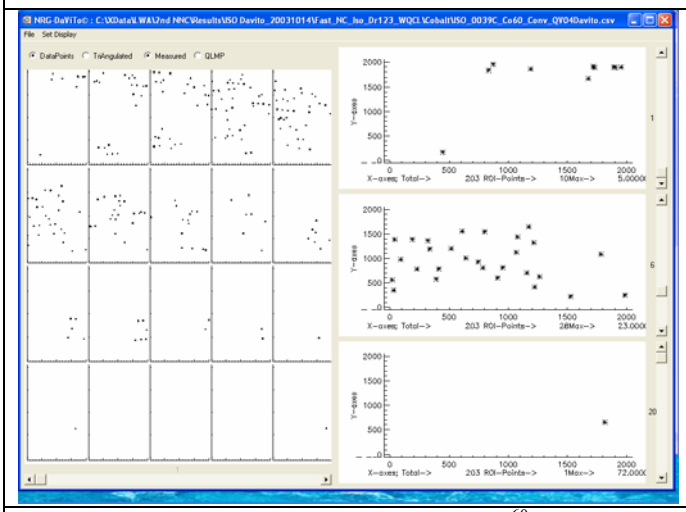

Figure A4.4 E Fractional net area data of ^{60}Co 1332 keV, IS0-0039; details 1, 6 and 20.

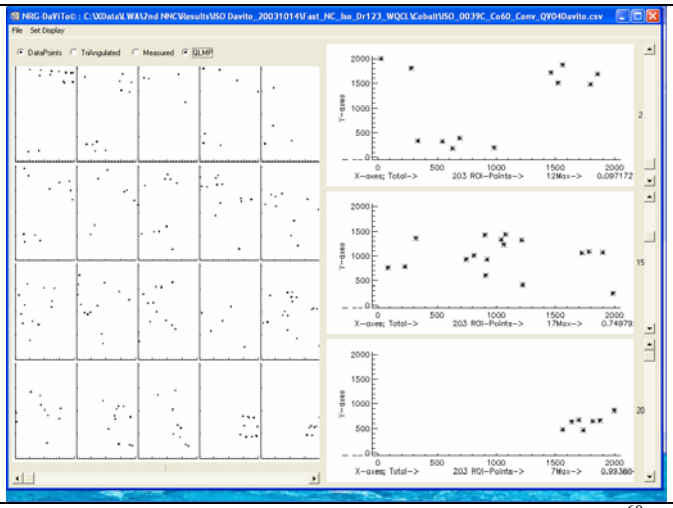

Figure A4.5 E Fractional statistically filtered data of ^{60}Co 1332 keV, run IS0-0039; details 2, 15 and 20.

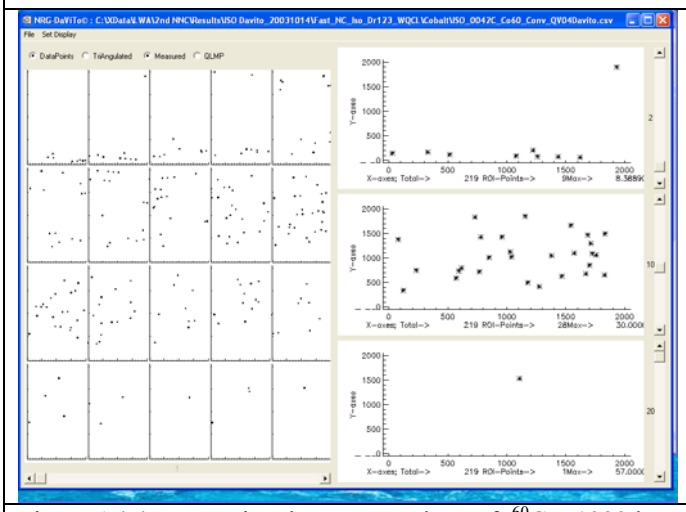

Figure A4.4 F Fractional net area data of ^{60}Co 1332 keV, IS0-0042; details 2, 10 and 20.

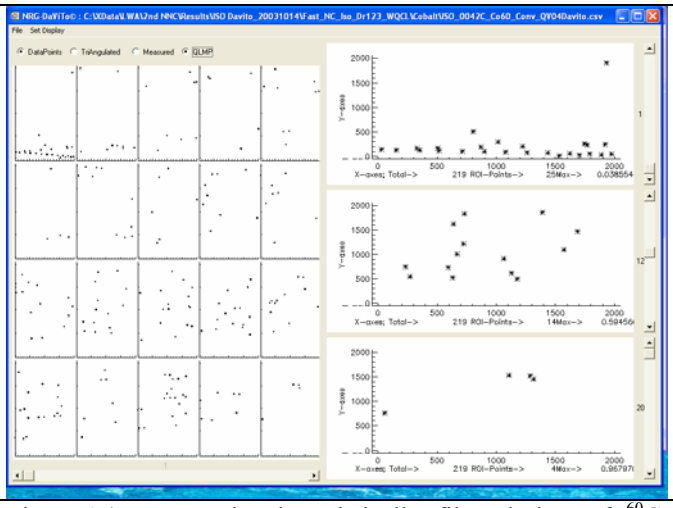

Figure A4.5 F Fractional statistically filtered data of ^{60}Co 1332 keV, run IS0-0042; details 1, 12 and 20.

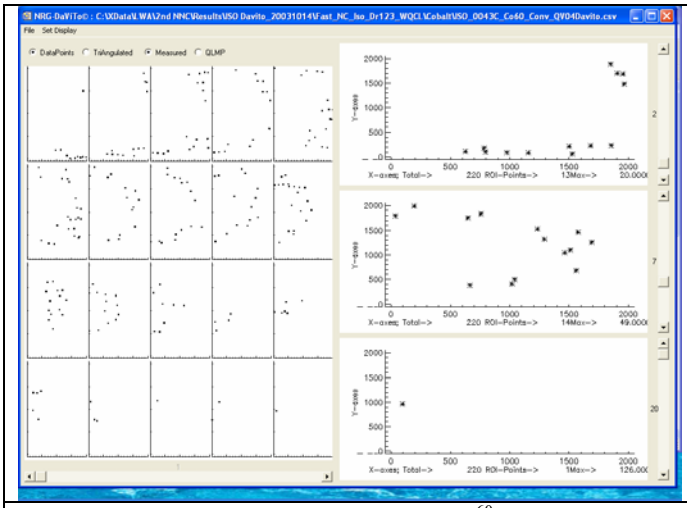

Figure A4.4 G Fractional net area data of ^{60}Co 1332 keV, run IS0-0043; details 2, 7 and 20.

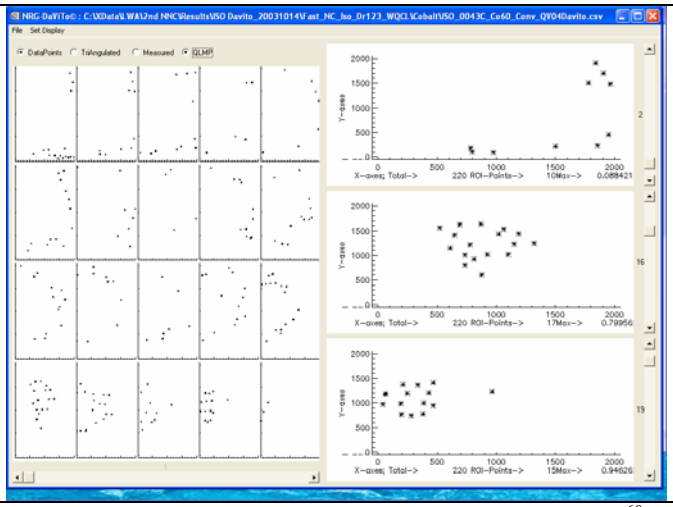

Figure A4.5 G Fractional statistically filtered data of ^{60}Co 1332 keV, run IS0-0043; details 2, 16 and 19.

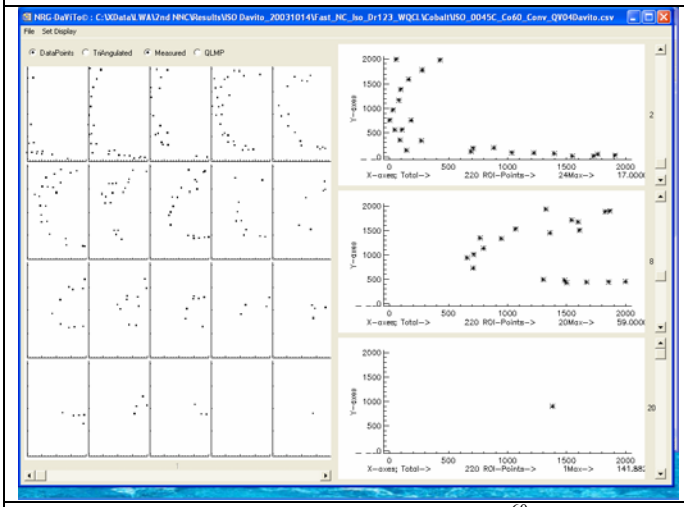

Figure A4.4 H Fractional net area data of ^{60}Co 1332 keV, IS0-0045; details 2, 8 and 20.

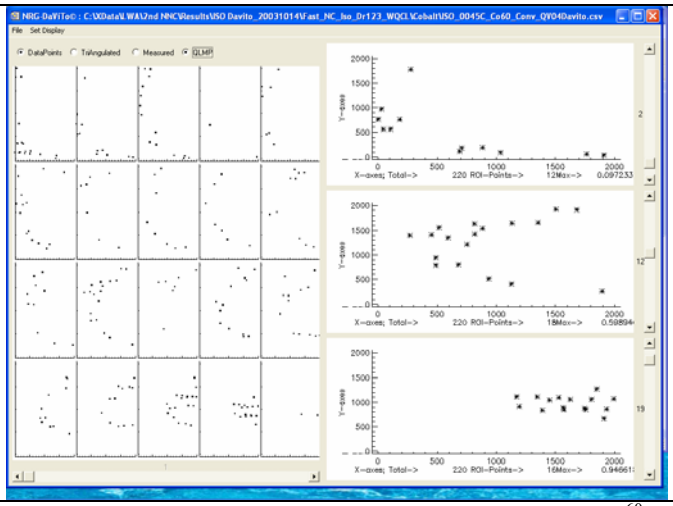

Figure A4.5 H Fractional statistically filtered data of ^{60}Co 1332 keV, run IS0-0045; details 2, 12 and 19.

A5 Fast scan of the ISO container with a *non-collimated* HPGe detector; caesium-137

Drum 123 has been replaced by
WQCL calibration drum number 13

Iso-, statistically filtered data plots and
fractional plots of collected and statistically filtered data

Measuring time 2 seconds per spectrum

Caesium-137 (661 keV)

Figure A5.1 Iso-plots of normalised at the maximum of collected data.

Figure A5.2 Iso-plots of collected data.

Figure A5.3 Iso-plots of statistically filtered data.

Figure A5.4 Fractional plots of net data.

Figure A5.5 Fractional plots of statistically filtered data.

Figure A5.1	Iso-plots; normalised at maximum of collected data of ^{137}Cs (fast scan *without collimator* and measuring time 2 s per spectrum).

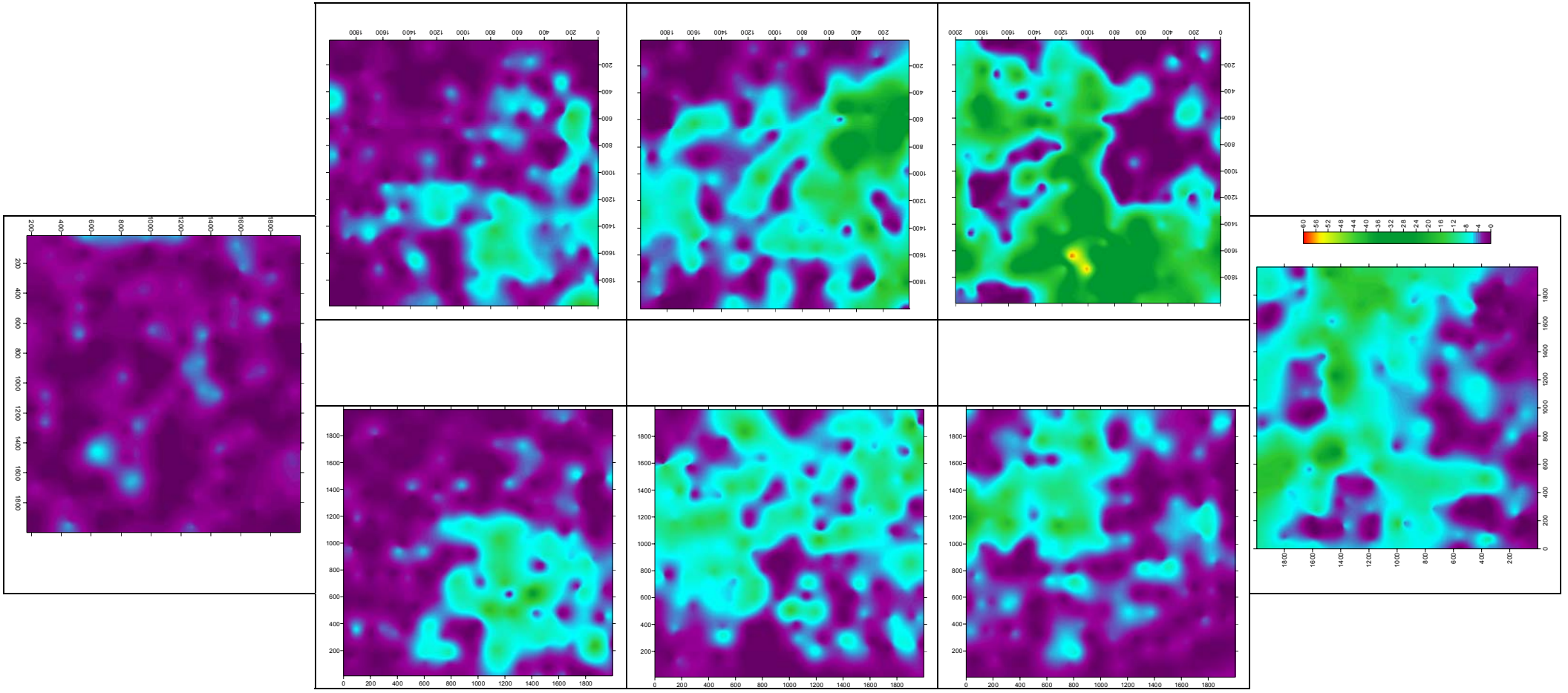

Scan results of ISO-0039 at the front side.	Scan results of ISO-0042 (top) and ISO-0038 (bottom).	Scan results of ISO-0043 (top) and ISO-0035 (bottom).	Scan results of ISO-0045 (top) and ISO-0033 (bottom).	Scan results of ISO-0030 at the backside (doors).

Figure A5.2	Iso-plots of collected data of ^{137}Cs (not normalized; fast scan *without collimator* and measuring time 2 s per spectrum).

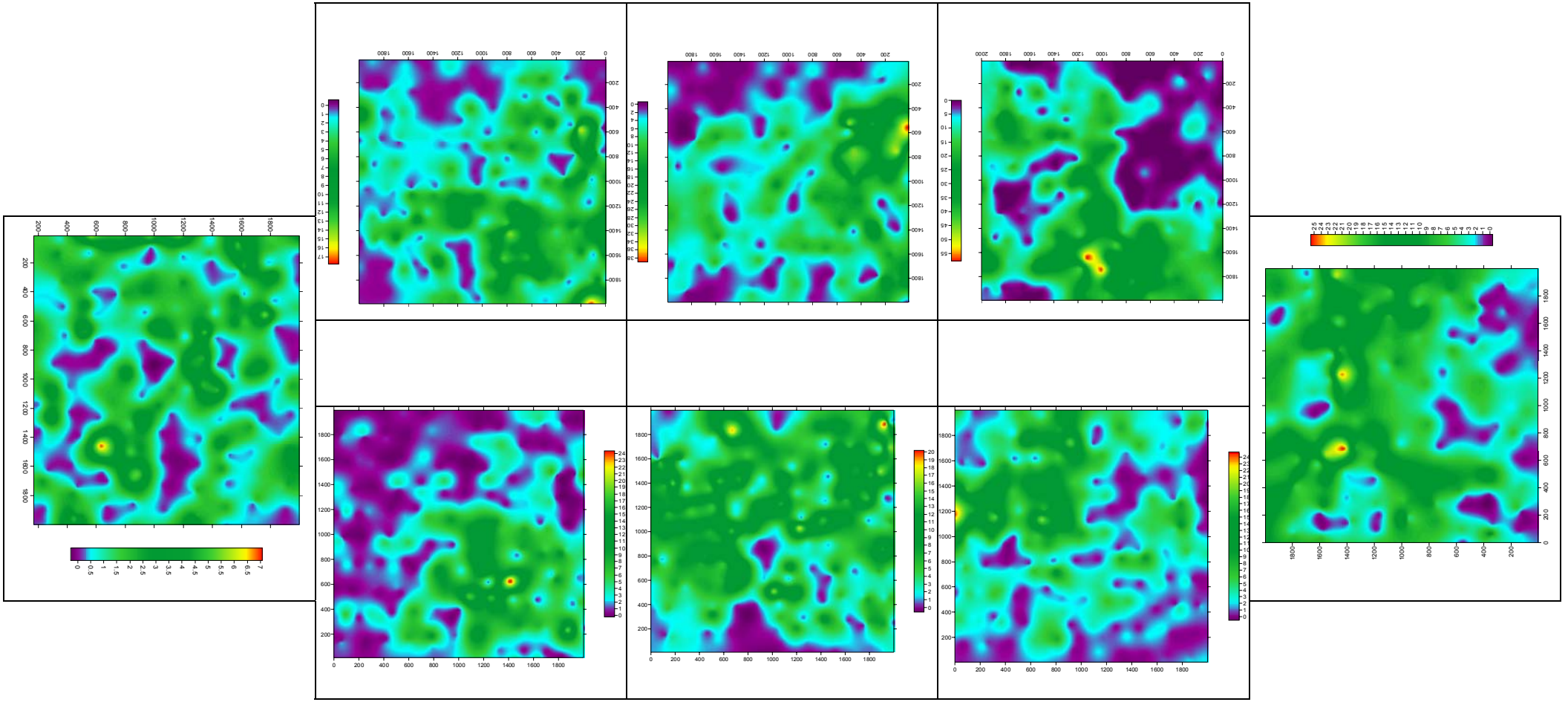

Scan results of ISO-0039 at the front side.	Scan results of ISO-0042 (top) and ISO-0038 (bottom).	Scan results of ISO-0043 (top) and ISO-0035 (bottom).	Scan results of ISO-0045 (top) and ISO-0033 (bottom).	Scan results of ISO-0030 at the backside (doors).

Figure A5.3	Iso-plots of statistically filtered data of ^{137}Cs (fast scan *without collimator* and measuring time 2 s per spectrum).

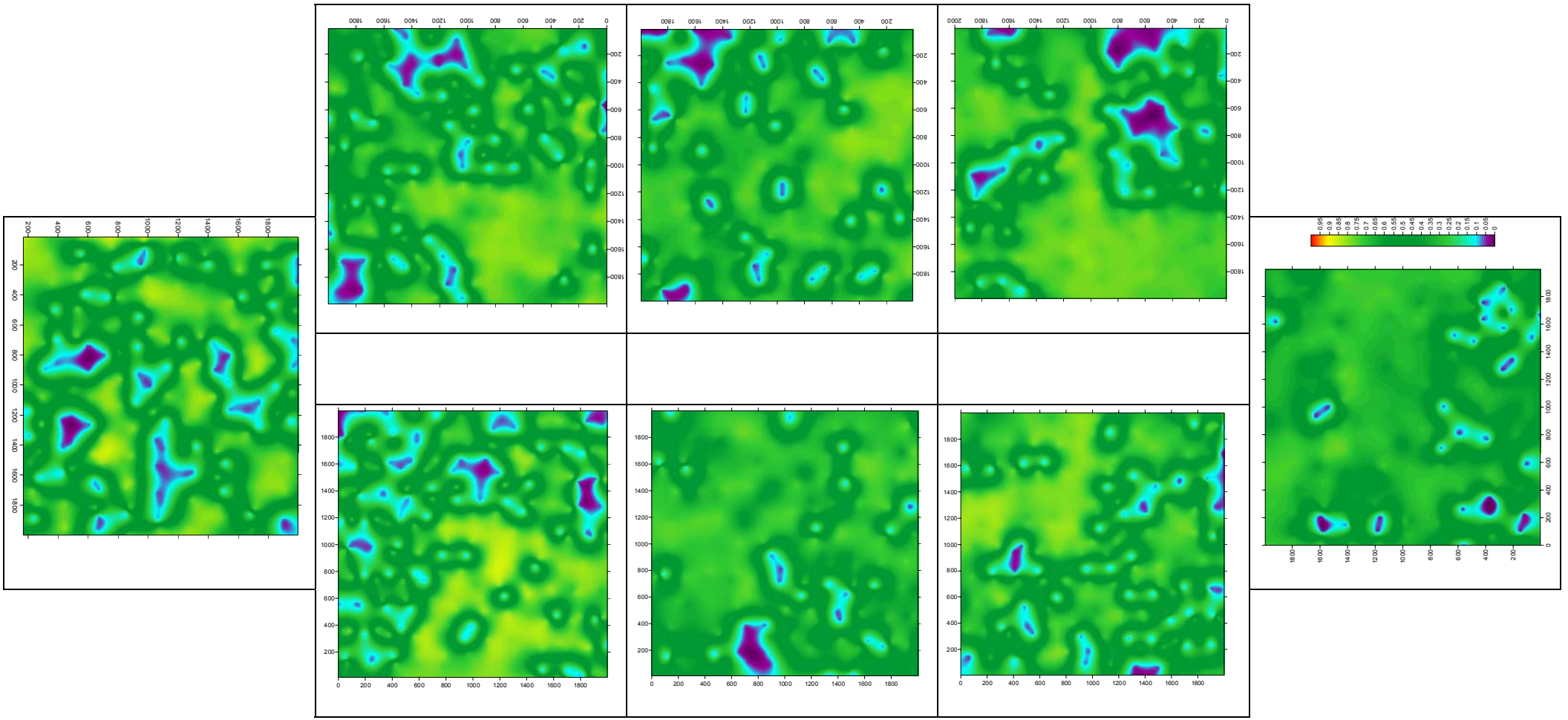

Scan results of ISO-0039 at the front side.	Scan results of ISO-0042 (top) and ISO-0038 (bottom).	Scan results of ISO-0043 (top) and ISO-0035 (bottom).	Scan results of ISO-0045 (top) and ISO-0033 (bottom).	Scan results of ISO-0030 at the back-side (doors).

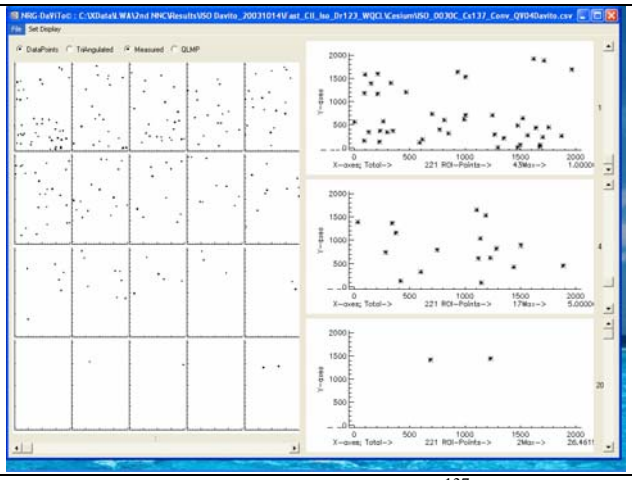

Figure A5.4 A Fractional net area data of ^{137}Cs 661 keV, run IS0-0030; details 1, 7 and 20.

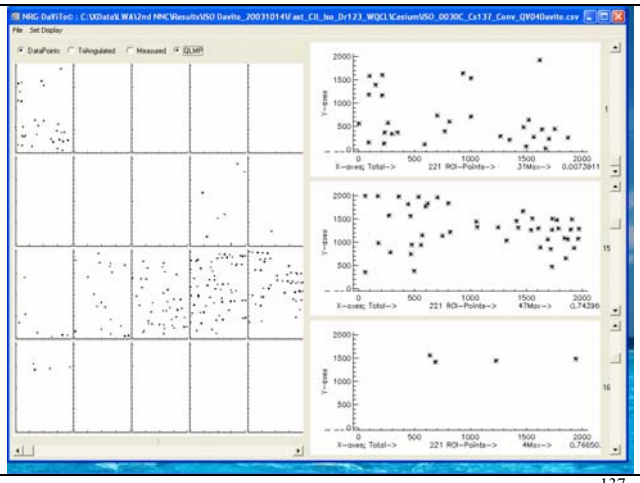

Figure A5.5 A Fractional statistically filtered data of ^{137}Cs 661 keV, run IS0-0030; details 1, 13 and 16.

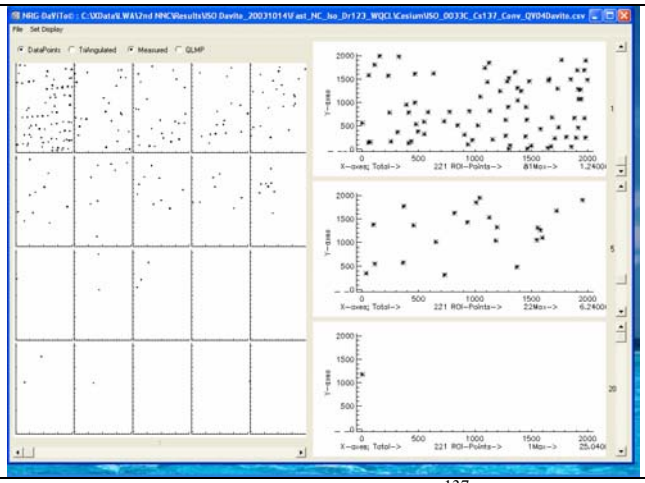

Figure A5.4 B Fractional net area data of ^{137}Cs 661 keV, IS0-0033; details 1, 5 and 20.

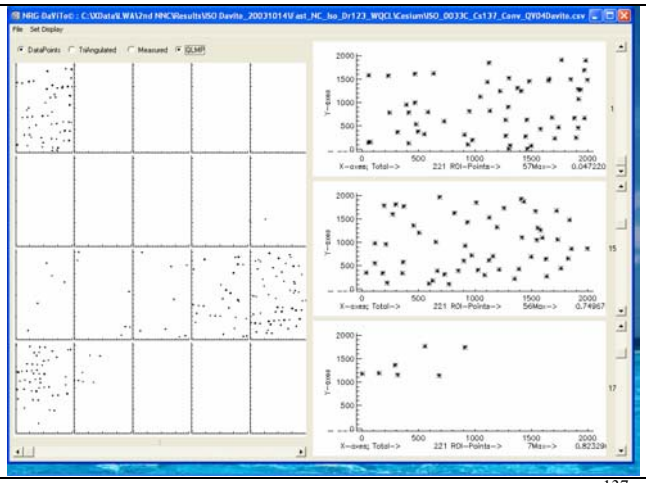

Figure A5.5 B Fractional statistically filtered data of ^{137}Cs 661 keV, run IS0-0033; details 1, 15 and 17.

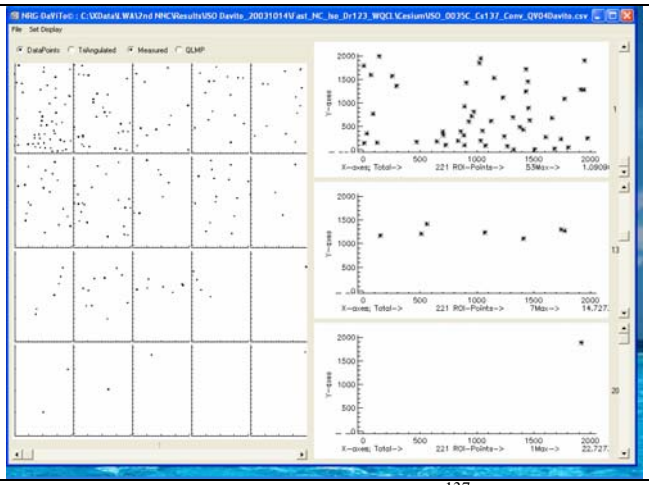

Figure A5.4 C Fractional net area data of ^{137}Cs 661 keV, IS0-0035; details 1, 13 and 20.

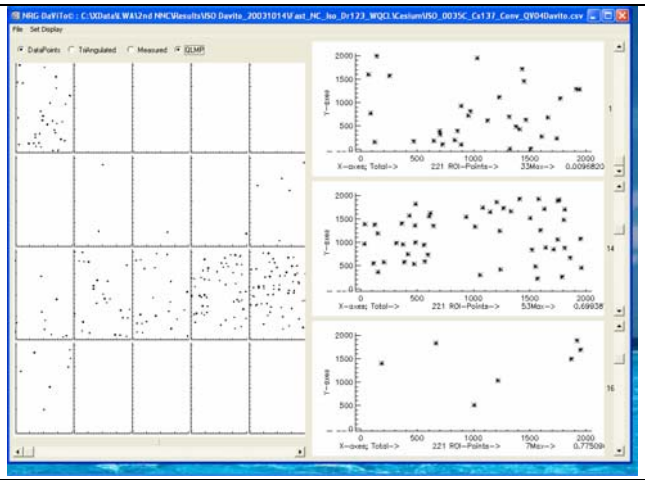

Figure A5.5 C Fractional statistically filtered data of ^{137}Cs 661 keV, run IS0-0035; details 1, 14 and 16.

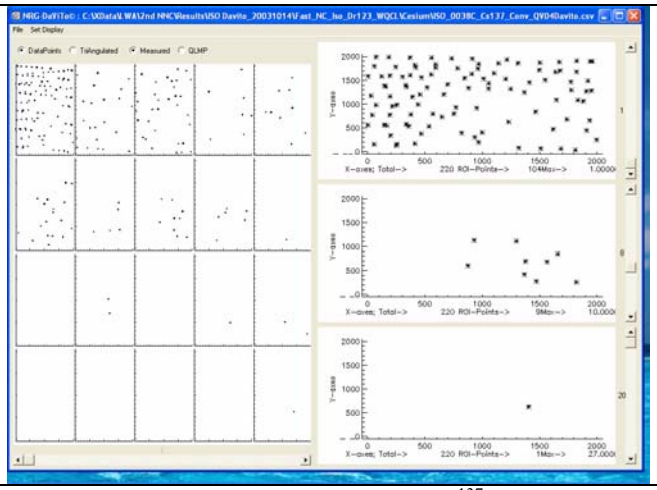

Figure A5.4 D Fractional net area data of ^{137}Cs 661 keV, run IS0-0038; details 1, 8 and 20.

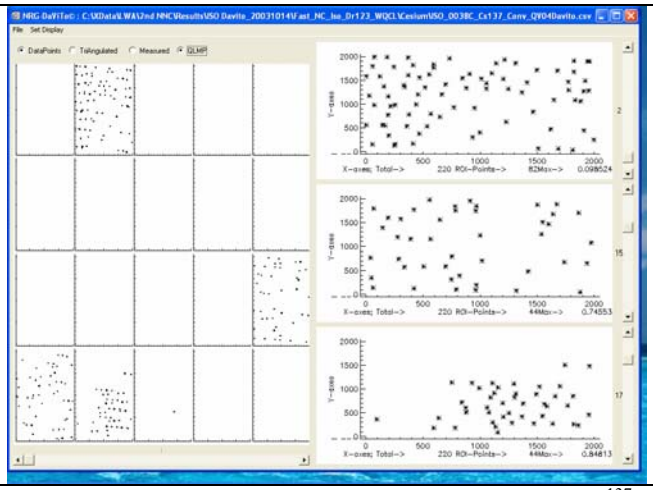

Figure A5.5 D Fractional statistically filtered data of ^{137}Cs 661 keV, run IS0-0038; details 2, 15 and 17.

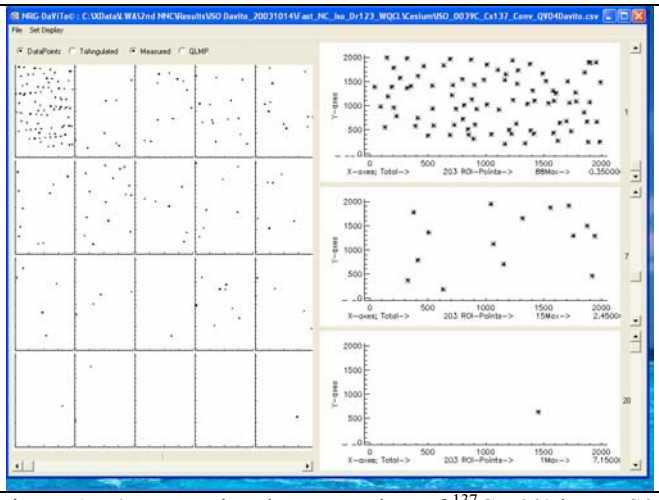

Figure A5.4 E Fractional net area data of ^{137}Cs 661 keV, IS0-0039; details 1, 7 and 20.

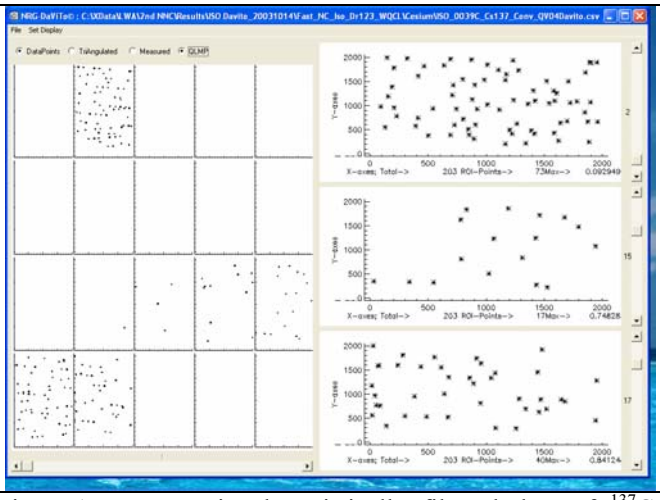

Figure A5.5 E Fractional statistically filtered data of ^{137}Cs 661 keV, run IS0-0039; details 2, 15 and 17.

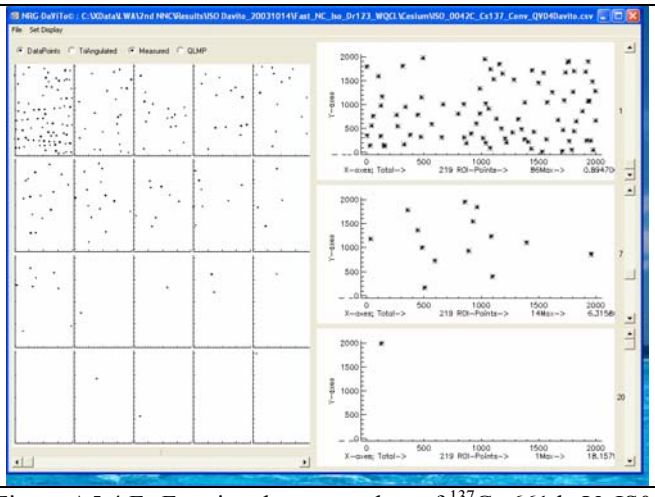

Figure A5.4 F Fractional net area data of ^{137}Cs 661 keV, IS0-0042; details 1, 7 and 20.

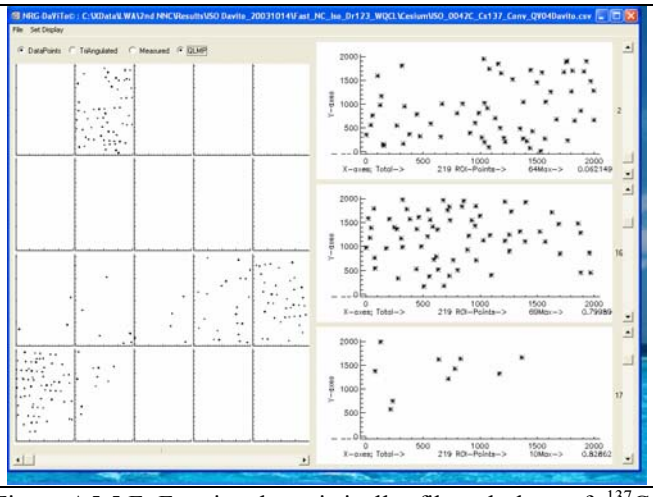

Figure A5.5 F Fractional statistically filtered data of ^{137}Cs 661 keV, run IS0-0042; details 2, 16 and 17.

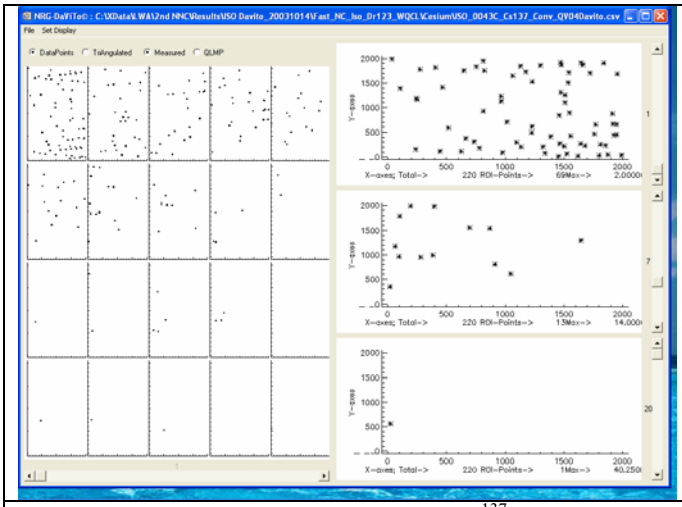

Figure A5.4 G Fractional net area data of ^{137}Cs 661 keV, run IS0-0043; details 1, 7 and 20.

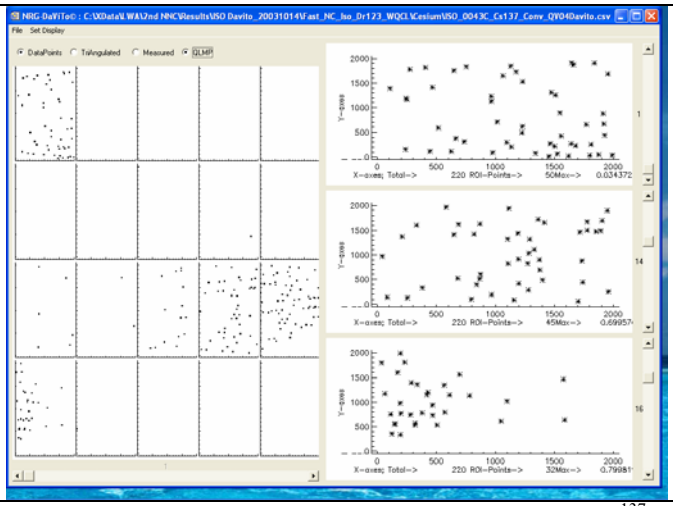

Figure A5.5 G Fractional statistically filtered data of ^{137}Cs 661 keV, run IS0-0043; details 1, 14 and 16.

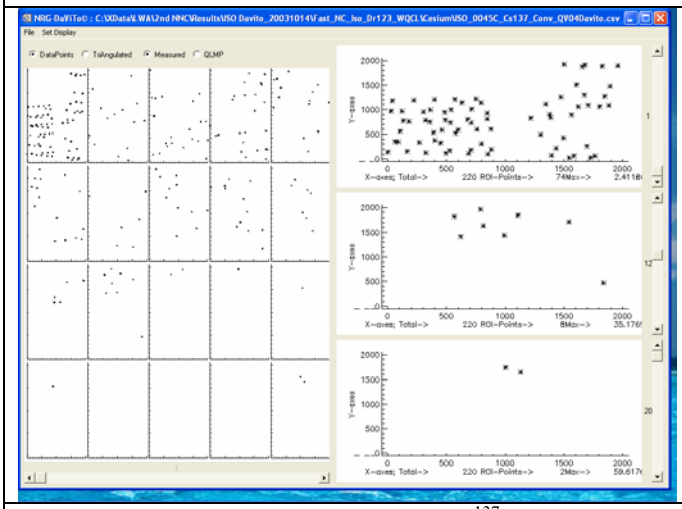

Figure A5.4 H Fractional net area data of ^{137}Cs 661 keV, IS0-0045; details 1, 12 and 20.

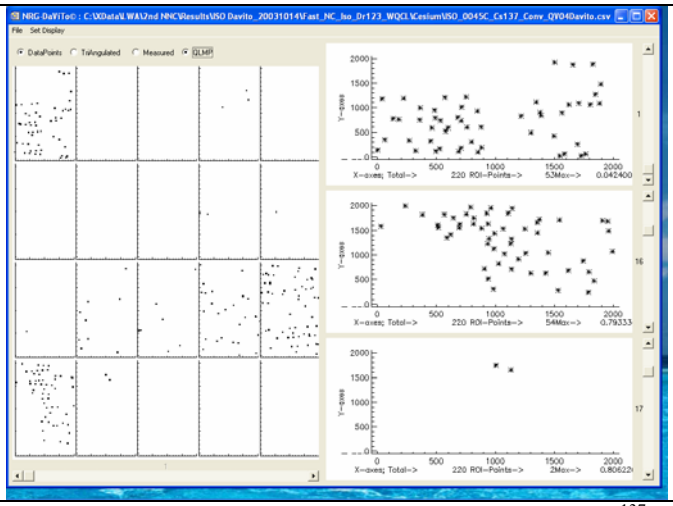

Figure A5.5 H Fractional statistically filtered data of ^{137}Cs 661 keV, run IS0-0045; details 1, 16 and 17.

A6 Transmission correction techniques for large-volume radioactive waste packages; calculation results

Table A6.1 Overview of the results of MCNP simulations for the original multi-energy transmission methodology. Revised methodologies 1 and 2. Specification of the Linac energy: 11 MeV

	Calculation methodology					True hydrogen mass fraction (%)								
Nr.	Density [kg/m^3] True/computed			Reference element		0.813 Computed mass fractions (%)			1.626 Computed mass fractions (%)			3.252 Computed mass fractions (%)		
	True	O	Ca	O	Ca	H	O	Ca	H	O	Ca	H	O	Ca
	Original methodology													
1		2.14		x		-10.52	-18.07	106.5						
2		2.15		x					-10.64	-16.33	105.1			
3		2.18		x								-10.68	-10.48	100.2
4	2.05			x		-4.959	-38.99	119.2	-4.338	-39.95	119.4	-3.068	-38.67	117.2
5			1.84	x		9.801	-94.50	152.8						
6			1.85	x					9.666	-92.47	151.1			
7			1.87	x								9.618	-85.67	145.5
8		2.14			x	-53.93	126.7	49.52						
9		2.15			x				-54.09	128.6	48.02			
10		2.18			x							-54.51	135.5	43.15
11	2.05				x	-46.19	98.47	65.06	-45.32	96.70	65.56	-43.55	96.31	64.05
12			1.84		x	-25.63	23.63	106.3						
13			1.85		x				-25.82	25.83	104.6			
14			1.87		x							-25.88	32.69	98.90
	Revised methodology 1													
15		2.14				13.38	-97.77	137.9						
16		2.15							-3.648	-39.63	114.2			
17		2.18										-13.56	-0.880	96.43
18	2.05					13.98	-102.1	144.0	-3.833	-41.63	120.0	-14.39	-0.934	102.3
19			1.84			15.57	-113.7	160.4						
20			1.85						-4.243	-46.09	132.9			
21			1.87									-15.77	-1.024	121.2
	Revised methodology 2													
22		2.14		x		-45.41	181.4	-						
23		2.15		x					-43.81	178.5	-			
24		2.18		x								-40.41	172.4	-
25	2.05			x		21.05	66.75	-	21.76	66.08	-	23.25	64.46	-
26			1.84	x		23.44	74.33	-						
27			1.85	x					24.10	73.16	-			
28			1.87	x								25.49	70.66	-
29		2.14			x	10.7	-	69.45						
30		2.15			x				11.437	-	68.35			
31		2.18			x							12.95	-	66.02
32	2.05				x	11.21	-	72.55	12.02	-	71.81	13.74	-	70.06
33			1.84		x	12.48	-	80.78						
34			1.85		x				13.30	-	79.51			
35			1.87		x							15.07	76.80	-

A7 Guideline for NDA characterization of fissile and non-fissile material in large-volume radioactive waste packages

A7.1 Introduction

The aim of this *NDA procedure for the NDA characterization of fissile and non-fissile material in large-volume waste packages* is to be a guideline to be used by institutes and companies that want to set up such systems.

Therefore the items discussed have to be read in general terms. Only when it is necessary essential are properties or specifications of hard ware and software specified in detail.

A7.2 Guideline for the NDA characterization of fissile material

Non-destructive measurements of fissile mass content of large radioactive waste packages requires in many cases passive and active measurement techniques to be applied. So procedures and approaches to be used are mainly based on modelling and, if it is possible, integrating passive and active methods.

It is advised to start with a checking capability based on passive measurements and if needed to proceed with active measurements if goals or objectives are not sufficiently reached.

Effectively, the choice of procedures and type of nuclear non-destructive measurements to be applied in view to quantify and/or to characterize fissile materials inside large waste packages depend on many parameters:

- Which fissile radionuclides have to be detected?
- What is the chemical composition of waste matrix?
- What is the hydrogenous (light elements) content of the waste matrix?
- What is the volume of waste packages?
- Can the contaminant distribution assumed to be homogeneous or not?
- What is the level of mass detection limit or/and sensitivity to be reached?
- Which kind of information is available on the isotopic distribution of the contaminant content (isotopic composition of uranium, plutonium, curium …)?
- What is expected maxim duration of a non-destructive measurement?
- Etc.

In general, fissile mass measurements deal with passive and usually also with active non-destructive techniques.

Passive measurement techniques that can be used are:

- Gamma spectrometry.
- Total neutron measurements.
- Neutron coincidence measurements.

Appliances of active measurement techniques have to be investigated step by step. It is advised to start first with checking the possibilities to apply active neutron measurements. If these measurements are not available than check the possibilities to apply active photon and neutron interrogation methodology by using an electron linear accelerator.

For large waste packages and crates, active measurement investigations and R&D often focussed on using high photon energy interrogation and high neutron intensity interrogation. Due to the high free mean path of such particles, mainly photons, one could strike the centre of such a large crate and hence dose fissile masses content.

Tomography could also be used to search for additional information such as the contaminant geometrical position, matrix density distribution and to support collected data interpretation and fissile mass declaration calculation.

Further, it is important to notice that an electron linear accelerator with a suitable energy and intensity is an appropriate system for active non-destructive measurements of radioactive large waste packages in order to characterize and to quantify the fissile mass of such a package.

A7.3 Guideline for the NDA characterization of non-fissile material

A7.3.1 Engineering and design of NDA equipment

The description of the properties of hard- and software to be used are based on the experiences gained with the 3DAS and PTP systems during the different *in situ* validation experiments, which results are presented in this report (see Section 2).

A7.3.1.1 Hardware

- *Detector and monitors.* The principle applied is that when one detector or monitor is not able to collect radiological data due to a too rough radiation environment another detector or monitor will take over, so that always one detector or monitor is able to provide radiological data. The following detectors are advised:
  - HPGe-detector. This semi-conductor detector can be collimated or open, this depends on detection principle applied e.g. accurate > PTP-system or scanning > 3DAS-system. This type of detector can operate up to an environmental dose rate level of about 200 μSv/h. The advised energy range to cover is from 50 keV up to 2000 keV.
  - CdZnTe-detector. This room temperature detector can be applied up to environmental dose rate level of about 2500 μSv/h. The disadvantage is that its energy resolution is not of the standard of a HPGe-detector, meaning that only principal photon energies can be analyzed. The advised energy range to cover is from 50 keV up to 1500 keV.
  - Dose-rate monitor. Advised is a pressurized ionization chamber up to 500 000 μSv/h.
  - Contamination monitor. By applying this type of monitors the sensitivity to gamma radiation must be minimal.
  - Neutron detector. By defining the specification of this detector an optimization has to be made between the detection of thermal-, epi-thermal- and fast neutrons.
- *NIM-electronics.* Analogue as well as digital processing electronics can be applied. Important is that the count rate throughput of the selected electronics is as high as possible, due to the fact that the selected combination of detector and electronics sets the limit of operating (e.g. performing gamma spectroscopy) in areas with elevated radiation levels. Special attention has to be given to the properties of the pre-amplifier (maximum power), spectroscopy amplifier (shaping time) and analogue digital converter (conversion time) and memory board (speed to store one pulse).
- Detector frame designed to scan the object or to measure accurately at well defined locations. Attention during the design has to be given to:
  - Selection of construction material. The construction material has to be able to be decontaminated as easily as possible. Advised are aluminium-oxidized profiles.
  - Strength of applied profiles. It is evident that such a frame will be transported or lifted in a number of occasions with a crane. Therefore it is advised that the profile that will be connected to the crane by webbing slings can withstand a bend-load of at least 3 times the total weight of the frame.

- Assembling and disassembling properties of the system. The assembling and disassembling of the system has to be logical and the amount of handlings to be performed has to be minimized. This is also valid for the number of tools to be used. Assembling and disassembling will be normally performed in areas with elevated radiation levels and by minimizing the time needed the received dose for technicians and or operators will also be minimized.
- Stability of the system and how to improve at the different measurement locations. The system can be engineered, like the developed *3D Rise* system, for operating in narrow areas, the stability of the system has also then still to be guaranteed.
- Transfer of the system to the (new) measurement location(s) along the large waste object. Transporting of the system has to be safe, easy and fast without loosing its stability during the transportation. Hereby, the dose received by the operators of the system will be reduced as well as the operational costs.
- Adjusting of the system to the (new) measurement location(s). See the point "Transfer of the system…." above.
- Registration of the distance between detector and the large waste object. In the case of a 3DAS-system the distance has to be controlled during a scan by cybernetics and by a PTP-system the distance can be measured by a measuring-tape.

A7.3.1.2 Software

The following software programs are advised:

- Gamma spectroscopy analyzing software.
  - PTP-system. Most commercial available software will function sufficiently. However, it is advised to test the software at background level and at an elevated level of about 90 % of the trough-put range. This test is to investigate if the software can handle the different low- and high-energy tail of the collected photo peaks.
  - 3DAS-system. Equal to PTP-system and the software has to have the following options:
    - To restart automatically a new data collection.
    - To define "real and live collection time" with at least a precision of 0.1 second.
- Conversion software. The aim of this software is to link collected radiological data with the actual measurement location.
- Statistical software. The aim of this software is to treat/filter collected data in order to detect irregularities that are statistical significant in the collected data.
- Imaging software. The aim of this software to produce iso-plots of collected data and statistically treated/filtered data in order to observe irregularities as hot-spots and patterns in collected data.

Special attention has to be given to data management and data handling between the different programs.

A7.3.1.3 Calibration

It is evident that for most large-volume waste objects no experimental calibration can be established. Therefore the calibration has to be estimated by means of appropriate software programs, like a software program as MCNP.

Further a large-volume waste object is in general a complex object to model, thus simplifications of the object have to be made. These simplifications have to be logical and meaning full. The first assessment can be, to assume that the large waste object contains a homogenous density and a uniform activity distribution. This simplification gives insufficient importance to the possibility to take into account detected activities at larger depths in the waste object.

At this moment it is advised to calculate the efficiency of a detector for a unique waste object as follows:

- Divide the waste object in a maximum of three zones of which each zone can be assumed to have a homogenous density but different from the adjacent zone.
- Divide each zone in a maximum of three equal layers with a uniform activity distribution of the nuclide of interest. For each layer the efficiency has to be calculated taking into account the shielding effects of the other layers. The sum of the three calibration coefficients of the different layers of one zone is of course equal to the calibration coefficient of the zone when this is not split-up in different layers. The aim of this subdivision in layers is that when it can be proved or assessed that an elevated radiation level is caused by an activity present at a greater depth this can be taken into account in the activity calculation of a specific nuclide.
- The simulated calibration factors have to be expressed in the dimension "Bequerel per outer surface of the waste object zone [Bq/m^2]". The sum of the individual surface zones is equal to the total outer surface of the waste object.

In this way a maximum of 12 calibration factors can be obtained (3 representing the uniform activity distribution of each zone, and 3*3 factors for the three layers of the three individual zones).

A7.3.2 Nuclide-specific activity calculation

The specific nuclide activity calculation can be based on the net count rate per surface area (see PTP-system), but also based on the statistically treated data (see 3DAS-system). This last calculation method is given in more detail below for one zone of the large waste object:

- Nuclide specific activity calculation based on statistically treated data.
  - Assess the percentage of the surface ($P_{Surface\ i}$) that has the following specific count rate:
    - $P_{Surface1}$: Greater than "Mean + 3* standard deviation".
    - $P_{Surface2}$: Between "Mean + 2* standard deviation and "Mean + 3* standard deviation".
    - $P_{Surface3}$: Between "Mean + 1* standard deviation" and "Mean + 2* standard deviation".
    - $P_{Surface4}$: Between "Mean + 1* standard deviation" and "Mean – 1* standard deviation".
    - $P_{Surface5}$: Between "Mean – 2* standard deviation" and "Mean – 1* standard deviation".
    - $P_{Surface6}$: Between "Mean – 3* standard deviation" and "Mean – 2* standard deviation".
    - $P_{Surface7}$: Less than "Mean – 3* standard deviation".
  - Calculate the average net count rate for the surfaces 1 to 7 for "$Nuclide_m$" as follows:
    - $N_{PSurface1}$ = "Mean + 3.5* standard deviation".
    - $N_{PSurface2}$ = "Mean + 2.5* standard deviation".
    - $N_{PSurface3}$ = "Mean + 1.5* standard deviation".
    - $N_{PSurface4}$ = "Mean".
    - $N_{PSurface5}$ = "Mean – 1.5* standard deviation".
    - $N_{PSurface6}$ = "Mean – 2.5* standard deviation".
    - $N_{PSurface7}$ = "Mean – 3.5* standard deviation".
  - Calculate the nuclide specific activity present in one zone of the waste package with:

$$A_{Zone\ j\ Nuclide\ m} = \Sigma\ (P_{Surface\ i} * \varepsilon_{Zone\ j\ Nuclide\ m} * N_{PSurface\ i;\ Nuclide\ m}),$$

in which $\varepsilon_{\text{Zone j Nuclide m}}$ is the total uniform calibration coefficient for the zone.

- Assess if collected data can be due to an activity located at a greater depth e.g. second or third layer. If yes, the following correction has to be made:
  - Assess the depth and the appropriate calibration efficiency $\varepsilon_{\text{Zone j Layer k Nuclide m}}$
  - Assess the surface with the elevated level caused by this activity $P_{\text{Surface Zone j Layer k}}$.
  - Assess the average net count rate due to the activity at a greater depth $N_{\text{PSurface Zone j Layer k; Nuclide m}}$
  - Assess the specific activity with

$$A_{\text{Zone j Layer k; Nuclide m}} = \Sigma(P_{\text{Surface Zone j Layer k}} * \varepsilon_{\text{Zone j Layer k Nuclide m}} * N_{\text{PSurface Zone j Layer k; Nuclide m}})$$

- The total specific activity can be calculated with:

$$A_{\text{Waste Package}} = \Sigma A_{\text{Zone 1}\rightarrow 3\text{; Nuclide 1}\rightarrow m} + \Sigma A_{\text{Zone 1}\rightarrow 3\text{ Layer 2}\rightarrow 3\text{; Nuclide 1}\rightarrow m}$$

In the above formula no corrections are applied for eventual activity that is counted double. This is due to fact that the accuracy is estimated to be about 50 % and these corrections are assumed at this moment to be not significant.

Note the results of the reported nuclide-specific activities and minimum detectable activities of important nuclides.

A7.3.3 NDA QA/QC characterization of a large waste object

A7.3.3.1 General information on the NDA characterization test

- Define the NDA QA/QC characterization test and eventual involved action criteria and eventual other special remarks.
- Describe the large waste item. Note the unique specifications of the waste item e.g. serial numbers eventually accompanied with digital pictures.
- Check if the available space around the large waste object is sufficient and note limiting distances.

A7.3.3.2 Preparations

- Adjust the detector frame at the (first) measurement location.
- Define the reference position(s). This position is important, because all collected data will be presented in relation to this position. In the case that the detector frame has to be adjusted at several locations around object the distances between reference positions have to be recorded accurately.
- Define the scan or measurements to be performed.
- Check if eventual limiting spaces have been taken into account by the set-up of the scan or measurement(s).
- Check the correct operation of the detector frame, like movement of axes, distance measurement, position data recording etc.
- Position the detector at the start position of the defined scan or at the first measurement location.
- Define the data collection specifications of mounted spectroscopy detector(s).
- Check the correct operation of the gamma spectroscopy system (see user manuals).
- Define the data collection specifications of mounted hand monitor(s).

- Check the correct operation of the mounted hand monitor(s) (see user manuals).

A7.3.3.3 Data collection

- Start all data collection programs e.g. detector and monitor position, gamma spectroscopy, dose rate, contamination etc. prior to movement of detectors and monitors according to the defined scan. In the case of a PTP-system just start the data collection of the gamma spectroscopy system. In the case of a 3DAS system, the following data collections have to be started:
  - Start the data collection of the position of the axes.
  - Start the data collection of the gamma spectroscopy system.
  - Start the data collection of mounted hand monitors.
  - Start the 3DAS-system to perform the defined scan. It is advised to wait till at least three gamma spectra are collected and all monitors are collecting data.
- Observe during the scan the data collection of the gamma spectroscopy system and hand monitors on abnormalities.

A7.3.3.4 Analysing collected data

In Section A7.2.4 the procedure to calculate the specific activity of a nuclide is explained in detail. The basis of this calculation procedure is an iso-plot of the nuclide of interest created on basis of collected data at the outer surface of the large waste object. This means that:

- All collected spectra have to be analyzed.
- The net count rate of the nuclide of interest has to be extracted out of all spectra and separately reported.
- All reported net count rates have to be linked to each individual measurement location. This location corresponds with a location at the surface of the large waste object.
- The just created data set can now be subject to statistical analyses. Important in this statistical treatment of the data set is that the link between the net count rate and its location may not be destroyed.
- The results of these additional calculations (statistical) including the net count rate data set will be used as input of graphical imaging software (this type of software is commercially available).
- The outputs of the graphical imaging software are iso-plots that are used to assess the fractions of the surface of the large waste object and the corresponding net count rates.
- The assessed fractions and corresponding net count rates are the input of the calculation formulas as given in section A7.2.4.